Microglia-nodes of Ranvier interaction during repair

Thomas Roux

THÈSE DE LA FACULTE DES SCIENCES DE SORBONNE UNIVERSITE

École Doctorale Cerveau, Cognition, Comportement (ED3C)

Présentée par **Thomas ROUX**

POUR OBTENIR LE GRADE DE DOCTEUR

SPÉCIALITÉ Neurosciences

Microglia-Nodes of Ranvier interaction during repair

Soutenue le 16 Décembre 2020

Devant la commission d'examen formée de :

Pr. Alain Trembleau	Président
Pr. Catherine Lubetzki	Directrice de thèse
Dr. Anne Desmazières	Co-directrice de thèse
Pr. Christine Stadelmann	Rapporteur
Dr. Alain Bessis	Rapporteur
Dr. Roberta Magliozzi	Examinatrice
Pr. Etienne Audinat	Examinateur

Remerciements

Tout d'abord, je tiens à remercier Alain Trembleau, Christine Stadelmann, Alain Bessis, Roberta Magliozzi, et Etienne Audinat de me faire l'honneur de juger ce travail de thèse.

Un immense merci au Pr Catherine Lubetzki et au Dr Anne Desmazières de m'avoir encadré depuis le tout début du master 2 jusqu'à aujourd'hui dans mon parcours scientifique. Merci pour votre soutien, votre patience, vos nombreux conseils et votre précieux compagnonnage. Merci à Bruno Stankoff pour son accueil dans l'équipe et ses conseils toujours constructifs.

Merci à tous ceux qui ont contribué à ce travail. Remerciement spécial à Rémi Ronzano avec qui j'ai partagé ce projet. Merci pour nos nombreux échanges sur nos résultats à chaque fois passionnants. Je te souhaite le meilleur pour la suite. Un immense merci à Marie-Stéphane, soutien indéfectible au sein du labo. Merci pour toute ton aide, ta disponibilité, et surtout ton sens de l'humour ! Merci à Melina qui m'a transmis beaucoup et avec qui j'ai fait mes premières armes au labo. Merci à Elisa précieuse voisine de bureau. Merci à Julien pour toute ton aide, ton efficacité.

Merci à toute l'équipe italienne à Vérone, Roberta, Valentina, Stephania, Lorenzo. Merci pour votre accueil, le temps que vous avez pris pour me former. Je garderai toujours un souvenir particulier de ces deux mois.

Merci également à tous les autres membres de l'équipe : merci à Boris, Nathalie et Marc, pour leurs précieux conseils. Merci à Anne-Laure pour nos discussions et ta bonne humeur. Merci à Elodie pour ta disponibilité et surtout les pauses blagues quotidiennes. Merci à Benedetta, Emilie, Matteo, Vito, Vanessa.

Merci à tous ceux de l'équipe d'à côté toujours prêt à rendre service et copains de déjeuner. Merci à Corentine, Laurent, Karim, Carlos, Jean-Baptiste, Emeric.

Merci à la plateforme d'imagerie ICM.quant, et à la plateforme HISTOMICS où j'ai passé un certain nombre d'heures. Merci à Dominique, Aymeric, Basile, Claire, Tudor, et Aurélien. Merci à Annick, Celia et Nicolas.

Merci à tous mes amis pour leur soutien. Merci à ma famille, tout spécialement à toi Adélaïde qui a dû supporter les moments de stress, de doute, les soirées et week-ends passés à travailler.

Table of Content

Table of Figures

Abbreviations

AIS	*Axon initial segment*
AnkG /R /B	*AnkyrinG /R /B*
APs	*Action potentials*
APP	*Amyloid precursor protein*
ATP	*Adenosine triphosphate*
CAMs	*Cell adhesion molecules*
Caspr	*Contactin-associated protein*
CNP	*2',3'-cyclic nucleotide 3'-phosphodiesterase*
CNS	*Central nervous system*
EAE	*Experimental autoimmune encephalomyelitis*
ECM	*Extracellular matrix proteins*
GalC	*Galactosylceramide*
IFN	*Interferon*
IGF	*Insulin-like growth factor*
IgG	*Immunoglobulin G*
IL-4	*Interleukin-4*
iNOS	*Inducible nitric oxide synthase*
K2p	*Two-pore domain potassium leak channel*
KIF	*Kinesin family member*
Kv	*Voltage-gated potassium channels*
LINGO1	*Leucine-rich repeat and Ig-domain containing1*
LPC	*Lysophosphatidylcholine*
MAG	*Myelin-associated glycoprotein*
MBP	*Myelin basic protein*
(MD)-macrophages	*Monocytes derives macrophages*
MHC-II	*Major histocompatibility complexes class II*
MR	*Mannose receptor*

MRI	*Magnetic resonance imaging*
MS	*Multiple sclerosis*
MTR	*Magnetization Transfer Ratio*
Nav	*Voltage-gated sodium channels*
NAWM	*Normal appearing white matter*
NF	*Neurofascin*
NG2	*Neural/glial antigen 2*
NGF	*Neurotrophin growth factor*
NrCAM	*Neuron-glia-related CAM*
Nrg-1	*Neuregulin 1*
OLs	*Oligodendrocytes*
OPCs	*Oligodendrocyte progenitor cells*
P2Y12r	*Purinergic receptor P2Y12*
p22phox	*Human neutrophil cytochrome b light chain*
PDGFRα	*Platelet-derived growth factor receptor α*
PET-MRI	*Positron emission tomography–magnetic resonance imaging*
PIB	*Pittsburgh Compound B*
PLP	*Proteolipid protein*
PNS	*Peripheral nervous system*
PPMS	*Primary progressive multiple sclerosis*
PPWM	*Periplaque white matter*
PSA-NCAM	*Polysialytated form of neuronal cell adhesion molecule*
RGC	*Retinal ganglion cells*
RRMS	*Relapsing-remitting multiple sclerosis*
Sema3	*Semaphorin 3*
SPMS	*Secondary progressive multiple sclerosis*
STED	*Stimulated emission depletion*

THIK-1	*Tandem-pore domain halothane-inhibited K+ channel 1*
TMEM119	*Transmembrane protein 119*
TNF-α	*Tumor Necrosis Factor-α*
TREK-1	*(TWIK)-related K+ channel*
TRAAK	*TWIK-related arachidonic acid stimulated K+ channel*

INTRODUCTION

Multiple Sclerosis (MS) is an inflammatory and demyelinating disease of the central nervous system (CNS) which can lead to neurodegeneration and permanent disability. Therapeutics to favor repair and neuroprotection are still lacking. How remyelination can be enhanced is thus a crucial question. However, the mechanisms underlying repair in MS are still only partially understood. The nodes of Ranvier, small excitable axonal domains allowing for the regeneration of action potentials, are a preferential target during demyelination. Moreover, we previously showed that node of Ranvier reclustering is an early event during (re)myelination, suggesting they could play a role in this process. It is also known that microglial cells, the resident immune cells of the CNS, are key players during remyelination. These cells are known to interact with different neuron subcompartments (soma, synapses, as well as axon initial segment, which shares a very similar composition to nodes of Ranvier), though the exact crosstalks between neurons and microglia in MS are still to be characterized. During my PhD, I focused on characterizing the interaction between neuron and microglia interaction at the nodes of Ranvier, in physiological as well as in pathological context.

I. Myelin, nodes of Ranvier and the myelination process

a) Composition and organization of myelinated fibers

The human central nervous system (CNS) can be divided into the two general anatomical categories of gray and white matter composed, respectively, of neuronal cell bodies and myelinated nerve fibers (Blackwood W et al., 1976).

Myelin is a multilamellar lipid rich structure, produced by oligodendrocytes in the CNS and by Schwann cells in the peripheral nervous system (PNS) that ensheathes myelinated axons. It consists of compacted spirals of plasma membrane extensions (Rio-Hortega, 1928). Its periodic structure has been visualized, using electron microscopy, as an alternance of electron-dense and lucent layers with a periodicity of about 12 nm (Aggarwal et al., 2011; Metuzals, 1963; Peters, 1960). Myelin is a hydrophobic structure with a high proportion of lipids (70-85%) and a low proportion of proteins (15-30%) (Baumann and Pham-Dinh, 2001). This unique molecular composition underlies its insulating properties, thereby favouring rapid nerve conduction (Waxman and Ritchie, 1993).

Louis-Antoine Ranvier (1835-1922), chair of anatomy at Paris College de France, was the first to describe periodic gaps along myelinated fibres, structures that now bear his name. Nodes of Ranvier are small (from 1.0 to 2.0 μm) unmyelinated segments between two adjacent myelin

segments (Landon and Williams, 1963; Salzer, 2003). Myelinated axons in the CNS are characterized by the alternance between nodes of Ranvier and internodes of myelin allowing saltatory conduction (Fig.1). Flanking the nodes are the paranodes representing the axoglial junction of the axolemma with uncompacted paranodal loops and segregating nodes from the juxtaparanodes before myelin segments.

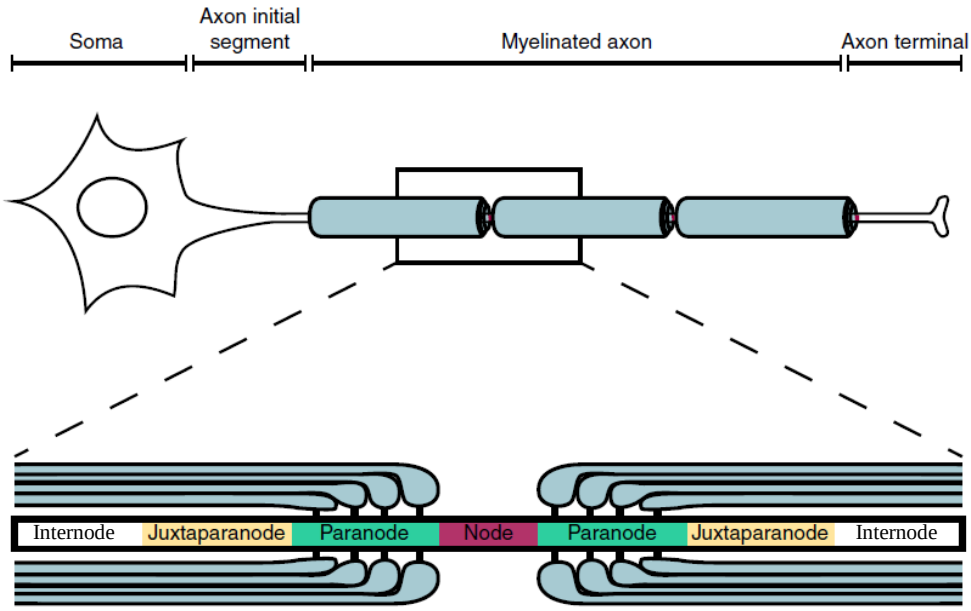

Fig.1/ The different domains of a myelinated neuron in the CNS.
Adapted from Arancibia-Carcamo et al. 2014

The molecular composition of the nodes of Ranvier has been extensively studied (for review, Lubetzki et al., 2020) (Fig.2). They are characterized by the high density of Nav channels allowing sodium entry and thus efficient depolarization of axons (Hodgkin and Huxley, 1952). Nav channels consist of a pore-forming α-subunit, sensitive to voltage and that regulates the ion flow; flanked by one noncovalently associated β-subunit (β1 or β3) and one covalently associated β-subunit (β2 or β4) (Catterall, 2000). Nine SCNA genes encode various α-subunit isoforms. In adult CNS nodes of Ranvier, Nav 1.1, Nav 1.2, and Nav 1.6 are the main isoforms identified (Arroyo et al., 2002). Nav 1.2 is expressed mainly in immature nodes whereas Nav 1.6 appears later in mature nodes (Boiko et al., 2001) and allow high firing rates. Nav 1.1 and Nav 1.8 are only expressed in a subset of neurons: Nav 1.1 in GABAergic neurons of the hippocampus and the cortex, retinal ganglion cells, Purkinje cells (Ogiwara et al., 2007; Schaller and Caldwell, 2003), and Nav 1.8 in the cerebellum and retinal ganglion cells (Black et al., 2000).

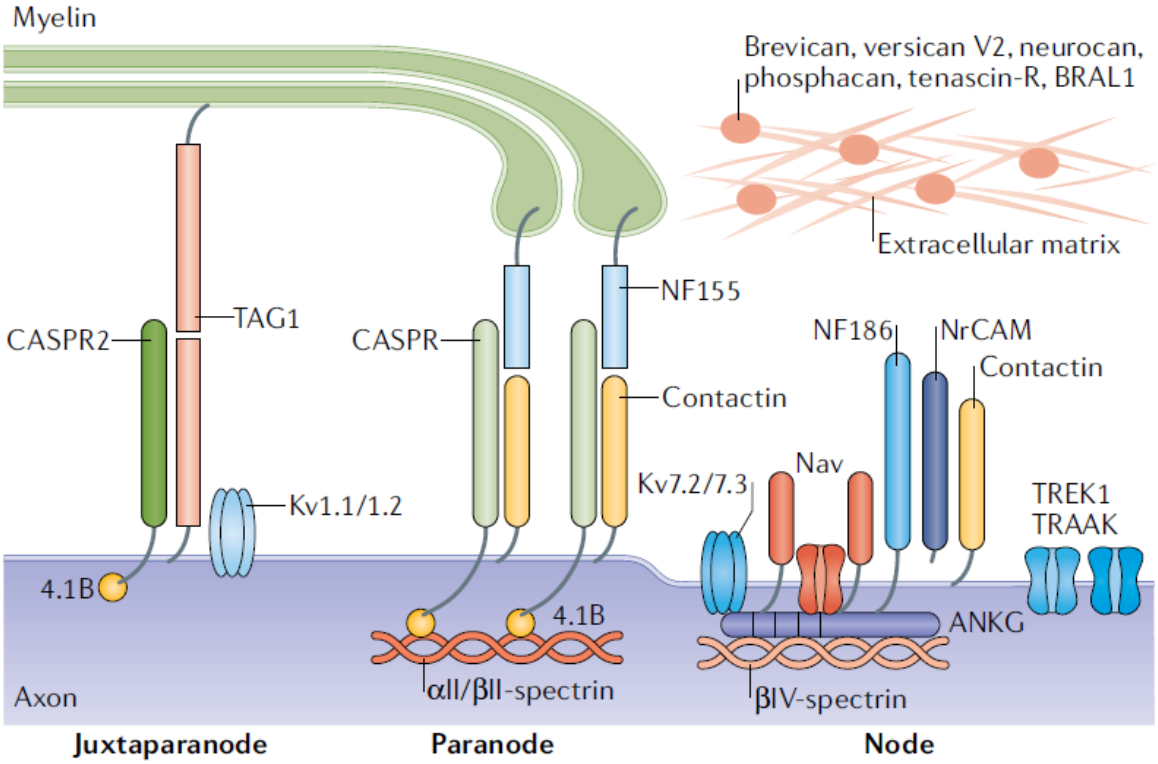

Fig.2/ Molecular composition of the node of Ranvier.
Schematic representation of the nodal, paranodal and juxtaparanodal molecular organization. The nodal domain is flanked by the paranodal axoglial junction, which acts as a diffusion barrier and separates the node from the juxtaparanodal domain. CASPR, contactin associated protein; NF, neurofascin. Adapted from Lubetzki et al. 2020.

β-subunits are glycoproteins encoded by a family of four SCNB genes (Kazen-Gillespie et al., 2000; Patton et al., 1994). They participate in modulating the gating properties of the α-subunits. β1, β2, and β4 isoforms are those mainly found in CNS nodes of Ranvier. β-subunits are transmembrane proteins that bind to the cell adhesion molecules (CAMs) Neurofascin (NF)-186, contactin and neuron glia-related CAM (NrCAM) (Berghs et al., 2000). This transmembrane complex is further anchored to the actin cytoskeleton through its direct interaction with the scaffold protein AnkyrinG, which in turn binds to βIV-spectrin (Garrido et al., 2003). βIV-Spectrin then associates with actin filaments. Extracellular matrix (ECM) molecules are enriched at the nodes, such as Brevican, versican V2, neurocan, phosphacan, tenascin R, or BRAL1 (Bekku et al., 2009; Oohashi et al., 2002). Voltage-gated potassium channels (Kv 7.2/7.3 and Kv3.1B) are also found at nodes and interact with AnkyrinG (Devaux et al., 2004; Pan et al., 2006; Schwarz et al., 2006). These channels are thought to stabilize the membrane resting potential, thereby allowing action potential amplitudes to be maximized (Battefeld et al., 2014). Furthermore, depending on neuronal subtypes other potassium channels have been described at the nodes like Kca3.1 in Purkinje cells (Gründemann and Clark, 2015). More recently thermosensitive and mechanosensitive TREK1 and TRAAK channels, which belong to the two-pore domain potassium leak channel (K2P) family have been identified in a subpopulation of nodes (Brohawn et al., 2019; Kanda et al., 2019). TRAAK contributes to the 'leak' K+ current by hyperpolarizing the resting membrane potential, thereby increasing Na+ channel availability for action potential propagation (Brohawn et al., 2019). Moreover, the very negative resting membrane potentials due to high leak K+ conductance at nodes of Ranvier should promote a quick recovery of voltage-gated Na+ channels from inactivation following each action potential, and instantaneous channel activation and deactivation of K2P channels minimizes the inter-spike interval. Thus, K2P channels permit high-speed and high-frequency action potential conduction (Kanda et al., 2019).

Directly flanking the nodes are the paranodes which mediate the formation of septate-like junctions between the uncompacted myelin paranodal loop and the axon and acts as a diffusion barrier to segregate the node from the juxtaparanodal domain (Baumgartner et al., 1996). They in particular allow to prevent juxtaparanodal Kv channels from diffusing into the node (Rios et al., 2003).

On the neuronal part, they are formed by the CAMs axonal contactin-associated protein (Caspr), and contactin (Einheber et al., 1997; Faivre-Sarrailh et al., 2000; Peles et al., 1997). They associate with the glial 155 kDa isoform of Neurofascin (NF-155) (Charles et al., 2002a; Tait

et al., 2000) on one hand, and to the cytoskeleton-anchoring protein 4.1B (Denisenko-Nehrbass et al., 2003; Menegoz et al., 1997) on the other hand which in turn binds to α2/β2-spectrin. The juxtaparanodes begin at the innermost axo-glial junction of the paranodes and extend for 5–15 nm. Their main feature is their high density of delayed rectifier voltage-gated potassium channels (Kv1.1, Kv1.2 and Kvb2 subunits), which might play a role in internodal resting potential support, in particular during development and injury (Rasband, 2010; Wang et al., 1993). They also contribute to the internodal resting potential and act to prevent repetitive firing. These ion channels are associated at juxtaparanodes to the CAMs Caspr2 and Tag1.

b) Functional properties of myelin and nodes of Ranvier

Myelin increases membrane resistance and decreases membrane capacitance (meaning less Na+ charge entry is needed to depolarize the cell), thereby stabilizing ionic charge as the axolemma is depolarized during action potential propagation (Arancibia-Cárcamo et al., 2017; Bakiri et al., 2011). The alternance of myelinated internodes and nodes of Ranvier permits the saltatory conduction along myelinated axons in vertebrates as a way of rapidly transmitting electrical impulses along large distances to target cells and tissues. Morphological axonal parameters are critical for conduction velocity, which increases with axon diameter, internodal length and myelin thickness (Freeman et al., 2016; Huxley and Stämpfli, 1949; Rushton, 1951; Smith and Koles, 1970). Moreover, nodal length can influence conduction speed. For a constant density of Nav channels at the node, lengthening of nodal gap increases conduction velocity (up to a certain maximum). On the opposite, an increased nodal length with a total number of nodal Nav channels kept constant decreases the speed (Arancibia-Cárcamo et al., 2017).

Therewith, myelin and oligodendrocytes also provide support to maintain axonal integrity and function. First, loss of myelin results in major axonal pathology. In EAE, after long-term demyelination, axonal loss is observed (Kornek et al., 2000). Secondly, it has been shown that oligodendrocytes provide essential trophic support to axons (Rasband et al., 2005; Saab et al., 2016), and other studies suggest their ability also to provide metabolic support (Fünfschilling et al., 2012). Mature oligodendrocytes use aerobic glycolysis, to participate in the metabolic support of myelinated axons, in which myelin delivers lactate to axons. Lactate is then metabolized in the axons, where access to other sources of energy is limited (Fig.3).

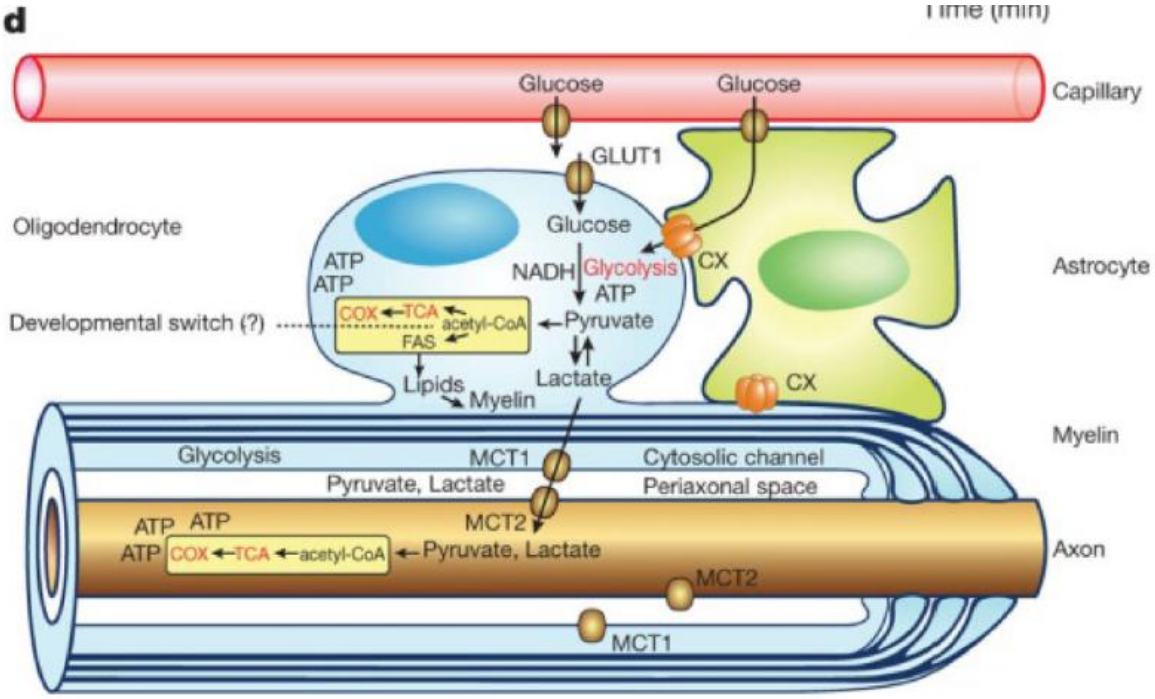

Fig.3/ Hypothetical model of metabolic coupling between oligodendrocytes and myelinated axons. Oligodendrocytes import glucose through GLUT1 (and possibly via astrocytes and gap junctions; CX, connexin) for glycolysis. Axons, largely shielded from the extracellular milieu, are separated by a thin periaxonal space from the oligodendroglial cytoplasm filling the inner loops of myelin ('cytosolic channel') and paranodal loops. Adapted from Funfschilling et al. 2012.

c) Myelination process and adaptive myelination

i. Oligodendrocyte lineage and myelin

In the CNS, myelin is produced by myelinating oligodendrocytes (OLs) (Rio-Hortega, 1921). Before that, the oligodendrocyte lineage follows a complex differentiation process (Fig.4). Oligodendrocyte progenitor cells (OPCs) are generated during embryogenesis from the ventricular neuroepithelium in the neural tube (Pfeiffer et al., 1993). Then OPCs differentiate in pre-myelinating oligodendrocytes which progress to immature OLs. Finally, these latter mature in myelinating OLs (Levine et al., 1993). Progression through the oligodendrocyte lineage is tightly regulated by a multitude of intrinsic and extrinsic cues, which control myelination both spatially and temporally during development and after myelination. These signals include growth factors, protein kinases, or extracellular matrix molecules (Bauer et al., 2009). Early OPCs are defined by the expression of platelet-derived growth factor receptor α (PDGFrα) and the proteoglycan neural/glial antigen 2 (NG2) (Nishiyama et al., 1996; Pringle et al., 1992). As their differentiation progress, OLs become less proliferative and start to express CNP and GalC (Zalc et al., 1981). Their arborization expand and they finally express myelin proteins (MBP, MAG, PLP) and begin to contact axons (Martini and Schachner, 1986). The maturation to myelinating OLs is achieved when they express the protein MOG (Solly et al., 1996).

In the CNS, *in vitro* (Watkins et al., 2008) as well as *in vivo* experiments (Czopka et al., 2013) have demonstrated that myelinating oligodendrocytes establish myelin sheaths in only a few hours. The deposition of the successive myelin layers is led by the inner tongue which wraps around the axon and extends laterally (Fig.5) (Snaidero et al., 2014). The dynamics of the actin cytoskeleton appears finely regulated to trigger myelin wrapping, with an actin polymerization at the leading edge of the inner tongue and subsequent depolymerization (Nawaz et al., 2015; Zuchero et al., 2015).

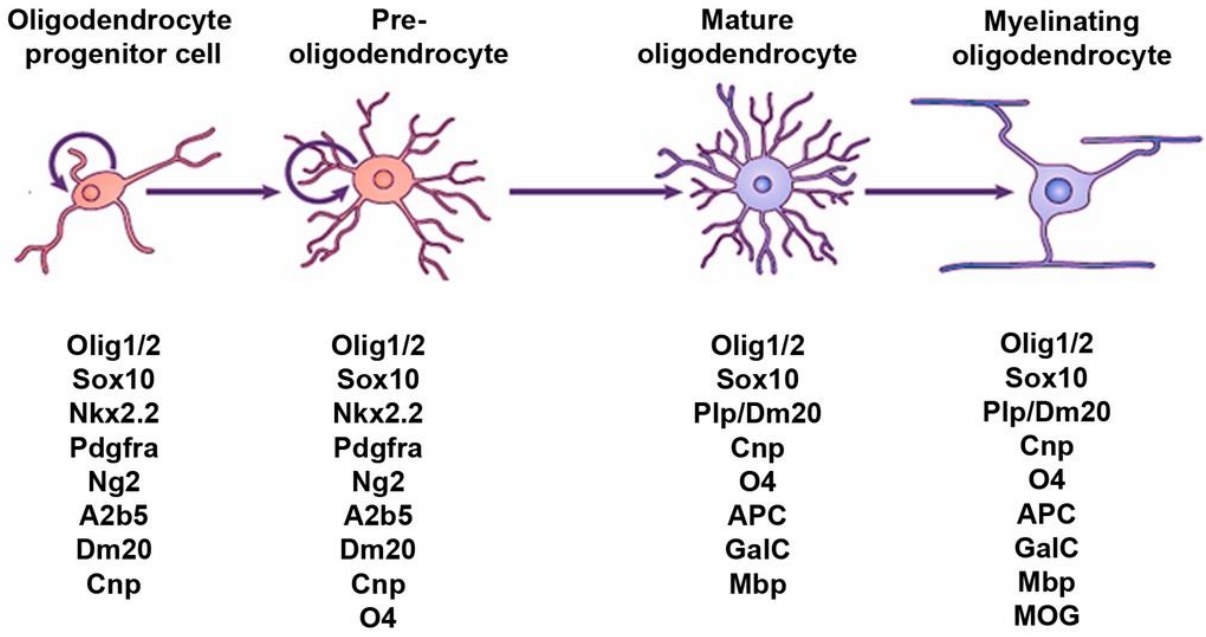

Fig.4/ Schematic representation of the development stages of the OL lineage.
The morphological (top) and antigenic (bottom) features of OPCs, pre-OLs, mature OLs and myelinating OLs are shown. Adapted from Traiffort et al. 2016.

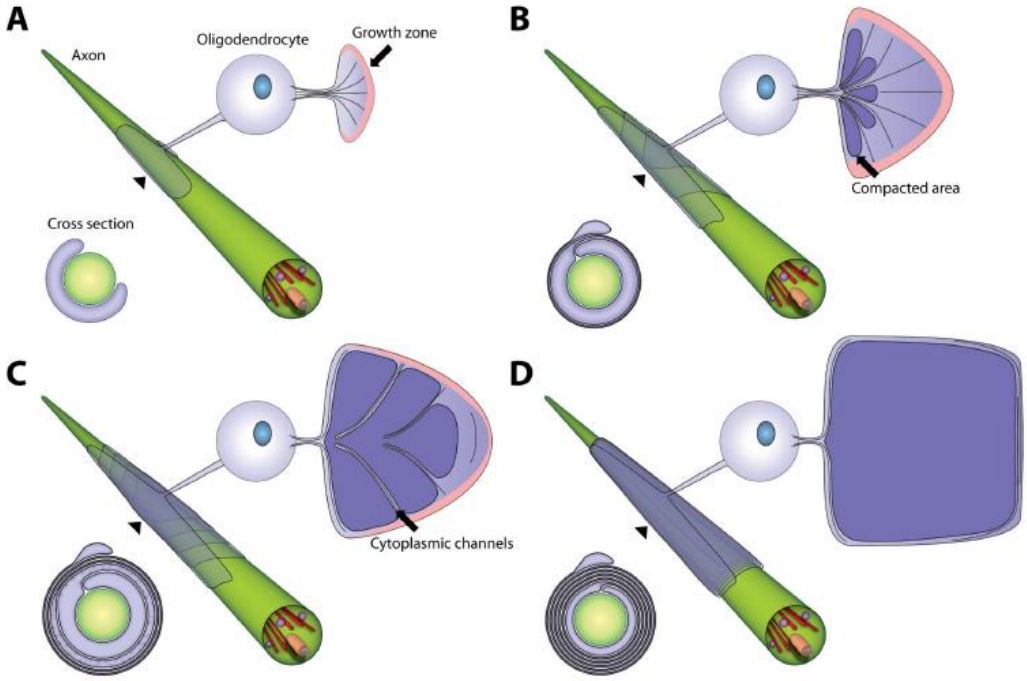

Figure.5/ Model of myelin biogenesis in the CNS.
(A-D) Model of a developing myelin sheath in a wrapped, unwrapped and cross section view. The unwrapped representation shows the geometry and the development of the sheath and the localization of the cytoplasmic channels, which connect the cell body and the growth zone at the inner tongue. The growth zone is colored in pink and compacted myelin in dark violet. The wrapped representation shows the position of the layers when wrapped around the axon. The cross sections show the state of compaction during myelin growth.
Adapted from Snaidero et al. 2014

Myelination is a highly regulated process. First, several seminal studies showed that a critical axon diameter is necessary for myelination to occur (Duncan, 1934; Matthews, 1968). Remahl & Hildebrand demonstrated that the spectra of myelinated axon diameter in the corpus callosum vary from 0.2 to 0.7 µm and from 0.6 to 1.2 µm in the spinal cord (Remahl and Hildebrand, 1982). Cultured oligodendrocytes can develop myelin membrane sheets in absence of neurons and can myelinate paraformaldehyde-fixed axons or synthetic fibers (Lee et al., 2012). These results confirmed the role of the axon diameter but also suggested that axonal cues might not be necessary to activate myelination. Moreover, intrinsic properties of OLs play a key role. Using microfibers, Bechler et al. showed that oligodendrocytes respond to fiber diameters and that spinal cord oligodendrocytes generate longer sheaths than cortical oligodendrocytes revealing that oligodendrocytes have regional identity (Bechler et al., 2015). Yet, *in vivo,* all eligible axons are not myelinated. Thus, several intrinsic axonal cues are known to influence (positively or negatively) myelination (Fig.6) as the axonal ligands Jagged-1 and Delta-1 (Wang et al., 1998), the neurotrophin NGF (Chan et al., 2004), the neuronal cell adhesion molecule PSA-NCAM (Charles et al., 2002a), or the leucine-rich repeat and Ig-domain containing1 (LINGO1) (Mi et al., 2005). The growth factor Nrg-1 and its receptor ErbB have been also implicated in CNS myelination process (Calaora et al., 2001; Canoll et al., 1996).

Furthermore, neuronal activity is known to impact myelination (Fig.6). First it was showed that blocking neuronal activity led to reduced OPCs proliferation and myelination (Barres and Raff, 1993; Demerens et al., 1996; Wake et al., 2011). Optogenetic experiments to direct neuronal activity also showed increased OPCs proliferation and survival following neuronal activation, resulting in increased oligodendrogenesis. In these experiments, mature oligodendrocyte number increased along with myelin-basic-protein protein expression and myelin sheath thickness coupled to behavioral improvement (Gibson et al., 2014). Moreover, it has been shown *in vitro* and *in vivo* in mice and zebrafish that the choice of the target axons is promoted by neuronal activity (Mitew et al., 2018; Wake et al., 2015). In zebrafish, Mensch et al. have shown that glutamate synaptic vesicular release enhance the number of myelin sheaths made by an individual oligodendrocyte and impact the selection of axons undergoing myelination (Baraban et al., 2018; Hines et al., 2015; Mensch et al., 2015).

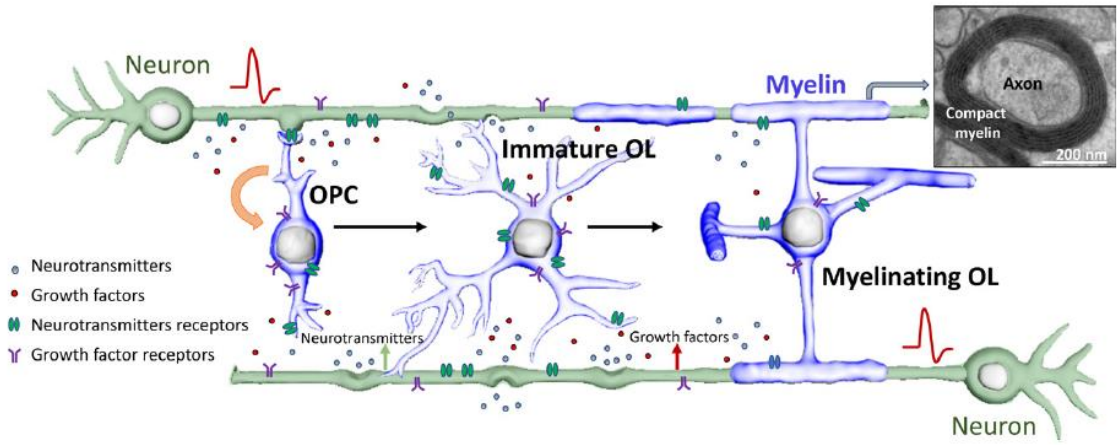

Fig.6/ Schematic showing oligodendroglial lineage development and de novo myelination. Action potential firing by active neurons results in the release of neurotransmitters (such as glutamate, GABA, ATP or acetylcholine) and/or growth factors (such as platelet-derived growth factor, brain-derived neurotrophic factor or neuregulin) via synaptic and non-synaptic mechanisms, and exert multifaceted influence upon both oligodendroglial lineage development and axonal ensheathment. Adapted from de Faria Jr et al. 2019.

Recently, the observation of partially myelinated neurons (Tomasi et al., 2012) led to the idea that the myelination pattern along axons and its modulation could participate in regulating axonal conduction and pave the way to the notion of adaptative myelination. Neuronal activity could modulate myelin plasticity which would in turn modulate neuronal networks. In 2014, Tomassy et al. showed that neurons, especially in the superficial layers of the cortex, display distinct longitudinal distribution of myelin suggesting a strategy to modulate long-distance communication (Tomassy et al., 2014). Thus, it has been established that nodes of Ranvier length and interval can modify conduction speed and contribute to the coordination of the coincident arrival of synaptic inputs from multiple axons (Arancibia-Cárcamo et al., 2017; Seidl et al., 2014). Ford et al. showed that internodes length and nodes of Ranvier diameter vary along axonal segments allowing optimization of the conduction velocities to ensure precise timed depolarization (Ford et al., 2015). In mice, OPCs keep proliferating and differentiating in adult CNS, with 5–20% of oligodendrocytes generated during adulthood (Young et al., 2013). Thus, the impact of neuronal activity on myelination in adult brain may result from the ubiquitous presence of OPCs throughout the adult mouse brain (Young et al., 2013). In rodent brain, adult NG2-positive OPCs are constantly migrating through the local environment, retracting, and extending their branched processes (Hughes et al., 2013). Myelin plasticity has been shown to play a role in learning processes. In human, increased brain white matter volume was observed in piano players (Bengtsson et al., 2005) or jugglers (Scholz et al., 2009), also suggesting

neuronal activity-induced increased myelin plasticity. Conversely, functional studies showed that socially isolated juvenile mice are hypomyelinated with fewer myelin sheaths produces by OLs. They also exhibit cognitive and behavioral alterations (Makinodan et al., 2012).

ii. Formation of Nodes of Ranvier

Formation of nodes of Ranvier in the CNS is a complex process. Susuki et al. demonstrated that the CNS nodes assembly involves three mechanisms: 1/stabilization of nodal components by ECM ; 2/ paranodal axoglial junctions that function as barriers to restrict the position of nodal proteins; and 3/axonal cytoskeletal scaffolds interacting with nodal markers (Susuki et al., 2013). They show that while mice with a single disrupted mechanism had mostly normal nodes, disruptions of two out of three mechanisms all lead to juvenile lethality, profound motor dysfunction, and significantly reduced Nav channel density. This major result support the hypothesis of complementary and compensatory mechanisms driving myelination (Fig.7).

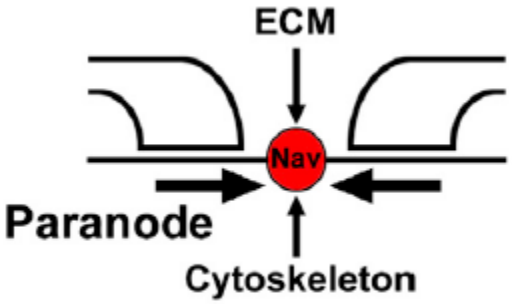

Fig.7/ Illustration showing the three mechanisms involved in CNS nodes of Ranvier formation
ECM, extracellular matrix. Adapted from Susuki et al. Neuron 2013.

Furthermore, the clustering role of oligodendroglial secreted cues was suggested by the Barres laboratory, showing that oligodendroglial secreted factors promote Nav channel clustering in CNS axons in retinal ganglion cell culture, in the absence of axoglial contact (Kaplan et al., 1997). These seminal results were confirmed and extended by our team on hippocampal GABAergic neurons (Freeman et al., 2015) with the identification of the clustering role of a contactin multimolecular complex comprising Phosphacan or Tenascin-R (Dubessy et al., 2019).

Secondly, it has been shown that paranodal junctions are important in the initial clustering of Nav channels (Rasband et al., 1999). In support of a role for paranodal junctions in the assembly of CNS nodes, researchers reconstituted paranodes by transgenic expression of glial NF-155 on a NF-null background. They found that this rescued the correct assembly of CNS nodes of Ranvier in the absence of NF186. However, data from paranodal mutant mice also suggested that paranodal junctions are dispensable for node assembly. Indeed, Nav channels accumulate at nodes in NF-null mice rescued with transgenic NF-186 (no reconstitution of the paranodal junctions) (Zonta et al., 2008).

Thirdly, concerning the role of cytoskeletal scaffolds, the interactions between AnkyrinG and CAMs or ion channels may promote their stable and restricted localization at nodes. AnkyrinG recruits βIV-spectrin to nodes, which in turn provides further linkage to the axonal cytoskeleton (Yang et al., 2007). Thus, the βIV-spectrin and ankyrinG based axonal cytoskeleton are important for stabilization of nodal Nav channel complexes. Furthermore, the work of Barry et al. revealed that AnkyrinG functions as an adaptor that links Nav channels to the anterograde molecular motor KIF5B during axonal transport suggesting that the axonal localization of Nav channels could rely on its interaction with AnkyrinG (Barry et al., 2014). More recently, our team showed that some nodal proteins are partially co-transported along the axon, suggesting a partial pre-assembly of the nodal complex prior to membrane targeting (Thetiot et al., 2020). Moreover, Nav channel binding to ankyrinG is both necessary and sufficient for channel clustering (Gasser et al., 2012). However, mice lacking nodal βIV-spectrin, which links AnkyrinG and Nav channels to the actin cytoskeleton, have relatively normal CNS nodes (Komada and Soriano, 2002). Indeed, compensatory mechanisms are involved: β1 spectrin, together with AnkyrinR (AnkR), could compensate for the loss of nodal AnkG and βIV spectrin (Ho et al., 2014; Liu et al., 2020).

Interestingly, nodal clustering mechanism may differ between neuronal subpopulations. Indeed, our team demonstrated the existence of nodal Nav clusters preceding myelination in

hippocampus experimental models *in vitro* and *in vivo* on GABAergic neurons, but not on pyramidal cells, suggesting that different mechanisms are at play to form nodes of Ranvier in the CNS. These node-like clusters correlated with accelerated axonal conduction, as shown by single neuron electrophysiological recording (Freeman et al., 2015) and might also play a key role in initiating myelination (Thetiot et al., 2020).

II. Demyelination and remyelination processes in Multiple Sclerosis and its experimental models

a) Natural course of Multiple Sclerosis

Multiple sclerosis (MS) is a chronic inflammatory demyelinating and neurodegenerative disease of the CNS leading to multiple foci of demyelination in white and grey matter of the brain and spinal cord. It is an autoimmune disease with predisposing genetic and environmental factors (Reich et al., 2018).

It is the most prevalent chronic inflammatory disease of the CNS, affecting >2 million people worldwide and currently incurable (GBD 2015 Neurological Disorders Collaborator Group, 2017). In Europe, prevalence is 1 out of 1000 people and thus is a frequent disease which constitute the first cause of non-traumatic handicap in young adults (Dubessy et al., 2014).

Some risk factors have been identified but remained scarce despite extensive clinical research. Smoking, and geographical gradient (at the expense of cold latitudes) are the two main known risk factors. Obesity, and mononucleosis are also associated with enhanced risk for developing MS. There is a sex ratio of 3 women for a man and the median age of onset is 30 (Compston and Coles, 2002; Reich et al., 2018).

The natural course of the disease is characterized in 85% of patients by the succession of relapses (relapsing-remitting phase) with various functional impairments (Fig.8): motor or sensory deficits, balance, or gait impairment. Oculomotor, optical, or urinary deficiencies are also common. For the 15% remaining patients, evolution is out of hand progressive (primary progressive) and linked to neurodegenerative processes. Among relapsing-remitting patients, around 50% will develop a secondary progressive form after 15-20 years of disease evolution (Dubessy et al., 2014).

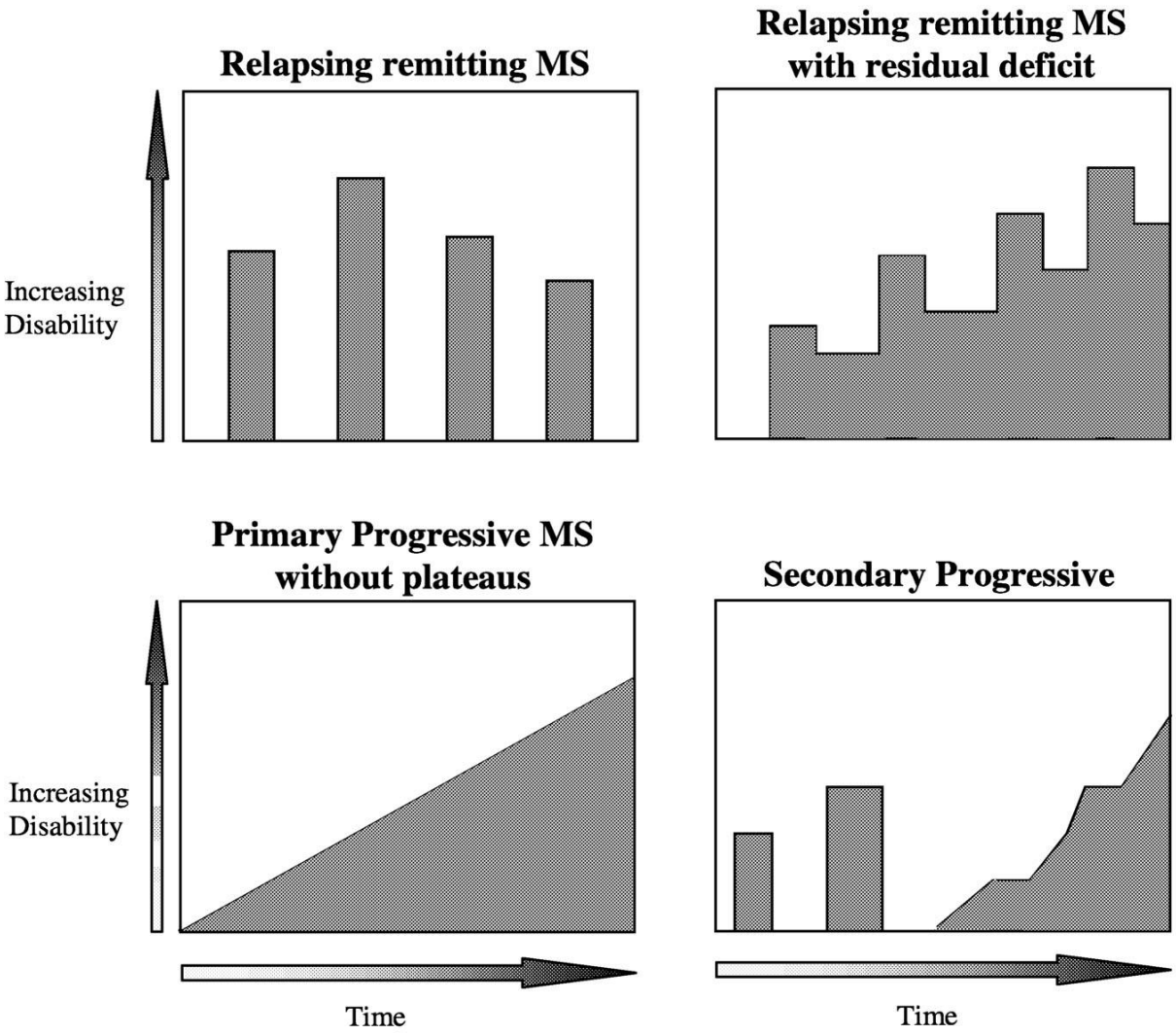

Fig.8/ Spectrum of disease course.
Adapted from Lublin and Reingold, 1996

To date, the main therapeutic angle used in MS is immunosuppressive/immunomodulatory therapy preventing inflammation and demyelination and thus relapses (Cree et al., 2019). On the other hand, the neurodegenerative part of the disease lacks therapeutical strategies. To achieve efficient immunosuppression in MS, some drugs decrease activation or proliferation of lymphocytes (teriflunomide, dimethyl-fumarate, interferonβ, glatiramer acetate), others prevent lymphocytes circulation (fingolimod) or their entry in the brain (natalizumab). Lastly, ocrelizumab suppresses a sub population of B lymphocytes (Rommer et al., 2019), probably interfering with antigen cell presentation.

b) Demyelination in MS

The demyelinated white matter lesions, responsible for relapses in MS, are characterized by inflammatory infiltrates composed of T cells, B cells and macrophages/microglia, demyelination, axonal loss, varying degrees of remyelination and glial scar formation. But white matter lesions from relapsing-remitting and chronic progressive disease significantly differ from each other.

The main white matter lesion type in relapsing multiple sclerosis is the actively demyelinating, inflammatory lesion, representing 35% of all lesions (Frischer et al., 2015). Active lesions are characterized by areas with sharp limits of demyelination. They can be either demyelinating or post-demyelinating according to macrophages population and their cytoplasm content (myelin degradation products). If demyelinating, myelin degradation products are visible in macrophages cytoplasm. Four histopathological profiles with active lesions have been described in MS (Lucchinetti et al., 2000) (Fig.9):

- Pattern I is characterized by T-lymphocytes and macrophages inflammation.
- Pattern II is very similar to pattern I, adding the presence of IgG and complement C9 deposition.
- Pattern III showed T-lymphocytes and macrophages inflammation, no IgG deposits, ill-defined lesions, and oligodendrocytes apoptosis.
- Pattern IV is similar to pattern III and showed T-lymphocytes and macrophages inflammation, no IgG deposits, loss of oligodendrocytes without apoptosis.

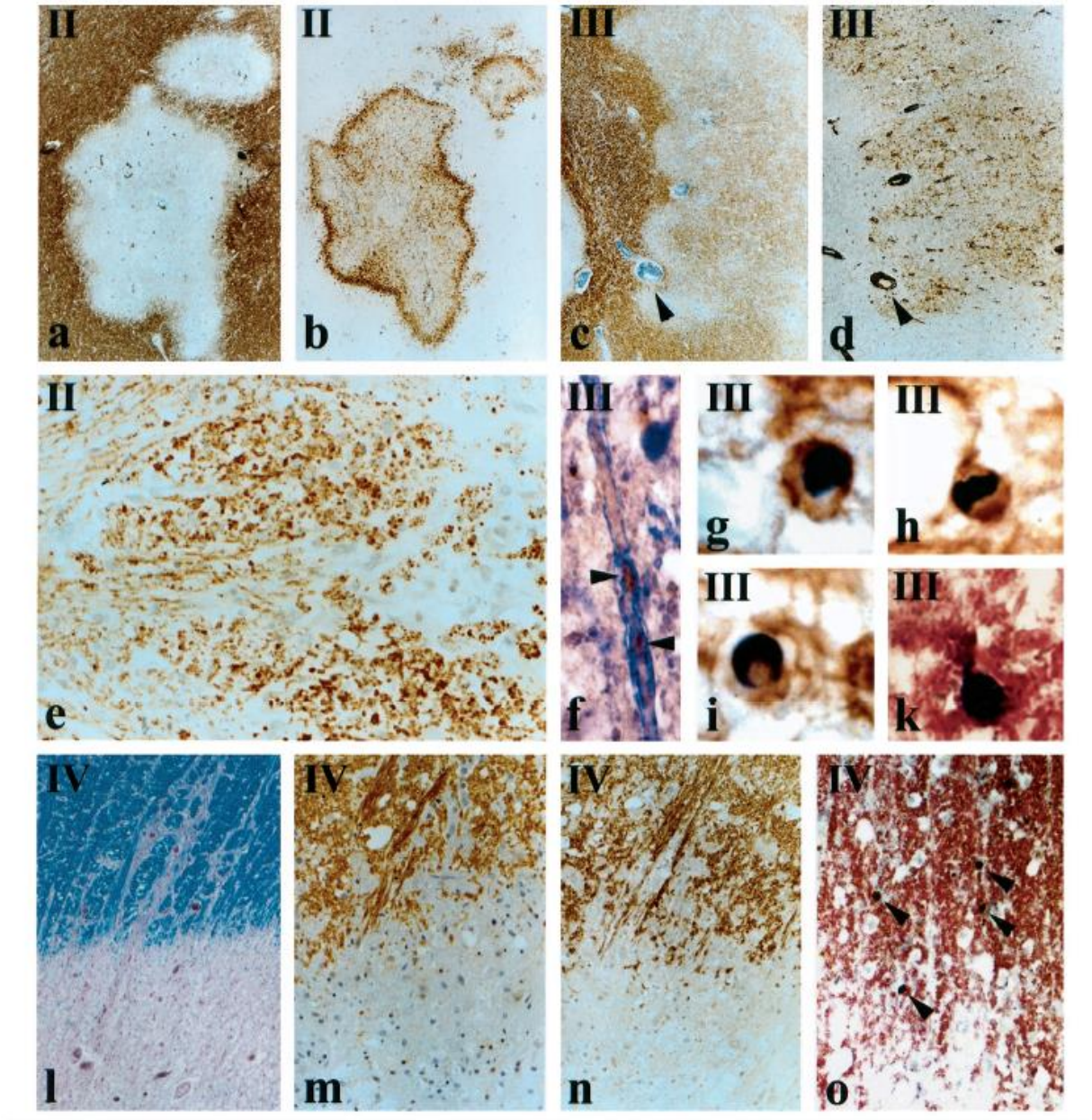

Fig.9/ Pattern of demyelination in active lesions.
Pattern II showing lesions with sharp limits (a; b), massive C9 deposition at the actively demyelinating border (e). Pattern III showing lesions with ill-defined borders (c, d), apoptotic oligodendrocytes (g-k). Pattern IV showing DNA fragmentation of oligodendrocytes is seen in the periplaque white matter (o).
Adapted from Lucchinetti at al. 2000

Very interestingly, at a given time point of the disease—as reflected in autopsy cases—the patterns of demyelination were heterogeneous between patients but were homogenous within multiple active lesions from the same patient. This suggests that various lesion mechanisms might exist according to each patient. White matter lesions of patients suffering from progressive multiple sclerosis are different and have originally been described as slowly expanding lesions. They are considered to be the morphological correlate of disease progression and are characterized by an accumulation of macrophages at the lesion edge that mediate active ongoing myelin breakdown and axonal damage (Prineas et al., 2001). However, a recent classification characterized more precisely these lesions calling them mixed active/inactive lesions (Fig.10) (Kuhlmann et al., 2017).

Thus, mixed active/inactive lesions are characterized by areas with sharp limits of demyelination and a rim of macrophages at the lesion edge. Two types are described, again depending on macrophages activity:

- Demyelinating (former smoldering or slowly expanding lesions)
- Post demyelinating (former chronic active lesions)

The significance of these mixed active/inactive lesions is still under debate (Jäckle et al., 2020). They are classically associated with the progressive stages of the disease. By applying the microglia-specific marker TMEM119, researchers demonstrate that cells accumulating at the lesion edge almost exclusively belonged to the microglial lineage (and were not monocyte-derived macrophages). By using a panel of markers characterizing their phenotype, they observed a preferential accumulation of pro-inflammatory cells at the lesion edge, indicating a crucial role of these cells in lesion progression. MRI studies identified a persistent phase rim (Absinta et al., 2016) or an iron rim at the lesion edge (Dal-Bianco et al., 2017) as potential in vivo markers for neuroimaging. These lesions may therefore be useful as a prognostic tool in multiple sclerosis patients (Luchetti et al., 2018).

Lastly, inactive lesions are fully demyelinated but without macrophages presence and characterized by a glial scar in their center with accumulation of astrocytes.

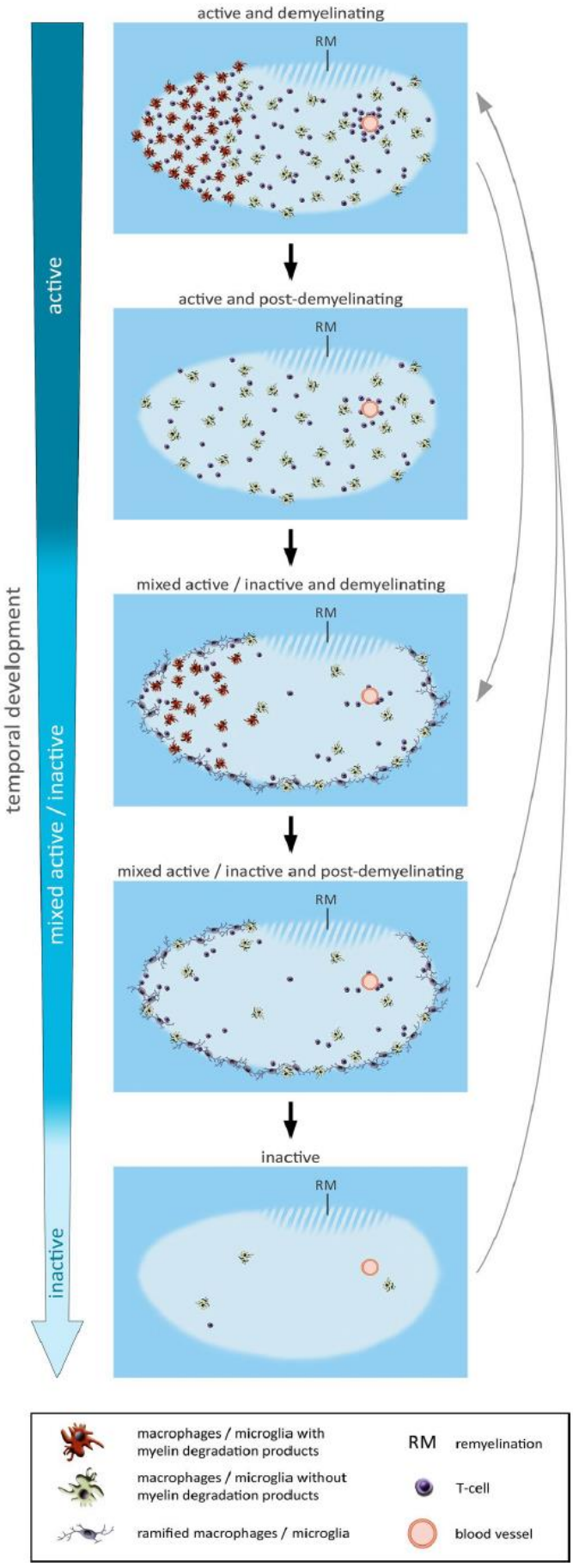

Fig.10/ Schematic diagram summarizing the temporal development of MS lesions.
Active and demyelinating lesions may develop into active and post-demyelinating or mixed active/inactive lesions.
Adapted from Kuhlmann et al. 2017

An extensive analysis of white matter plaques in a large sample of MS autopsies showed that active plaques were most often found in early disease, whereas at later stages, mixed active/inactive and inactive lesions predominated. The presence of early active plaques rapidly declined with disease duration. Moreover, depending on the clinical course (relapsing-remitting vs. progressive MS), plaque type distribution differed significantly: most plaques in acute monophasic and relapsing-remitting MS (RRMS) were active. Disease duration, clinical course, age, and gender contribute to the dynamic nature of white matter MS pathology (Frischer et al., 2015).

Furthermore, pathological processes without demyelination have also been described in MS supporting the idea that MS is not only a myelin disease. Focal axonal degeneration before demyelination (Nikić et al., 2011) and acute axonal injury without any demyelination after experimental oligodendrocytes ablation were found (Oluich et al., 2012) in MS experimental models and MS tissues. Howell et al. showed that a significant early alteration in Nfasc155+ paranodal structures occurs within and adjacent to actively demyelinating white matter MS lesions that are associated with altered axonal organization (Howell et al., 2006). Moreover, focal changes have been documented in normal-appearing white matter of MS months to years before the appearance of MRI gadolinium-enhancing lesions. In these foci, clusters of activated microglia are found in the absence of demyelination or clear leukocyte infiltration, distinguishing them from the traditional demyelinating active and mixed active/inactive lesions (van der Valk and Amor, 2009).

c) Remyelination

i. Remyelination in experimental models

Richard and Mary Bunge demonstrated after demyelination induced in subpial cord by cerebrospinal fluid exchange that demyelinated axons can acquire new myelin sheaths (Bunge et al., 1961). Remyelination relies on the rapid repopulation of the demyelinated lesion with glial progenitor cells and their subsequent differentiation into myelinating oligodendrocytes. Thanks to this physiological process an efficient conduction is restored (Smith et al., 1979). Studies of experimental models of demyelination, induced either by immunological, viral, or

chemical means, have demonstrated that remyelination is usually very rapid and efficient and is associated with improved neurological function (Franklin and Goldman, 2015).

Indeed, long ago it was shown that the degree of axonal loss in experimental allergic encephalomyelitis (EAE) is greater in areas of active demyelination than in areas with remyelination (Kornek et al., 2000). Pohl et al. reported that a selective genetic ablation of OLs to induce demyelination was followed by axonal injury (Pohl et al., 2011). Several more recent studies demonstrated that remyelination favors neuroprotection. First, Irvine & Blakemore showed that rescuing remyelination in irradiated mice (to prevent endogenous remyelination) after cuprizone induced demyelination allows to decrease axonal loss (Irvine and Blakemore, 2008). Moreover, Mei et al. showed that accelerated remyelination during inflammatory demyelination prevents axonal loss and improves functional recovery (Mei et al., 2016).

Remyelination follows several crucial steps which have been extensively studied in this last decade (Fig.11). The first question was to isolate the cell population leading to the generation of myelinating OLs. Tripathi et al. examined the fates of PDGFRα/NG2 cells in the mouse spinal cord during experimental autoimmune encephalomyelitis showing that most of these cells differentiate in OLs expressing myelin markers as CNP or Opalin. These results suggest that adult OPCs are the major source of new OLs during remyelination (Gensert and Goldman, 1997; Levine and Reynolds, 1999; Tripathi et al., 2010). On the other hand, several studies have shown that human mature oligodendrocytes transplanted into demyelinated areas of the rat spinal cord survived but were unable to remyelinate (Crawford et al., 2016; Keirstead and Blakemore, 1997; Targett et al., 1996). But, interestingly, others suggested that new myelin sheaths can be generated by existing oligodendrocytes without the need for de novo oligodendrogliogenesis (Duncan et al., 2018; Wood and Bunge, 1991).

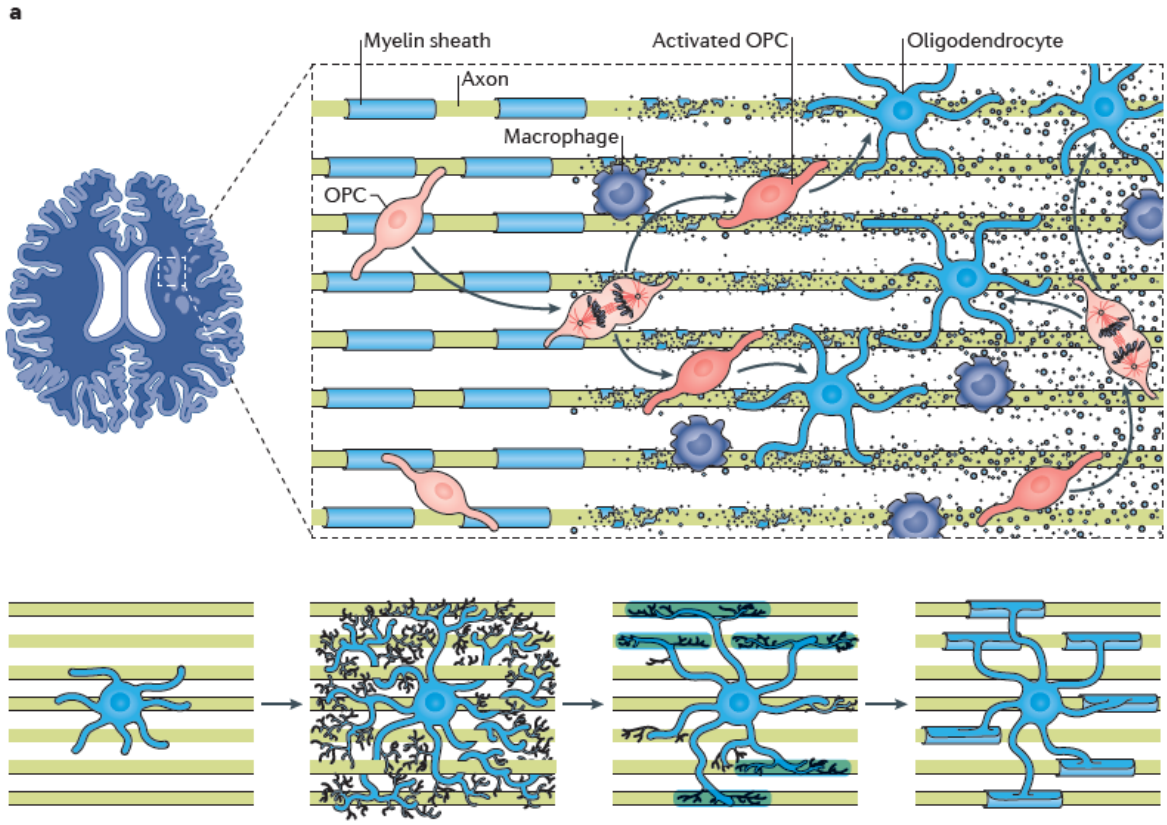

Fig.11/ The biology of remyelination. Following damage to myelinated areas in the CNS, remyelination is initiated by activation of oligodendrocyte progenitor cells (OPCs). These become activated (as represented by the color change), divide, and form new oligodendrocytes. Note the presence of macrophages in the lesion. Following oligodendrocyte differentiation, myelin formation proceeds in three steps, as shown in the sequence illustrated in the lower panel: the formation of multiple processes and the expression of myelin proteins such as myelin basic protein, the initial wrapping of the axon by an elaboration of myelin membrane and, finally, the formation of multilayered and compacted sheaths by the continued elaboration of membrane, further wrapping of the axon and extrusion of the cytoplasm. Adapted from Franklin & French-Constant 2017.

For remyelination to occur, activation (visible by morphological and behavioral changes), proliferation, and migration of OPCs are necessary. The order in which these events occur is still under debate. Some transcription factors (TCF7L2 and SOX2), normally absent in the normal CNS OLs lineage, are detected after myelin injury, permitting enhanced proliferation, and priming for differentiation (Fancy et al., 2009). Next, the importance of migration was underlined by Boyd et al. who showed that some MS lesions lack sufficient OPCs to drive remyelination suggesting a failure in migration (Boyd et al., 2013). Moreover, it was demonstrated in the lab that increasing OPCs recruitment towards demyelinated areas by overexpression of attractive guidance cues (Semaphorin 3F) accelerates remyelination after experimental demyelination (Piaton et al., 2011).

Thirdly, to myelinate denuded axons, OPCs need to differentiate in myelinating OLs. To do so, OPCs must exit the cell cycle (Casaccia-Bonnefil et al., 1997). How OPCs switch from a proliferating to a differentiating stage remains elusive. One hypothesis is based on cell density. When the number of OPCs reaches a certain level, proliferation stops, and differentiation starts (Hughes et al., 2013). Others investigated about potential positive or negative cues. Several studies showed that myelin debris could inhibit OPCs differentiation (Plemel et al., 2013; Robinson and Miller, 1999). Using inhibitors of the retinoid X receptor pathway, it was showed that aging macrophages are less effective to clear myelin debris, leading to inhibition of OPCs differentiation (Natrajan et al., 2015). Glial environment can also promote OPCs differentiation. Thus, it has been shown that activated microglia can secret various cues promoting remyelination (Miron and Franklin, 2014; Psachoulia et al., 2016).

Furthermore, it is now clear from an abundant literature on the subject that other glial cells contribute to this process of myelin repair. A pro-remyelinating environment including cytokines, growth factors, ECM, and adhesion molecules, expressed in an appropriate manner, participates to favor activation, proliferation, migration, and differentiation of OPCs (Franklin, 2002). In this context, Miron et al. (Miron et al., 2013) showed that macrophage switch to M2 phenotype drives OPCs differentiation. Preventing this switch could thus prevent efficient repair. Moreover, El Behi et al. showed, comparing remyelination after grafting lymphocytes from healthy donors or from MS patients in spinal cord demyelinated lesions that lymphocytes derived cytokines help OPCs differentiation through microglia modulation (El Behi et al., 2017). Others showed the role of neuronal activity on repair. Electrically active demyelinated axons can form new glutamatergic synapses with OPCs present within areas of demyelination. Through sensing axonal activity via AMPA and kainate receptors, OPCs can exit the cell cycle

and undergo differentiation (Etxeberria et al., 2010; Gautier et al., 2015). More recently, Ortiz et al. using optogenetic experiments reported an increase of OPC differentiation and extensive remyelination after activation of demyelinated axons (Ortiz et al., 2019).

Regarding astrocytes, there are also evidence that they can help to clear debris (Skripuletz et al., 2013). They are abundant in glial scar in inactive lesions. Whether it brings more damage or inhibits repair is still under debate (Pekny et al., 2014). For example, it has been suggested that reactive astrocytosis is also common in the normal appearing white matter (NAWM) (Zeis et al., 2008). On the other hand, studies using ethidium bromide demyelination confirmed the need for these cells in remyelination, as elimination of astrocytes resulted in remyelination only by Schwann cells, unless transplanted astrocytes were reintroduced (Franklin et al., 1991). Furthermore, it has been showed that perinodal astrocytes can regulate myelin structure (thickness and gap length) and could thus contribute to adaptative (re)myelination (Dutta et al., 2018).

ii. Remyelination in MS

After the demyelinating insult, endogenous remyelination can also occur spontaneously in MS (Prineas and Connell, 1979). Classically, remyelinated areas are known in MS as “shadow plaques”. Shadow plaques are fully remyelinated lesions in MS brains (Fig.12). They are called “shadow” because of the pale staining compared to normally myelinated areas. It is related to the thinner myelin sheaths and shorter myelin internodes typical of newly formed myelin in remyelinated areas. Thus, shadow plaques demonstrate that complete repair of MS plaques is possible, although it is more common to observe only limited repair at the edge of lesions. Furthermore, the location of a lesion influences the likelihood of remyelination, with subcortical lesions showing more signs of remyelination than periventricular or cerebellar lesions (Goldschmidt et al., 2009).

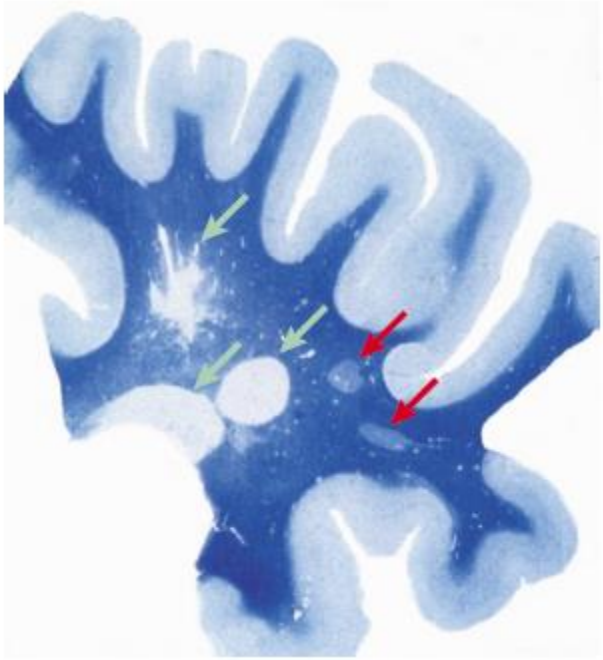

Fig.12/ Lesions in MS. Section of the forebrain of a multiple sclerosis patient.

The section is stained with Luxol Fast Blue to reveal myelinated areas in the subcortical white matter. The green arrows indicate three areas from which the myelin staining is absent, representing three foci or plaques of chronic demyelination. The red arrows indicate 'shadow plaques', in which the demyelinated axons have undergone remyelination. Adapted from Franklin 2002.

Even if we know that this process is partial and becomes rarer with age and disease duration, it has been suggested that remyelination in MS may be more extensive than previously thought. One detailed neuropathological study of two MS cases showed that nearly 50% of white matter analyzed was remyelinated (or remyelinating). Increased density of macrophages and microglia at the lesion border correlated significantly with more extensive remyelination. (Patani et al., 2007). In another study, in 20% of the patients, the extent of remyelination was extensive with 60–96% of the global lesion area remyelinated (Patrikios et al., 2006). Subgroups of MS patients with either extensive or limited remyelination were identified, suggesting that in addition, genetic factors may influence the ability of lesions to remyelinate. Moreover, it has been suggested that remyelinated areas could be difficult to distinguish from intact white matter (Neumann et al., 2020) implying that remyelination might be underestimated in MS brains. Moreover, a PET-MRI study using a myelin marker ([11C]PIB) showed a great variability of myelin content changes between patients, that might indicate inter-individual myelination capacity. This PET study also demonstrated that dynamic remyelination was inversely

correlated with clinical disability (Bodini et al., 2016). El behi et al., using the lymphocytes graft paradigm described above, confirmed diverse remyelination patterns depending on these different patients (El Behi et al., 2017).

It has, however, been suggested that remyelination is a transient phenomenon and that remyelinated shadow plaques may become affected by new bouts of demyelination (Prineas et al., 1993). Bramow et al. observed that remyelinated areas were more vulnerable than the normal-appearing white matter to new demyelination, including active demyelination in secondary progressive multiple sclerosis. Recurrent slowly expanding demyelination, affecting remyelinated areas, and the load of slowly expanding demyelination correlated with incomplete remyelination (Bramow et al., 2010). Moreover, using lesion segmentation from MTR images, an MRI study showed the occurrence of second round of inflammatory demyelination in pre-existing lesions (Brown et al., 2014; Campbell et al., 2012).

It has further been shown that failure in OPCs recruitment and differentiation increased with age (Shields et al., 1999; Sim et al., 2002; Wolswijk, 1998). Indeed, it has been suggested that repetitive rounds of demyelination/remyelination could alter remyelination processes (Prineas et al., 1993). Lucchinetti at al. showed that 30% of lesions in MS lack sufficient OPCs for remyelination, whereas in the other 70%, sufficient OPCs are present but remyelination fails at the later stages of differentiation and/or myelin sheath formation (Lucchinetti et al., 1999) corroborating what is known from experimental models.

Taken together, these results suggest that promoting remyelination is a promising therapeutic goal to prevent axonal degeneration and associated handicap burden. Finding the factors leading to a failure of remyelination or why some patients remyelinate better than others are thus key questions in the MS research field.

d) Nodes of Ranvier in demyelination and remyelination

i. Nodes of Ranvier fate during demyelination

In EAE, a disruption of nodes of Ranvier with loss of Nav nodal clusters has been reported in both the optic nerves (Craner et al., 2003) and the spinal cord (Craner et al., 2004a). The loss of nodal clusters is associated with a diffuse expression of Nav channels along demyelinated axons. Similar disruption of Nav nodal clusters were reported in the corpus callosum following cuprizone-induced demyelination, or after focal lysophosphatidylcholine (LPC) demyelination (Pfeiffer et al., 2019).

Alterations of Nav localization in experimental demyelination models are associated with changes in Nav isoform expression. Nav1.6, the mature isoform of Nav expressed at nodes in the adult normal CNS, is reduced after demyelination, whereas Nav1.2, which is normally restricted to immature nodes and unmyelinated fibers, is detected in various models (Craner et al., 2003, 2004a; Pfeiffer et al., 2019; Rasband et al., 2003).

The few neuropathological studies that addressed the fate of nodal structures in post-mortem CNS tissue from patients with MS demonstrated that nodes of Ranvier on white matter demyelinated axons were profoundly altered or disrupted and a diffuse redistribution of Nav channels was detected along denuded axons (Fig.13) (Coman et al., 2006).

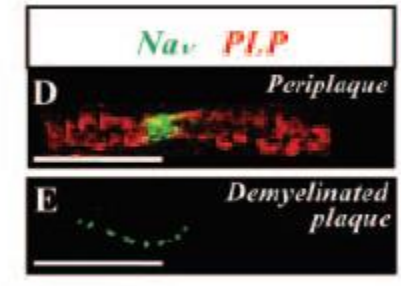

Fig.13/ Nav channels in demyelinated plaques.
Nav channels form dense nodal clusters in the periplaque (D), whereas diffuse immunoreactivity is detected in the demyelinated plaque (E). Adapted from Coman et al. 2006.

ii. Nodes of Ranvier assembly in remyelination

Our team has previously shown that nodal proteins can recluster prior to redeposition of myelin in remyelinating lesions suggesting that it could be an early event in repair (Fig.14) (Coman et al., 2006).

Newly formed internodes are shorter than existing internodes (Young et al., 2013). Of note, the average internode length decreases with normal aging (Lasiene et al., 2009) which might suggest that even without demyelinating disease, remyelination takes place throughout life. These changes could have profound effects on the proper function of the neural circuit, as the efficiency of impulse conduction is a function of internode length (Brill et al., 1977).

Moreover, long-term imaging of myelin remodeling after myelin ablation in zebrafish has shown that new sheaths are positioned almost exactly where the ablated ones were located, indicating that node-like clusters could serve as landmarks for myelin positioning in regenerating sheaths (Auer et al., 2018).

Smith et al. observed in 1982 new loci of inward membrane current as early as 4 days after LPC injection, i.e. 3 days before the onset of remyelination suggesting that saltatory conduction precedes remyelination in axons demyelinated with LPC (Smith et al., 1982). They made the hypothesis of precursors of nodes of Ranvier with aggregates of sodium channels which form along the demyelinated axolemma prior to remyelination, a hypothesis which is in line with the prenodal clusters detected in MS tissue by Coman et al (see above).

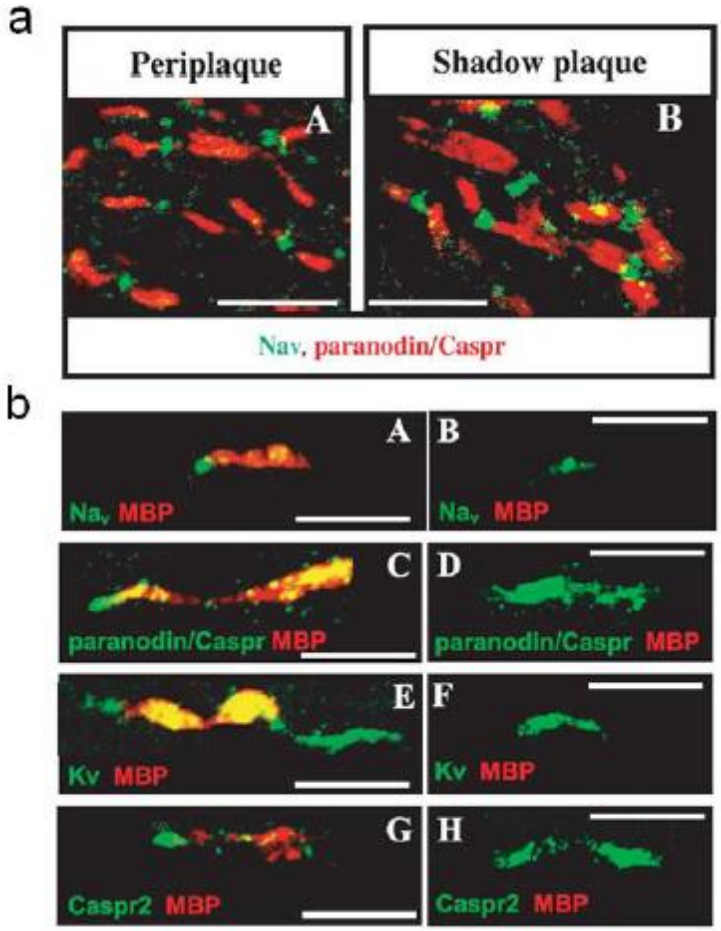

Fig.14/ Nodal and perinodal proteins aggregation during remyelination in MS tissue
(a) Nodal (Nav, green) and paranodal (Caspr1, red) aggregation is similar in periplaques and shadow plaques (remyelinated). Scale bar, 10µm. (b) Immunostainings of nodal and perinodal proteins (Nav, Caspr1, Kv, Caspr2) in partially remyelinated plaques. Whereas aggregates were detected on some denuded MBP-negative fibres (B, D, F, H), MBP-positive myelin sheaths were always associated with nodal and perinodal clusters (A, C, E, G). Scale bar: 10 mm. Adapted from Coman et al., 2006.

This seminal study has been confirmed recently by our team which showed nodal-like clusters before remyelination in an *ex vivo* model of murine cerebellar slices (Fig.15) (Lubetzki et al., 2020).

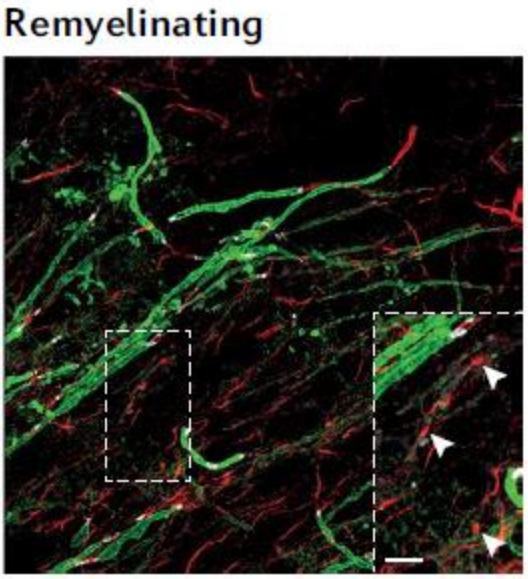

Fig.15/ Node-like structures in remyelination.

Node-like structures in red are indicated by arrowheads in the inset. Scale bar 20 nm in main figure and 5 nm in inset. Adapted from Lubetzki et al. 2020.

iii. Consequence of Nodes of Ranvier alterations on neuronal physiology

In the pathological state, nodal disruption drastically affects axonal function and integrity by participating to conduction failure (Faivre-Sarrailh and Devaux, 2013). It has also been suggested by us and others that nodal or paranodal alterations could be an early event during demyelinating events. As an example, Howell et al. showed that a significant early alteration in Nfasc155+ paranodal structures occurs within and adjacent to actively demyelinating white matter lesions before axonal disruption (Howell et al., 2006). These alterations were associated with damaged axons. They confirm this result showing an association between microglial activation and axon/oligodendrocyte pathology at nodal and paranodal domains in NAWM of MS cases and in EAE. The extent of paranodal axoglial (neurofascin-155+/Caspr+) disruption correlated with local microglial inflammation and axonal injury in MS NAWM. These changes were independent of demyelinating lesions and did not correlate with the density of infiltrating lymphocytes (Howell et al., 2006). Disruption of the axoglial was reversible and coincided with the resolution of microglial inflammation. Paranodal damage and microglial inflammation persisted in chronic EAE. Axoglial integrity could be preserved by the administration of minocycline, which inhibited microglial activation (Howell et al., 2010).

Moreover, Nav channels redistributed along the axon might act as a double-edged sword, participating in an adaptive response to injury on one hand and contributing to neurodegeneration on the other. Craner et al. showed that the redistributed Nav1.6 isoform, which produce a persistent sodium current, could be a key driver of neurodegeneration owing to the accumulation of intra-axonal sodium and a subsequent calcium overload. By contrast, the re-expression of Nav1.2 was considered less damaging, as this isoform produced a less persistent sodium current than the Nav1.6 channels (Craner et al., 2004b). In addition, supporting these observations, hyperexcitability, ectopic spike generation and failure of action potential propagation at the presynaptic terminals have been recorded in demyelinated fibers (Hamada et al., 2017).

iv. Nodes of Ranvier and glial cells (Fig.16)

Astrocytes processes have been observed to contact the node of Ranvier in a several species such as rabbit or rat (Black and Waxman, 1988; Ffrench-Constant et al., 1986; Sims et al., 1985; Waxman and Black, 1984; Waxman and Swadlow, 1976).

In addition to astrocytes, contacts between NG2 cells and nodes of Ranvier were detected in the cerebellum and in the optic nerve (Butt et al., 1999). It was confirmed in a more recent study where 33-49% of nodes of Ranvier were contacted in the optic nerve, corpus callosum, and spinal cord (Serwanski et al., 2017). In the same work, 95% of nodes were contacted by astrocytes (Serwanski et al., 2017). Using electron microscopy and STED (stimulated emission depletion) super resolution microscopy the authors showed the presence of dual glial insertion at some nodes and further revealed that NG2 cell processes contacted the nodal membrane at discrete points, while astrocytes had broader processes that surrounded the nodes. Such ultrastructural analysis revealed that NG2 cells extend fine finger-like projections that often contact both the nodal axolemma and outermost paranodal myelin loops, while they confirmed that astrocytes extend broader processes covering the entire nodal gap, suggesting different roles of the two glial cell types at the node and different ways to interact with nodes.

Recently, Zhang et al brought ultrastructural evidence of microglial contacts with nodes of Ranvier and myelin in rat corpus callosum (Zhang et al., 2019) (Fig. 16).

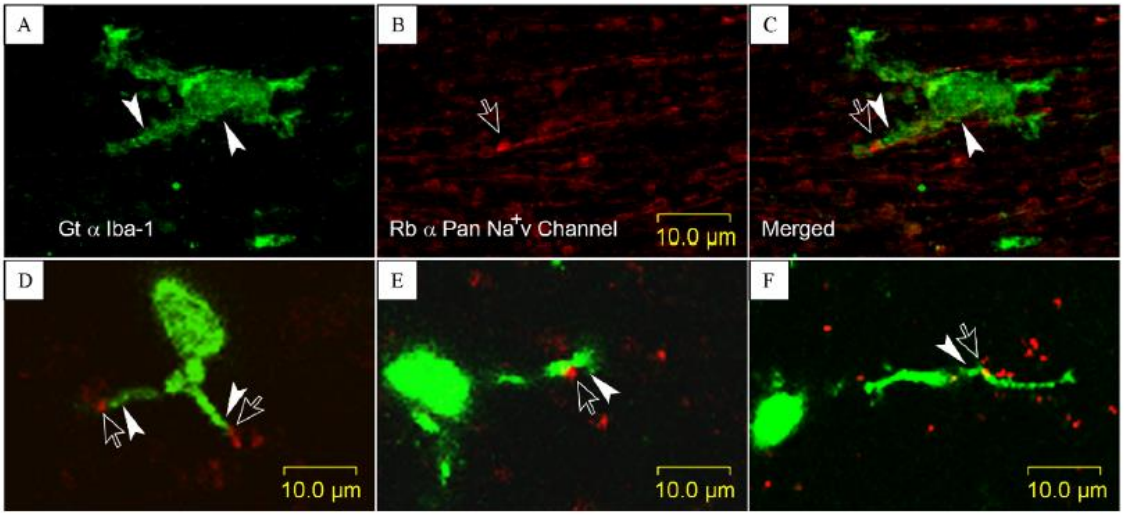

Fig.16/ Direct contacts of microglia processes (green) with nodes of Ranvier (red).
Adapted from Zhang et al. 2019.

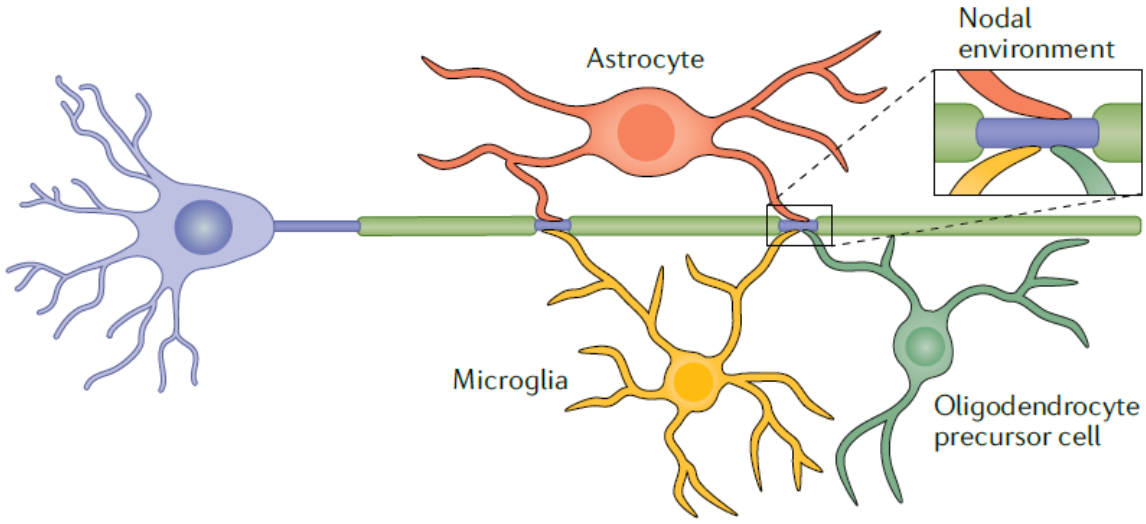

Fig.17/ Neuroglial interactions at the node of Ranvier.
Schematic representation of neuroglial contacts at the node of Ranvier in the CNS. Nodal structures have been shown to be contacted by perinodal astrocytes, oligodendrocyte precursor cells and here, microglial cells. suggesting that the node could act as a 'hub' for neuroglial communication. Adapted from Lubetzki et al. 2020.

III. Microglia: a new major player in MS

a) Description and function of microglial cells

Microglia originate from the yolk sac and populate the CNS during early embryonic development (Ginhoux et al., 2010). They are maintained thereafter throughout life by local proliferation, not from replacement by bone-marrow-derived circulating elements (Ajami et al., 2007). They represent 5-10% of brain cells (Lawson et al., 1990).

Microglia are highly ramified cells that have a multitude of fine, exceptionally motile processes that continuously survey the environment. Through this surveillance, microglia detect diverse extracellular signals, and consequently, translate, integrate, and respond to maintain brain homeostasis (Davalos et al., 2005; Nimmerjahn et al., 2005; Salter and Stevens, 2017). It is estimated that resident microglia scan the entire volume of the brain over the course of a few hours (Nimmerjahn et al., 2005), suggesting that they have homeostatic functions in the healthy brain. Moreover, process motility can change dramatically in response to extracellular stimuli, including neuronal activity and neurotransmitters (Li et al., 2012).

Initially described as the innate immune cells of the brain, many other microglial functions have been established. For example, microglia also guide neural development (Schafer et al., 2012; Ueno et al., 2013), in part by responding to local changes in the brain microenvironment and by interacting with developing neurons. Many of these functional interactions are spatially and temporally controlled and include phagocytosis of apoptotic cells, synaptic pruning (Parkhurst et al., 2013), modulation of neurogenesis (Torres et al., 2016), and regulation of synapse plasticity and myelin formation (Hagemeyer et al., 2017; Wlodarczyk et al., 2017). Very recently, Hammond et al. showed using RNA-sequencing that various subsets of microglia which expressed unique sets of genes exist depending on age, brain localization, and diseases (Hammond et al., 2019). Moreover, Hickman et al., using RNA sequencing, found that microglia have a distinct transcriptomic signature and express a unique cluster of transcripts encoding proteins for sensing endogenous ligands and microbes, for which the name sensome was proposed. (Hickman et al., 2013).

Microglia also play a role in (re)myelination (Bar and Barak, 2019; El Behi et al., 2017; Miron et al., 2013). Early studies using microglia and oligodendrocytes cocultures showed that microglia stimulate the expression of MBP and PLP in oligodendrocytes, suggesting a positive role for microglia in myelination (Hamilton and Rome, 1994). Recently, Wlodarczyk et al

showed that transient CD11c+ microglia subpopulation promotes myelination through IGF-1 (Wlodarczyk et al., 2017). Moreover, injection of IL-4-activated microglia into the cerebrospinal fluid of rodents with EAE resulted in increased oligodendrogenesis in the spinal cord and improved clinical symptoms (Butovsky et al., 2006). The newly formed oligodendrocytes were spatially associated with microglia expressing major histocompatibility complex class II proteins and IGF-1.

b) Classification of microglia phenotypes in health and disease

Thus, microglia display spatial and temporal-dependent identities in the CNS. Microglial heterogeneity is closely related to the environment and cellular interactions that are provided in a time, space, and disease-specific manner (Bogie et al., 2014). To date, none of the described studies have been able to define whether there is one microglial subset specialized in neuronal support and another subset specialized in immune functions. As such, the question as to how microglia shifts between these two functions remains unanswered.

As seen above, microglial cells constantly survey their environment. In case of an insult or modification of the environment, they become “activated”. This term defines any physical or biochemical changes away from the microglial homeostatic state (M0) and include rapid proliferation, migration to the site of pathology, phagocytosis of cells and debris, and production of the cytokines and chemokines necessary to stimulate microglia and other brain and immune cells. Following injury in the developing or adult CNS, microglia activation is the first cellular response, as shown in models of traumatic brain injury, demyelination, inflammation, excitotoxic injury and ischemia–hypoxia. Following injury, microglia proliferate and extend processes to the site of damage, responding to chemoattractant signals released from injured cells (Davalos et al., 2005).

Historically, the M1-M2 paradigm was used to study microglial activation states (Colonna and Butovsky, 2017). M1 refers to pro-inflammatory microglia, while M2 refers to an “alternative” activation state, known to promote repair. M1 cells are obtained *in vitro* after exposition to interferon-γ whereas M2 cells are observed after exposition to IL-4. M2 cells have been later separated between M2a, M2b and M2c, corresponding respectively to alternative, type II alternative and deactivation states. One of the main caveats of such a classification is that microglial milieu *in vitro* is likely to largely differ from the complex environment *in vivo*. Thus,

it is now well known that microglia can adopt a spectrum of phenotypes, surpassing the classical and oversimplified M1-M2 dichotomy (Fig.17) (Mosser and Edwards, 2008).

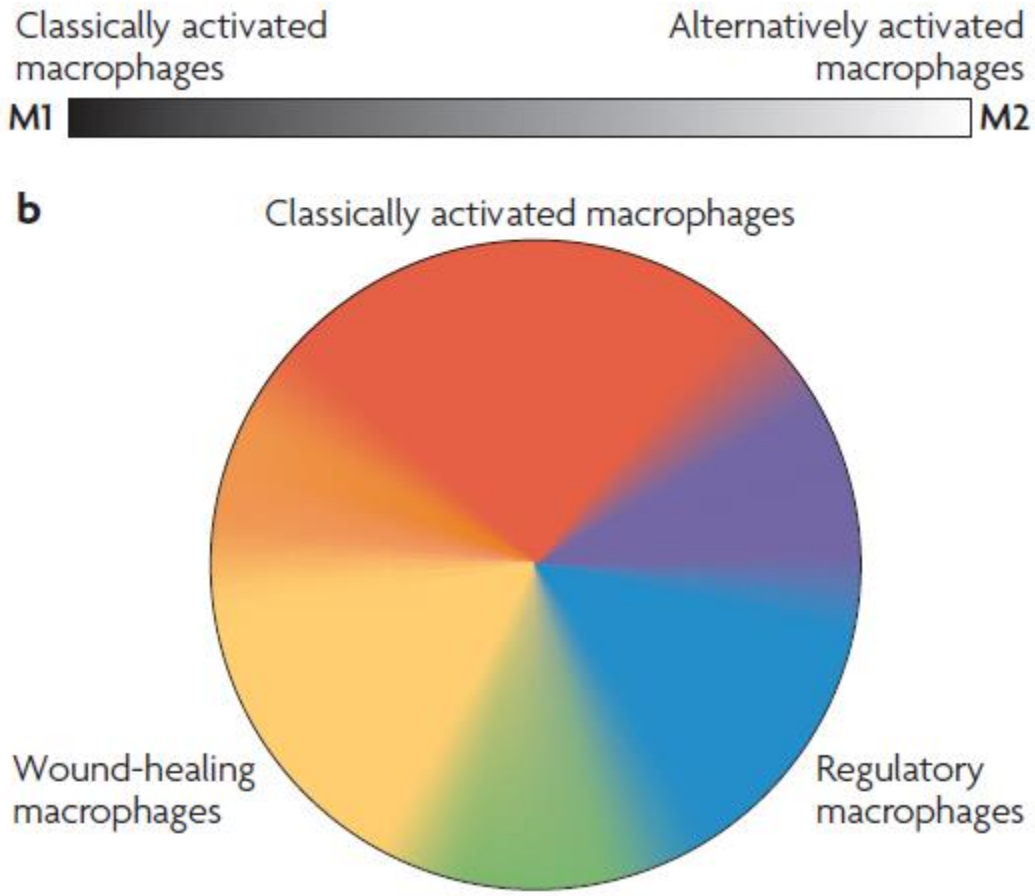

Fig.18/ Full spectrum of macrophage activation
Opposition between the old dichotomy in gray above and a new paradigm below
Adapted from Mosser & Edwards Nat Rev Immunol 2008

Two other major issues had to be addressed in order to decipher roles and mechanisms by which microglia act in the brain: 1/how to distinguish in pathology resident microglia from blood-derived macrophages; 2/how to classify microglia by their multiple phenotypes. Indeed, under specific host conditions, like inflammatory processes within the CNS that lead to the disruption of the blood-brain barrier integrity, peripheral monocytes can migrate into the CNS parenchyma (Mildner et al., 2009). In these circumstances, infiltrated peripheral monocytic cells and activated microglia acquire a similar morphology and share common myeloid marker expression (CD68, Iba1, major histocompatibility complexes class II (MHCII)…). However,

the two myeloid populations may have completely different functions during CNS diseases and therefore a reliable identification system for either cell type is critical to investigate in detail their respective contribution to human CNS diseases.

Recent studies brought tools and markers to answer these questions (Fig.18). First, TMEM 119, a cell-surface protein of unknown function was found to be specific to resident (i.e. derived from the yolk sac) microglia and was not expressed in monocyte-derived (MD) macrophages (Bennett et al., 2016; Butovsky et al., 2014; Satoh et al., 2016). Then, the purinergic receptor P2Y12r, a Gi-coupled receptor for nucleotides like ATP/ADP, was used to identify homeostatic microglia (M0) (Mildner et al., 2017). This microglial marker was shown to be stable over lifespan and absent of perivascular or meningeal macrophages. An example of application of such markers in human pathology has been brought by Zrzavy et al. In MS, they showed that homeostatic microglia stained with P2Y12r antibodies was significantly reduced in NAWM compared to controls and completely lost in active and chronic active lesions (Zrzavy et al., 2017). Early stages of demyelination and neurodegeneration in active lesions contained microglia with a pro-inflammatory phenotype, which expressed molecules involved in phagocytosis (CD68), oxidative injury (iNOS and p22phox), antigen presentation and T cell co-stimulation (CD86). Moreover, on average 43% of Iba1+ cells were TMEM119+ and there was a decreasing gradient of TMEM119+ cells from initial to advanced active lesions. In later stages, the microglia and MD-macrophages in active lesions changed to a phenotype that was intermediate between pro- and anti-inflammatory activation with the expression of pro-repair markers such as CD206 or CD163. In inactive lesions, the density of microglia/MD-macrophages was significantly reduced and microglia in part converted to a P2Y12r+ phenotype, i.e. become homeostatic. These results demonstrate the loss of the homeostatic microglial signature in active multiple sclerosis with restoration associated with disease inactivity.

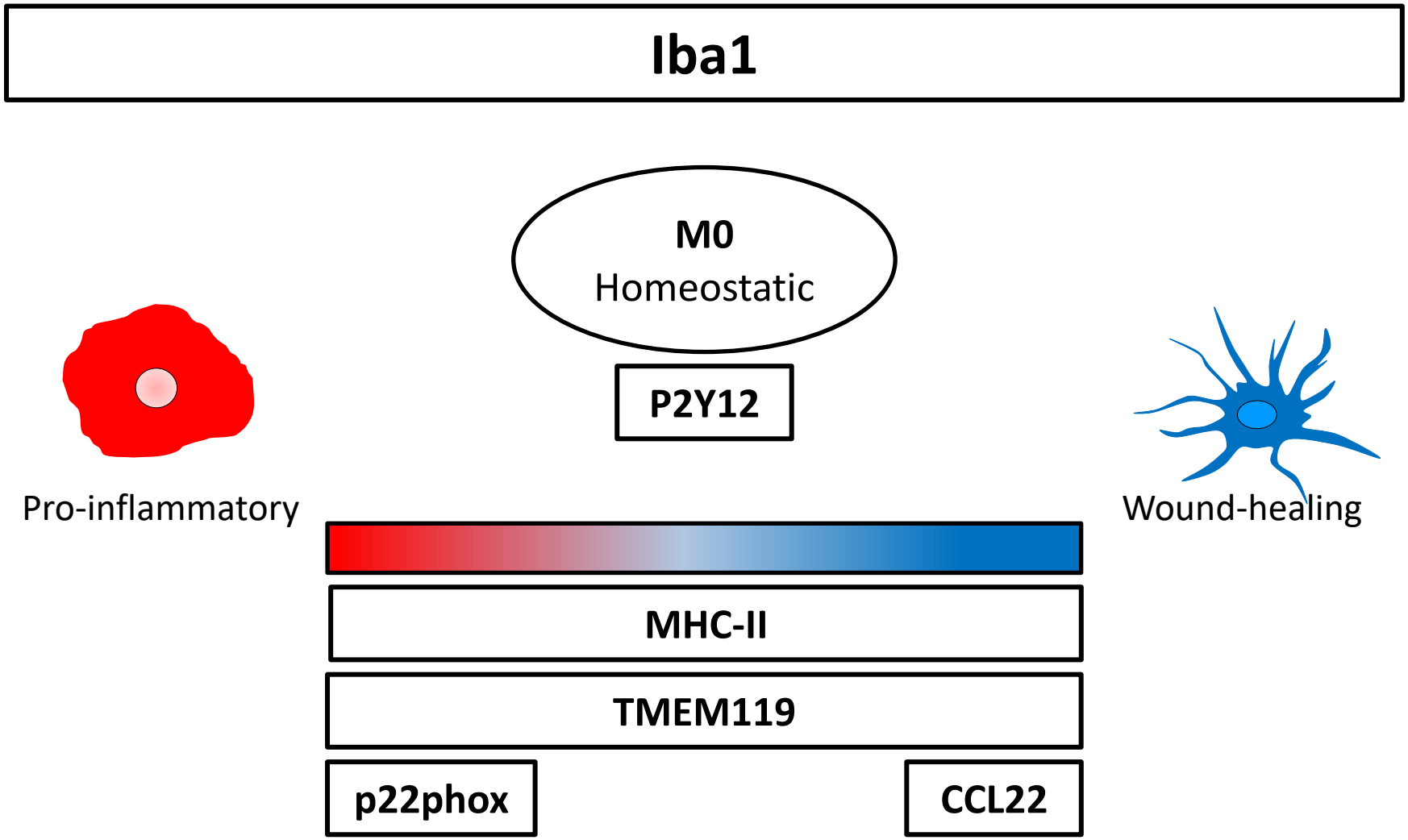

Fig.19/Microglia markers in human tissues

c) A dynamic and social cell

As described before, microglial cells are highly motile cells allowing to interact with all their environment as glial cells for instance. As an example, it has been shown that microglia can contact axonal initial segment (AIS) in healthy conditions. These interactions were lost following brain injury (Baalman et al., 2015). Others showed that AIS were maintained after demyelination but not after inflammation (Clark et al., 2016). AIS disruption was preceded by microglial reactivity and correlated with increased microglia/AIS contact and expression of pro-inflammatory factors. Moreover, pharmacological intervention can prevent and reverse these microglial changes and lead to the protection of AIS integrity. They also showed that microglial-AIS interactions increase with disease progression in both the cuprizone and EAE models and precede myelin loss and AIS disruption.

Other neuronal structures can be contacted. One study showed that microglial processes closely apposed neuronal perikarya and apical dendrites. Upon activation, cortical microglia can migrate to and strip synapses from neuronal area (Trapp et al., 2007). Aside from neuronal synapses, neuronal soma has recently been identified as a site of microglial interaction, relying on purinergic signaling and being possibly involved in microglia-induced neuroprotection (Cserép et al., 2019; Hughes and Appel, 2020).

d) Microglia and Multiple Sclerosis: a dual role.

Initially in MS, microglia were thought to only participate to the inflammatory processes and thus to the demyelinating mechanisms. Later, it was demonstrated that they also play an essential role in repair. In fact, the majority of infiltrating macrophages and activated microglial cells in active lesions in MS display an intermediate activation status. Double staining with anti-CD40 and anti-mannose receptor (MR, an “alternative” state marker) revealed that approximately 70% of the CD40-positive macrophages in MS lesions also expressed MR (Vogel et al., 2013).

The M1 (pro-inflammatory)–M2 (pro-repair) paradigm has been useful to characterize the functional phenotypes of macrophages and microglia in different disorders. However, as said above, recent reports indicate that macrophages and microglia show a remarkable plasticity and can likely adopt a spectrum of polarizations depending on environmental cues. Furthermore, M1-associated inflammatory secreted cues by macrophages, which were

previously considered as stimulating neuroinflammation and neurodegeneration, can also stimulate CNS repair early steps (see below).

Moreover, the complexity of these processes is increased by the fact that resident microglia and blood-derived macrophages could have separate roles. Using serial block-face scanning electron microscopy, researchers showed that monocyte-derived macrophages associate with nodes of Ranvier and initiate demyelination, whereas resident microglia appear to clear debris. Gene expression profiles confirm that monocyte derived macrophages are highly phagocytic and inflammatory, whereas those arising from microglia demonstrate an unexpected signature of globally suppressed cellular metabolism at disease onset (Yamasaki et al., 2014).

i. A role in inflammation

The contribution of microglia to demyelination and inflammation in MS has been extensively studied. Thus, blocking microglial activation represses the experimental MS model EAE (Heppner et al., 2005). This is in agreement with the fact that microglia participates early in the pathological process (Ponomarev et al., 2005). The mechanisms by which microglia play its inflammatory role are multiple. One of them is the secretion of various cues as nitric oxide or TNF-α which participate in disruption of the blood-brain barrier, oligodendrocyte injury and demyelination, and axonal degeneration (Bitsch et al., 2000; Smith and Lassmann, 2002).

Microglia also seem to be linked to disease progression in MS. Positron emission tomography (PET) studies in relapsing and progressive MS using the mitochondrial translocator protein TSPO, which is up-regulated in activated microglia, demonstrated that microglial activation is a significant predictor of disability in progressive MS (Airas et al., 2018). NAWM as well as periplaque white matter (PPWM) displays diffuse, sometimes quite extensive microglial activation. This is especially a feature of tissue samples from patients with a long disease duration and a progressive disease course (Zrzavy et al., 2017).

Microglia clusters are also the hallmark of the so-called “preactive” lesions in MS among NAWM. They were first observed using post-mortem MRI-guided sampling of NAWM in a number of patients with progressive MS where microglial clusters were detected in close

vicinity to microvessels surrounded by lymphocytic infiltrates (De Groot et al., 2001; van der Valk and Amor, 2009).

ii. Microglial role in repair

On the other hand, accumulating evidence for their need in repair was established. For example, researchers demonstrate that macrophage depletion impairs remyelination following lysolecithin-induced demyelination (Kotter et al., 2001). In order to examine the role of MD-macrophages in CNS remyelination, adult rats were depleted of monocytes using clodronate liposomes and demyelination induced in the spinal cord white matter using lysolecithin (Kotter et al., 2005). In situ hybridization for MBP revealed a delayed remyelination in liposome-treated animals. Macrophage reduction corresponded with delayed recruitment of PDGFRa+ OPCs, which preceded changes in myelin phagocytosis, indicating a macrophage effect on OPCs, which is independent of myelin debris clearance. In EAE, inhibition of microglia activation results in a delayed onset of EAE symptoms, but also exhibit an increased disease severity and delayed recovery from neurological dysfunction (Lu et al., 2002). Furthermore, stimulation of microglia activation before and at disease onset dampens EAE severity and promotes timely recovery from neurological deficits (Bhasin et al., 2007).

Otherwise, microglia can promote CNS repair in animal models by clearance of inhibitory myelin debris (Fig.19). The latter has been shown to interfere with recruitment and differentiation of OPCs (Neumann et al., 2009; Robinson and Miller, 1999), thus highlighting myelin debris clearance as an essential step in remyelination. Furthermore, the ability of microglia/macrophages to phagocytose myelin debris decreases with age, and this decrease is associated with a reduction in remyelination efficiency (Ruckh et al., 2012). Thus, myelin debris clearance is key for remyelination and neuroprotection (Lampron et al., 2015).

Microglia can also produce pro-regenerative factors such as activin A and insulin-like growth factor 1 (Miron et al., 2013). Oligodendrocyte differentiation was enhanced *in vitro* with M2 cell conditioned media and impaired *in vivo* following intra-lesional M2 cell depletion. Blocking M2 cell–derived activin-A inhibited oligodendrocyte differentiation

during remyelination in cerebellar slice cultures. Microglia might also promote OPC proliferation (Giera et al., 2018).

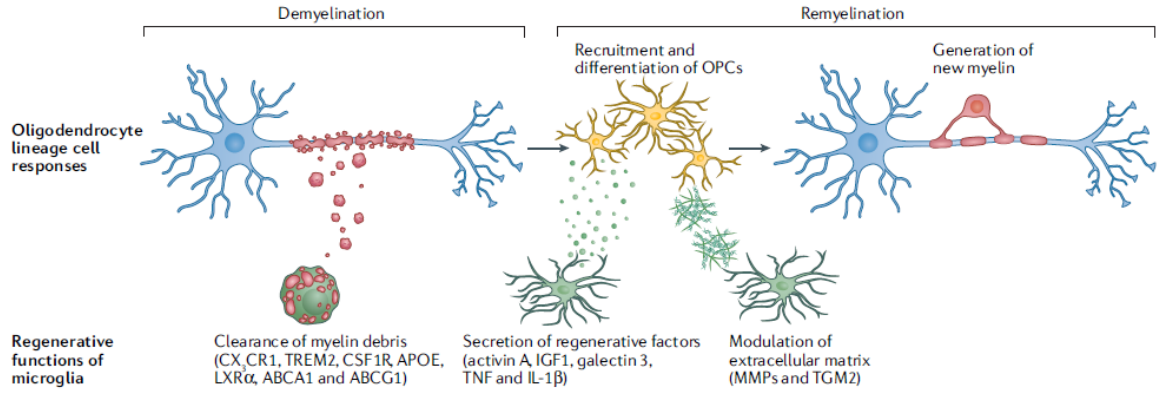

Fig.20/ Pro-remyelination functions of microglia. Microglia drive remyelination by facilitating OPC recruitment and differentiation into oligodendrocytes, which generate new myelin. Adapted from Lloyd and Miron 2019.

In post-mortem tissue of multiple sclerosis, active lesions with ongoing remyelination have relatively higher numbers of M2 macrophages than chronic lesions which do not remyelinate. Authors demonstrated a switch from M1 to M2 microglia during remyelination (Miron et al., 2013). Very recently, two teams proposed two different mechanisms. Lloyd Nat Neuro 2019 showed a death of pro-inflammatory microglia before repopulation with a pro-regenerative population during white matter remyelination being positively regulated by type-1 IFN signaling (Lloyd et al., 2019). Locatelli et al. in contrast reported a M1 to M2 switch during lesion evolution, with the hypothesis that this switch contributes to repair, without death of pro-inflammatory microglia (Locatelli et al., 2018). But Lloyd et al. looked at microglia whereas locatelli et al. focused on phagocytes originated from the periphery, which could explain the two opposite observed mechanisms and underlines that resident microglia and peripheral macrophages probably do not have the same role during repair.

Moreover, in addition to its role in demyelination, the pro-inflammatory microglia might also play a role in remyelination. Inhibition of macrophage activation or density by minocycline or toxin-encapsulated liposome administration respectively was associated with reduced remyelination (Kotter et al., 2001; Li et al., 2005; Miron et al., 2013). Foote et al. showed that inflammation stimulates remyelination in areas of chronic demyelination (Foote and Blakemore, 2005). In addition, remyelination is impaired in transgenic animals lacking inflammatory cytokines such as TNF-α and IL-1h, MHCII, or T-cells (Arnett et al., 2001;

Bieber et al., 2003; Mason et al., 2001). A very recent study (Cunha et al., 2020) showed that the pro-inflammatory response depends on myeloid differentiation primary response 88 (MyD88). MyD88- deficient mice and zebrafish were not only impaired in the degradation of myelin debris, but also in initiating the generation of new oligodendrocytes for myelin repair. They identified reduced generation of TNF-α in lesions of MyD88-deficient animals, a pro-inflammatory molecule that was able to induce the generation of new pre-myelinating oligodendrocytes thus showing that pro-inflammatory phagocytic signaling is required for initiating the generation of new oligodendrocytes.

Thus, microglia is a key player in repair. Despite its participation in inflammatory processes during demyelination, microglial cells are necessary, not only to clear myelin debris, but also participate, in connection with axons and other glial cells, to repair.

Aims of the dissertation

My thesis project aimed at deciphering the interactions between microglia and nodes of Ranvier, in particular in repair.

A previous study in our lab showed that Nav clusters can be identified without any myelin apposition in remyelinating areas suggesting that nodal protein clustering could be an early event in remyelination (Coman et al., 2006). Moreover, nodes of Ranvier have been identified as a putative preferential target in CNS inflammatory diseases (Nikić et al., 2011; Oluich et al., 2012). As shown in introduction, the role of microglia in repair has been extensively studied (Franklin and ffrench-Constant, 2017), but the mechanisms involved are still poorly understood. Recently, Baalman et al. showed an interaction between microglia and AIS, which share a similar molecular composition with nodes of Ranvier (Baalman et al., 2015). Others showed interaction between neuronal soma and microglia (Cserép et al., 2019). Moreover, interactions between other glial cells and nodes of Ranvier have been identified (Lubetzki et al., 2020; Serwanski et al., 2017).

The first part of my work aimed at analyzing interactions between microglia and nodes of Ranvier in experimental models. We identified stable microglia-nodes contacts and showed that these contacts were reinforced during remyelination. We then observed a correlation between neuronal activity and the percentage of nodes contacted by microglia, suggesting that microglia might sense neuronal physiology/health through these interactions. We then demonstrated a role of K+ fluxes in mediating this effect. We also showed that these microglia-nodes contacts are involved in repair capacity, by demonstrating that their inhibition correlates with a reduction of the microglial switch towards a pro-repair state and with a decreased remyelination rate.

The second part of my thesis, which corresponds to work in progress, aims at characterizing node-microglia interactions in human control and MS tissues. We know that no experimental models can reproduce exactly what is happening in MS. Thus, we asked whether this interaction exists in human control and MS tissues and its frequency. We then searched to decipher microglia phenotypes according to lesion types and how they correlate with nodal interaction. We thus studied whether different microglia subtypes could interact with nodes of Ranvier and in which environment.

RESULTS

ARTICLE

Microglia, the resident immune cells of the CNS, play a major role in brain homeostasis and repair. They are known to participate in myelin repair in Multiple Sclerosis (Franklin and ffrench-Constant, 2017), but the exact mechanisms of microglial crosstalk with surrounding cells are still poorly understood. In particular, the mechanisms underlying microglia-neuron communication in the white matter remain largely unknown. Recently, Baalman et al. showed an interaction between microglia and axon initial segment, which share a similar molecular composition with nodes of Ranvier (Baalman et al., 2015). Moreover, interactions between other glial cells and nodes of Ranvier have been identified (Lubetzki et al., 2020; Serwanski et al., 2017).

Here, we identify nodes of Ranvier as a direct and stable site of interaction between microglia and axons, in both mouse and human tissue. Moreover, microglial contacts co-exist on a given node with contacts from astrocytes and OPCs processes, establishing the node as a privileged site for axons to interact with their glial environment. Using dynamic imaging, we further highlight the preferential interaction of microglial processes with nodes of Ranvier along myelinated fibers, showing that microglial process contacting nodes of Ranvier have reduced dynamics compared to processes moving freely or contacting internodal areas. We further showed that microglia-node interaction increased during remyelination and is modulated by neuronal activity and associated potassium release, with THIK-1 ensuring their microglial read-out. Disrupting axonal K+ flux following demyelination correlates with microglial pro-inflammatory polarization and decreased remyelination rate.

Taken together, these findings identify the node of Ranvier as a major site for microglia-neuron communication, participating in the pro-remyelinating effect of microglia after myelin injury.

Microglia-neuron communication at nodes of Ranvier depends on neuronal activity through potassium release and contributes to myelin repair.

(Short title: Microglial interaction at nodes of Ranvier in health and repair)

Ronzano R. 1#, Roux T.1,2#, Thetiot M.1, Aigrot M.S.1, Richard L.3, Lejeune F.X.1, Mazuir E.1, Vallat J.M.3, Lubetzki C.1,2#, Desmazières A.1#*

[1]Paris Brain Institute, ICM, Sorbonne University, Inserm U1127, CNRS UMR 7225, Pitié-Salpêtrière hospital, Paris, France.
[2]Assistance Publique des Hôpitaux de Paris (APHP), Neurology Department, Pitié-Salpêtrière hospital, Paris, France.
[3]Centre de Référence National des Neuropathies Périphériques Rares et Département de Neurologie, Hopital Universitaire, Limoges, France
[#]These authors contributed equally to this work
*Corresponding author : Anne Desmazieres; anne.desmazieres@icm-institute.org

Abstract

Microglia, the resident immune cells of the central nervous system, are key players in healthy brain homeostasis and plasticity. In neurological diseases, such as Multiple Sclerosis, activated microglia either promote tissue damage or favor neuroprotection and myelin regeneration. The mechanisms for microglia-neuron communication remain largely unkown. Here, we identify nodes of Ranvier as a direct and stable site of interaction between microglia and axons, in both mouse and human tissue. Using dynamic imaging, we highlight the preferential interaction of microglial processes with nodes of Ranvier along myelinated fibers. We show that microglia-node interaction is modulated by neuronal activity and associated potassium release, with THIK-1 ensuring their microglial read-out. Disrupting axonal K+ flux following demyelination polarizes microglia towards a pro-inflammatory phenotype and decreases remyelination rate. Taken together, these findings identify the node of Ranvier as a major site for microglia-neuron communication, participating in the pro-remyelinating effect of microglia after myelin injury.

Introduction

Microglial cells are the resident immune cells of the central nervous system (CNS), where they represent 5-10% of the cells [1]. This is a heterogeneous population, which participate in normal brain development, homeostasis, and maintenance of neuronal function, as well as learning and memory, by modulating neurogenesis, neuronal survival, wiring and synaptic plasticity [2–4].

In the healthy brain, microglia dynamically survey their environment with their motile processes, as well as with nanoscale sensing filopodia [5–7]. Process motility is modulated by ATP, chemokines, neurotransmitters, extracellular potassium concentration [5,8–10], among other cues, and integrated through microglia receptors, in particular the purinergic P2Y12 receptor, the fractalkine receptor CX3CR1 and the recently identified two-pore domain potassium channel THIK-1 [10–12].

Microglia are activated in most neurological pathologies, including neurodegenerative diseases, epilepsy, autism, psychiatric disorders and stroke [2,4]. In multiple sclerosis (MS), a CNS inflammatory, demyelinating and neurodegenerative disease, activated microglia can contribute to neuronal loss, but they are also important to favor myelin regeneration, in particular through removal of myelin and neuron debris [13–16]. Remyelination depends on the phenotype of activated microglial cells, with a polarization from M1 (pro-inflammatory) to alternatively activated M2 (pro-regenerative) microglia, though this vision of a M1/M2 polarization is clearly oversimplified [17–20]. The pro-inflammatory signature is observed early following injury and is associated with deleterious microglial activity if maintained inappropriately [14,21,22]. However, cells with a pro-inflammatory signature also stimulate proliferation and recruitment of oligodendrocyte precursors cells (OPCs) towards the lesion, whereas pro-regenerative microglial cells promote OPCs differentiation into myelinating oligodendrocytes [14–16,22]. These experimental data are consistent with results showing an enrichment in pro-regenerative microglia in remyelinating lesions [14–16].

It is established that microglia sense neuron activity and can modulate neuron function or detect early neuronal damage [9,11,23–29]. Aside from neuronal synapses, neuronal soma has recently been identified as a site of microglial interaction, relying on purinergic signaling and possibly involved in microglia-induced neuroprotection [11,28,29]. Axon initial segment (AIS) has also been identified as a site of microglia-neuron contact, with description of microglial processes overlapping AIS in healthy brain, which vary following brain injury and inflammation [30,31].

Along myelinated fibers, the nodes of Ranvier are short unmyelinated domains allowing action potential regeneration and propagation. Astrocytic processes have been described to contact nodes of Ranvier, with a role in nodal length modulation and in ionic buffering. OPCs processes also contact nodes, although the prevalence of these contacts as well as their physiological role remain elusive [32]. Direct contacts of microglia on myelin sheaths and nodes of Ranvier have recently been observed in rat corpus callosum [33]. We therefore tested, in control and demyelinated CNS, the hypothesis that nodes of Ranvier might be a preferential site for axon-microglia communication.

Here we identify nodes of Ranvier as a site for microglia-neuron communication, in mouse and human CNS, suggesting they could play the role of a "neuro-glial communication hub". We show that microglia-node interactions are modulated by neuronal activity and potassium ion release and provide evidence of their influence in microglia-dependent remyelination capacity after experimental demyelination.

RESULTS

Microglia contact nodes of Ranvier in vivo in mouse and human tissues

The nodes of Ranvier, short unmyelinated axonal domains, allow direct access to the axonal surface of myelinated axons. We thus addressed whether microglia can contact axons at the nodes of Ranvier.

By performing immunostainings and 3D reconstruction on adult mouse fixed tissue, we first observed that microglia (Iba1+ cells) contact nodes of Ranvier (AnkyrinG+ structures surrounded by paranodal Caspr+ staining) in CNS grey (cortex and cerebellum, Figure 1Aa-b) as well as white matter (corpus callosum and cortico-spinal tract, Figure 1Ac-d), thus confirming and extending a previous observation in rat corpus callosum [33]. The vast majority of microglial cells contact multiple nodes, through cell soma or processes (at the tip or "en-passant"), with the preferential area of contact being along the node and extending to the junction of the node and the paranode (Figure 1A). This was confirmed by an electron microscopy study following immunostaining with Iba1 antibody, to visualize microglial processes. Longitudinal views of nodes delineated by the paranodal loops on both sides and contacted by microglial processes show that these processes directly contact the nodal axolemma (Figure 1B) and that the microglial process sometimes extends towards the first paranodal loops (Figure 1Bb, b').

Knowing that nodes can also be contacted by astrocytes and OPCs, we next addressed whether a single node could be contacted by multiple glial cell types. We performed co-stainings in adult mouse spinal cord tissue for microglia (Iba1) and astrocytes (GFAP, Figure 1C) or OPCs (PDGFRα, Figure 1D). Our results, showing that a single node can be contacted simultaneously by multiple glial processes, suggest that the node of Ranvier could be a neuro-glial "hub".

Microglia-node contacts were further detected in human post-mortem hemispheric white matter of healthy donors (Figure 2), as shown using a specific marker for resident microglia (TMEM119, Figure 2A-B) and a marker of homeostatic microglia (P2Y12R, Figure 2C).

Microglia-node of Ranvier contacts are stable and their frequency increases during remyelination

To assess the extent of microglia-neuron contacts at nodes, we first quantified the percentage of nodal structures contacted by microglial cells in adult mouse dorsal spinal cord. As shown in Figure 3B and E, 26.3 ± 3.7% of nodes are contacted by microglia. To assess whether these contacts correspond to microglial cell random scanning of the local environment or to a directed and/or controlled interaction, we then quantified the stability of the contacts, using *in vivo* live-imaging of mouse dorsal spinal cord (Figure 3H) [34] from CX3CR1GFP/+/Thy1-Nfasc186mCherry double-transgenic mice allowing to detect both microglia (GFP) and nodes of Ranvier (Nfasc186mCherry). We detected that both microglial processes and soma are motile over long periods of time. However, when selecting nodes initially contacted by microglia (Figure 3I, Figure S1A-C and Movies 1-4), we observed that microglia-node contacts were maintained along the vast majority of 1 hour movies, as well as 3 hour movies (Figure 3J-K and Figure S1D-E respectively). This suggests that microglia-node contact is a regulated interaction rather than a random scanning.

We then used the same methods to assess microglia-node interaction following a demyelinating insult (focal demyelination induced by lysophosphatidylcholine, LPC, Figure 3A). As nodes are deeply disrupted by demyelination [35], we excluded demyelinated areas and instead analyzed the perilesional area (i.e., the periphery of a demyelinated lesion, where nodal structures are preserved despite paranodal abnormalities; 7 DPI). Remyelinating lesions (11 DPI) and

corresponding Shams, injected with LPC carrier (NaCl 9‰) were also analyzed (Figure 3C-G and Figure S1).

We found that the frequency of interaction (i.e. the percentage of nodes contacted by microglia) was unchanged in the perilesional area (perilesional: 37.6 ± 2.7% vs sham: 31.8 ± 4.0%; Figure 3C-E). In contrast, the stability of the interaction was significantly decreased in perilesional tissue at the peak of demyelination (one-hour movies, 88.4 ± 3.1% of timepoints with contact) compared to control and 7 DPI Sham (98.9 ± 1.1% and 100±0.0% respectively, Figure 3J). Similar results were obtained with the longest sequence of consecutive timepoints with contact, with a reduction of 25% of contact stability (Figure 3K). In contrast, the frequency of interaction was significantly increased during remyelination (60.9 ± 1.9% of nodes of Ranvier contacted; Figure 3E and G) compared to control and 11DPI Sham (18.2 ± 1.6%; Figure 3E and F), with a stability similar to controls (Figures 3J-K and S1; Movies 2-4). These findings were corroborated in the three-hour acquisition's studies (Figure S1D-E).

The increased frequency of interaction upon remyelination suggests that microglia-node communication might play a role in the repair process, whereas decreased stability in the perilesional area (where demyelination is not yet detected) might be an early event preceding demyelination.

Microglial processes interact preferentially with the nodes of Ranvier compared to the internodes

To study microglia-node interaction with an increased temporal and spatial resolution, we used the organotypic culture of mouse cerebellar slice model, which present a preserved cytoarchitecure and is highly accessible for live-imaging and pharmacological treatments [36,37].

We first showed, using CX3CR1GFP/+ cerebellar fixed tissue, that microglia also contact nodes of Ranvier during developmental myelination, both *in vivo* and *ex vivo* (Figure S2A and S2B, respectively). In myelinating tissue *ex vivo*, the percentage of nodal structures contacted is similar to adult myelinated tissue (21.8 ± 3.4%, Figure S2C), with no significant bias towards mature nodes of Ranvier or immature nodal structures (node-like clusters and heminodes, Figure S2D). In fully myelinated slices (Figure S2E), the percentage of nodes of Ranvier contacted by microglia is similar to *in vivo* results (23.9 ± 4.0%, Figure S2G). Following LPC treatment, and in agreement with our *in vivo* observations, the percentage of nodal structures contacted in remyelinating slices (Figure S2F) is increased compared to control condition (46.0 ± 3.2%, Figure S2G), without any bias towards mature or immature structures (Figure S2H).

Having established the similarity of *ex vivo* and *in vivo* models for the analysis of microglia-node interaction, we then used CX3CR1GFP/+ cerebellar slices transduced to express β1NaVmCherry (nodal structures, in red) along Purkinje cell axons (10-min movies; Figure S3A-B and Movies 5-7) to gain deeper insight into the dynamics of microglia processes at nodes. We first compared microglial process tip dynamics when contacting an internodal or a nodal area along the axon in myelinated slices (Figure 4A, Control, Movies 5 and 6, respectively). The rate of microglial process contact is significantly increased at nodes compared to internodes (81 ± 8% of time frames per movie with contact at nodes, vs 52 ± 5% at internodes, Figure 4B) as well as the maximum number of consecutive timeframes with contact (14.0 ± 2.2 frames at nodes vs 8.2 ± 1.1 frames at internodes, Figure 4C). Similarly, the number of consecutive timeframes without contact is increased at internodes (8.5 ± 1.2 frames vs 3.9 ± 1.6 frames at nodes, Figure S3C). Regarding microglial contacts at nodes, these parameters are similar in remyelinating slices (rem) compared to control slices (Figure 4A, 4F-G, Movie 7 and Figure S3E).

Microglial process behavior is modified at the nodes of Ranvier

To further assess how microglial process motility and behavior could be modified at the vicinity of a node, we further analyzed the trajectory of process tips with nodal contact or without contact (wo contact) at imaging onset (Figure 4D-E). The total length of the trajectory was unchanged along 10 min (wo contact 28.1 ± 4.0 µm vs nodal contact 26.1 ± 4.4 µm, Figure 4D), as well as the mean instantaneous velocity (wo contact: 2.6 ± 0.4 µm/min vs nodal contact: 2.2 ± 0.4 µm, Figure 4E). However, the microglial process tip remained in the direct vicinity of the node contacted compared to non-contacting tips, which frequently move away from their initial position (mean distance from origin, wo contact: 3.06± 0.4 µm vs nodal contact: 1.77 ± 0.4 µm, Figures 4D and S3D).

In remyelinating slices, the mean distance from origin was also reduced for processes contacting nodes (wo contact: 2.88 ± 0.7 µm and with nodal contact: 1.20 ± 0.5 µm, Figure 4H and S3F). Interestingly, the mean velocity was in that case significantly decreased by a half for process tips contacting a node compared to non-contacting ones (wo contact: 2.1 ± 0.3 µm/min vs node: 1.2 ± 0.3 µm/min, Figure 4I). Hence, the total length of the trajectory covered in 10 min was decreased when contacting a node (wo contact: 24.9 ± 3.7 µm vs node 15.8 ± 4.2 µm).

Taken together, these data suggest the existence of (an) underlying mechanism(s) attracting and/or stabilizing microglia at nodes of Ranvier, an interaction which is strengthened in the remyelinating context. We thus questioned which signal(s) could be regulating this interaction.

CX3CR1, P2Y12 and P2Y13 are not required for microglia-node interactions in physiological condition

Various signaling pathways mediating neuron-microglia crosstalk have been uncovered in physiological and pathological contexts [38]. Among them, we first focused on CX3CR1 pathway, taking advantage of the fact that CX3CR1-GFP mouse strain corresponds to a knock-in of GFP into the CX3CR1 gene locus, leading to a loss of function of this gene in homozygous mice. By comparing CX3CR1GFP/GFP with CX3CR1GFP/+ littermates in myelinated cultured slices, we found no significant difference in the percentage of nodes contacted (25.1 ± 2.5% vs 20.8 ± 2.6% respectively, Figure S4A-B).

The microglial P2Y12 purinergic receptor has also been involved in multiple microglia-neuron interactions. In order to address whether this pathway was required for microglia-node contact, we first inhibited the P2Y12R receptor specifically using PSB0739 (1 µM), a highly potent P2Y12 antagonist, and found that it is not required for microglia-node interaction (15.1 ± 1.2% of nodes contacted in control vs 15.5 ± 1.7% following treatment, Figure S4C-D). To further assess the potential role of the P2Y receptor family and exclude any compensatory mechanisms, we also inhibited P2Y13R, which participates in microglia dynamics control 39, concomitantly to P2Y12R by using the MRS2211 inhibitor (50 µM). Again, there was no significant variation in the number of nodes contacted in control vs treated slices (15.1 ± 1.5% vs 14.3 ± 1.3% respectively, Figure S4E-F), confirming that P2Y12R and P2Y13R are not required for microglia-node interactions in physiological condition.

Neuronal electrical activity modulates microglia-node interaction

As reciprocal interactions between electrically active neurons and microglia have been established, we then addressed whether changes in neuronal activity might impact microglia-node contacts. Purkinje cells are spontaneously active in organotypic cerebellar slices, as

assessed by loose-cell attached recordings (n=13 cells from 9 animals, Figure S5A). To modulate neuronal activity, we used two pharmacological agents, Apamin (Apa, 500 nM) and Tetrodotoxin (TTX, 500 nM). Apamin is a blocker of SK2 channels, which leads to a specific increase of Purkinje cells firing in the cerebellum [40], while TTX is a well described blocker of action potential generation through voltage-gated sodium channel inhibition [41]. Apamin treatment lead to a 60% increase of Purkinje cell firing instantaneous frequency (Ctrl: 16.09 ± 3,47 Hz; Apamin: 26.12 ± 7,14 Hz, Figure S5B-C), whereas TTX completely blocked their activity (Figure S5A-B). Following 1h TTX treatment of myelinated slices, microglia-node contacts were significantly decreased by 20% (21.3 ± 2.4% nodes contacted in control vs 16.9 ± 2.0% in treated slices, Figure 5A-C), while a 1h Apamin treatment on myelinated slices significantly increased by 20% the percentage of nodes contacted (16.9 ± 1.7% nodes contacted in control vs 20.4 ± 1.2% in treated slices, Figure 5D-F).

Taken together, these data demonstrate that microglial contacts at nodes are modulated by neuronal activity, adding further insight into the role of microglia as a neuronal activity sensor.

Microglia-node interaction is modulated by potassium release at nodes

Recent works suggest that microglia dynamics can be modulated by extracellular potassium concentration. To assess the potential involvement of nodal potassium flux in microglia-node interaction we first treated myelinated cultured slices with the large spectrum inhibitor of potassium channels tetraethylammonium (TEA, 30 mM) for 1h (Figure 6A). This resulted in a 40% decrease of microglia-node interaction, with 11.4 ± 1.1% of the nodes contacted in the treated slices, compared to 18.8 ± 1.1% in control condition (Figure 6B-C). High concentration of TEA is expected to decrease Purkinje cells activity, which would lead to reduced interaction. We thus compared the normalized effects of TEA and TTX and observed that the reduction of microglia-node interaction is more pronounced after TEA treatment than after TTX treatment

(40% and 20% decrease respectively), suggesting that the outward potassium current existing at axonal resting potential may also participate in modulating microglia-node interaction.

We then addressed how TEA impacts the dynamics of microglial process in myelinated slices, by comparing processes contacting a node or an internode (Figure 6D-I). Contrary to the preferential interaction of microglial processes at nodes found in untreated slice cultures (Figure 4), in the TEA treated slices, the dynamics of contact was similar between processes with internodal or nodal contact (49.7 ± 4.9 % of timeframes with contact at internodes vs 55.2 ± 9.3 % at nodes, Figure 6E) and consecutive number of timeframes with contact was comparable (internode: 8.5 ± 0.9 frames; node: 10.0 ± 1.8 frames; Figure 6F). Similarly, in myelinated slices treated with TEA, the process trajectory and velocity are not significantly different for processes with and without nodal contacts (Figure 6G-I).

To confirm the role of K+ flux in microglia-node interaction, we treated myelinated cultured slices for 1 hour with tetrapentylammonium (TPA, 50 µM), a blocker of THIK-1, a two-pore domain channel recently identified as the main K+ channel expressed in microglia (Figure 6J). We observed a significant 36% decrease of microglia-node interaction, with 10.8 ± 1.2% of the nodes contacted in the treated slices, compared to 17.1 ± 1.4% in control condition (Figure 6K-L), an effect which amplitude is similar to the effect of TEA treatment.

Taken together, these results confirm that microglial preferential interaction with nodes of Ranvier depends on potassium level within the nodal area, with a key role of microglial THIK-1 K+ channel.

Alteration of microglia-node interaction by K+ channels inhibitors polarizes microglia towards a pro-inflammatory phenotype and reduces remyelination

Having confirmed that node-microglia communication also depends on K+ flux in remyelination (Figure 7A-C), we next addressed whether altering microglia-node interaction at remyelination onset could affect the repair process in LPC-demyelinated cultured cerebellar slices. To address this question, we thus treated cerebellar slices with either TEA or TPA at the onset of remyelination and studied whether this could affect the microglial switch from pro-inflammatory towards pro-regenerative phenotype, by quantifying the percentage of microglial cells expressing the pro-inflammatory marker iNOS (Figure 7D-E, TEA and Figure 7H-I, TPA). We observed a significant 21% increase in iNOS+ population following TEA treatment (ctrl: 57.2 ± 0.90% ; TEA: 69.5 ± 1.7%; Figure 7E), and a significant 26% increase following TPA treatment (ctrl: 60.0 ± 1.02%; TPA: 75.9 ± 2.2%; Figure 7I). Microglia-node K+ signaling dysregulation at onset of remyelination thus results in increased pro-inflammatory microglia.

We next quantified the rate of remyelination of Purkinje axons in demyelinated slices treated with TEA or TPA, compared to untreated slices (Figure7F-G and J-K). We observed a significant 24% decrease of the remyelination rate following TEA treatment (ctrl: 47.7 ± 2.6%; TEA: 36.4 ± 2.5%; Figure 7G), and a significant 23% decrease following TPA treatment (ctrl: 37.5 ± 2.7% ; TPA: 28.9 ± 1.7%; Figure 7K).

Taken together these data demonstrate that nodal K+ modulates the remyelination process, by promoting the pro-regenerative phenotype of microglia after myelin injury. This effect is associated and likely mediated by changes in microglia-node of Ranvier interaction.

Discussion

Here we show that microglia establish direct contacts at nodes of Ranvier both in mouse and human tissue. These microglial contacts co-exist on a given node with contacts from astrocytes and OPCs processes, establishing the node as a privileged site for axons to interact with their glial environment. Using *in vivo* and *ex vivo* mouse models, we show that this interaction is stable in healthy tissue but also during remyelination, with an increased percentage of nodes contacted in this latter situation. In addition, we provide evidence that microglial process contacting nodes of Ranvier have reduced dynamics compared to processes moving freely or contacting internodal areas, reinforcing the hypothesis of a specific interaction rather than a random "surveilling" contact between microglia and nodes of Ranvier. This preferential interaction at the nodes of Ranvier depends on neuron activity and potassium ion release. When altering this interaction during remyelination by disrupting nodal K+ flux or blocking microglial K+ channels, microglial cells acquire a more pro-inflammatory phenotype, which associates with reduced remyelination (model Figure 8).

Microglial contact at nodes is stable and depends on neuronal activity and physiological status of the tissue

We show that nodes of Ranvier are specific sites for neuron-microglia interaction, this interaction likely corresponding to microglial sensing of neuronal activity, mediated through specific signaling. We first observed that the majority of microglial cells interact with nodes of Ranvier, regardless of the CNS area considered, with about a fifth to a fourth of the nodes contacted in healthy condition in spinal cord and cerebellar mouse tissue. The increased rate of contact in remyelinating condition could be linked to neuronal transient hyperactivity [43], but it might also be related to the reduced density of nodes detected in remyelinating tissue. Whether frequency of nodal contacts depends on the neuronal subtype or activity pattern is unknown.

Using live-imaging we were able to demonstrate for the first time the stability of these microglia-nodes contacts, strongly arguing for a specific interaction rather than a random survey of the local environment by microglial processes. Whether the reduced interaction stability in perilesional tissue relates to altered axonal physiology or increased local inflammatory signals, remains uncertain.

When addressing the mechanisms supporting these microglia-nodes interactions, we demonstrate that neuronal activity and nodal efflux of potassium are playing a key role, by showing that pharmacological inhibition of nodal and perinodal potassium channels leads to a 40% decrease of the contact, and that blocking THIK-1, the main microglial potassium channel linked with K+ homeostasis [10] reproduces this effect. Various potassium channels have been suggested to be at play at the node, depending on the neuronal subtype considered, with Kca3.1 being present at nodes of Ranvier in Purkinje cells [44] and TRAAK and TREK channels recently described as playing a major role at PNS nodes, and in several CNS areas, such as the cortex, hippocampus and spinal cord [45,46]. Thus, the microglia-node interaction may be modulated through axonal potassium efflux mediated by various players depending of the neuron considered, with the microglial THIK-1 channel allowing the read-out of this signal.

The node of Ranvier: a neuron-glia communication hub?

It has previously been described that OPCs and perinodal astrocytes contact nodes of Ranvier [32], and that these cells might interact at a given node [47]. We now show that microglia can also form multipartite contacts with these other glial cell types, which suggests that nodes of Ranvier may act as a hub of intercellular communication in the CNS. This is further supported by our 3D reconstruction data showing that microglia establish a physical contact both with the nodal constituents and the other contacting glial cell.

This nodal "communication hub" could in particular participate in transmitting information on neuronal function and neuronal health to the glial environment and glia could in return modulate neuronal physiology. Oligodendroglial lineage cells have been shown to sense neuronal activity, which modulates their proliferation, differentiation and the myelination process [41,48,49]. Furthermore, electrophysiological paired recordings show that OPCs adjacent to neurons can sense their discharge, and extracellular stimulation induces slow K+ currents in OPCs, showing they could sense K+ variations linked with activity [50]. This suggests that both OPCs and microglia could have a read-out of neuronal activity at nodes through similar signaling pathways. Nodal protein clusters could further guide myelination initiation along some axons both in development and repair [51,52].

In addition to this node-OPCs dialog, astrocyte-node interaction has been implicated in buffering K+ at the node [53], but also recently in the regulation of axonal conduction velocity, by modulating nodal gap length and myelin thickness. This later effect relies on the secretion of Serpine2 [54], a thrombin inhibitor also expressed by microglial cells in mice [19,55]. This neuron crosstalk with multiple glial cells at node could be of importance for network synchronization and adaptive plasticity in healthy condition, as well as adequate repair in disease [49].

Microglia-node of Ranvier interaction in disease: damaging or protective?

Activated microglia are known to have a dual role in disease, with a deleterious impact in case their pro-inflammatory phenotype is maintained inappropriately, and an active role in repair, in particular when they acquire a pro-regenerative phenotype [14,21]. Activated microglia have been observed in normal appearing white matter (NAWM) in MS tissue and MS models, together with nodal area alteration [56–58]. In addition, some nodes of Ranvier are contacted by macrophages even prior demyelination and it has been hypothesized that they might be an early site of axonal damage [57]. It appears however that the cells actively attacking nodal domains are

rather monocyte derived macrophages than microglial cells [59]. Our observation that microglial-node contact is destabilized in perilesional area at the peak of demyelination is compatible with this observation.

An increased microglia-node interaction might favor remyelination

In both our *in vivo* and *ex vivo* models, we report that microglia contact nodal structures, including heminodes and node-like clusters at the onset of remyelination. Strikingly, as observed in our *ex vivo* model, the microglial cell processes at nodes are less motile during ongoing remyelination compared to control myelinated tissue. This reinforced attraction/stability could be linked to increased potassium release at the sites where nodal structures reagregate or to increased microglial sensitivity to this K+ signal in a remyelinating condition. Indeed, this pathway and other(s) could synergize, such as P2Y12R, which is known to potentiate THIK-1 [10].

Nodes of Ranvier disruption and reassembly following demyelination have a major impact on neuronal physiology. In addition, several lines of evidence have shown that neuronal activity affects the (re)myelination process [41,60,61]. Early nodal reclustering along axons might lead to restored saltatory-like (or "microsaltatory") axonal conduction [32] and generate a local increase of K+ efflux. This local modulation might trigger microglial behavior changes and participate in the regulation of microglial activation state by neuronal activity [62,63], including the pro-inflammatory to pro-repair switch observed concomitantly to the onset of remyelination [14,64,65]. Intracellular K+ decrease has been associated with microglial inflammasome expression [10,66]. The axonal K+ locally released at nodal structures when they reassemble could thus contribute to modulate microglial K+ flux and subsequently limit inflammasome expression in the microglial cells with nodal contacts. Conversely, the restoration of stable microglial contacts at

nodal structures could allow for microglia to buffer reassembled nodal area and modulate activity at nodes, as neurons may be transiently hyperexcitable at onset of remyelination [43,67].

To address the functional role of microglia-node interaction in repair, we took advantage of the modulation of the microglia-node interaction by potassium flux. We first inhibited potassium efflux at onset of remyelination and further targeted THIK-1, the main channel implicated in microglial K+ conductance [10]. Interestingly, THIK-1 channel is expressed in microglial cells in the CNS in healthy as well as MS tissues [55,68]. These different pharmacological approaches promote a more pro-inflammatory profile of microglial cells, associated with decreased remyelination. This suggests that neuron dialog with microglia through K+ signaling might favor myelin regeneration.

This hypothesis is further supported by our observation that, in remyelinating mouse dorsal spinal cord lesion following LPC-induced focal demyelination, microglia contacting nodal structures have a more pro-regenerative phenotype, with a 31% increase of IGF1+ pro-regenerative cells and a 35% decrease of iNOS+ pro-inflammatory cells in node-contacting microglial population compared to the non-contacting cells (data not shown). Microglia contact at nodal structures could allow for a read-out of the neuron physiological status and orientate microglial phenotype, which in turn could modulate neuronal survival and remyelination. This reciprocal interaction might be of importance in different pathological contexts in the CNS.

Recent data suggest that the impact of neuronal activity on OPCs recruited at the lesion follows a two-step mechanism, with consecutive time windows, first facilitating proliferation of OPCs, then promoting OLs differentiation and myelination [43,60,61,69]. This parallels the biphasic activation of microglial cells following demyelination, with a switch from the pro-inflammatory to the pro-regenerative state, with recently published data suggesting that both stages are required for optimal repair [14,16,65]. Our results show that the recovery of a stable microglia-node

interaction at onset of remyelination could influence the microglial phenotypic switch and contribute to accumulation of pro-regenerative microglia. Neuronal activity could then play a role in remyelination both through direct OL lineage regulation and indirectly though modulating microglial phenotypic orientation.

The preferential interaction of the main glial cell types at nodes of Ranvier forming a "neuro-glial communication hub" may thus contribute to efficient repair orchestration.

Methods

Animal care and use

The care and use of mice conformed to institutional policies and guidelines (UPMC, INSERM, French and European Community Council Directive 86/609/EEC). The following mouse strains were used: C57bl6/J (Janvier Labs), CX3CR1-GFP (gift from Prof S. Jung, Weizmann Institute of Science, Israel; 70) and Thy1-Nfasc186mCherry (gift from Prof P.J. Brophy, University of Edinburgh, UK).

Focal demyelination of mouse spinal cord

Following intraperitoneal injection of Ketamin/Xylazin in NaCl 9‰ (respectively 110/25 mg/kg, Centravet), a small incision was made between thoracic and lumbar vertebrae to access the spine and inject with a glass capillary 1µl of lysophosphatidylcholin diluted into NaCl 9‰ (LPC, 10mg/ml; Sigma-Aldrich) or NaCl 9‰ for the sham condition. Following surgery, mice were stitched and placed into warming chambers (Vet tech solution LTD, HE011). At either 7-day post-injection (7dpi, peak of demyelination) or 10-11 dpi (early remyelination phase), the mice were euthanized with Euthasol (Centravet) and transcardially perfused with 2% PFA (Electron Microscopy Services).

Spinal glass window surgery

Surgery protocol was adapted from Fenrich et al., 2012. Briefly, following an intraperitoneal injection of Ketamin/Xylazin as described above, the dorsal skin and muscles were incised, and the spine immobilized with two spinal forks placed at T12 and L2 vertebrae, with Tronothane 1% (Lisa-Pharm) applied at the point of junction with the forks. Two staples were then fixed along the transverse processes of the vertebrae as a support for a reshaped paperclip, stabilized with glue (Cyanolite) and dental cement (Unifast Trad 250 mg/250mg, GC Dental Products Corp). A dorsal laminectomy was performed using a high-speed drill with a carbide bur. Spinal cord was then hydrated with a solution PBS/penicillin-streptomycin/Naquadem (Dexaméthasone 0.05%, Intervet) and LPC (or NaCl) was injected as described above. A glass window cut from a glass coverslip (Menzel-Glaser, 0.13-0.16 mm) was cleaned, dried and placed above silicon (Kwik-Sil, World Precision Instruments) directly applied on the spinal cord. The window was fixed with glue and dental cement. Finally, the animal received a subcutaneous injection of Buprenorphine (0.1 mg/kg, Centravet) and was placed in the warming chamber.

Cerebellum organotypic slice culture

Ex vivo culture protocol was adapted from [36,37]. Briefly, P8 to P10 mouse cerebella were dissected in ice cold Gey's balanced salt solution complemented with 4.5 mg/ml D-Glucose and penicillin-streptomycin (100 IU/mL, Thermo Fisher Scientific). They were cut into 250µm parasagittal slices using a McIlwain tissue chopper and the slices placed on Millicell membrane (3-4 slices per membrane, 2 membranes per animal, 0.4 µm Millicell, Merck Millipore) in 50% BME (Thermo Fisher Scientific), 25% Earle's Balanced Salt Solution (Sigma), 25% heat-inactivated horse serum (Thermo Fisher Scientific), supplemented with GlutaMax (2 mM,

Thermo Fisher Scientific), penicillin-streptomycin (100 IU/mL, Thermo Fisher Scientific) and D-Glucose (4.5 mg/ml; Sigma). Cultures were maintained at 37°C under 5% CO2 and medium changed every two to three days. Experiments were analyzed at 4 days in vitro (DIV) for myelinating condition and at 10 to 11 DIV for control and remyelinating conditions.

Lentiviral transduction of cerebellar slices

For live-imaging *ex vivo*, nodes of Ranvier were detected using β1NavmCherry expressed under the control of the Synapsin promoter. Briefly, the pEntr-β1NavmCherry plasmid was recombined with the pDestSynAS (generated by Philippe Ravassard, ICM), using the Gateway LR clonase kit from Thermo Fisher Scientific 37; detailed description on demand) and the corresponding lentivirus produced by the ICM vectorology plateform. Transduction was performed immediately following slice generation by addition of the lentiviral solution directly onto the slices placed on Milicell membranes (1 µl/slice at a final concentration of 10^9 VP/µl).

***Ex vivo* treatments**

As culture systems may lead to increased variability between animals, we always cultured the slices from a given animal on two membranes. One of these membranes was treated, while the second one was kept untreated. This allowed us to minimize the potential variability and to do paired experiments.

To induce demyelination, for each animal, the slices on one membrane were incubated overnight at 6 DIV in 0.5 mg/ml LPC added to fresh culture medium, while the other membrane was kept as control.

To study microglia-node interaction in myelinated tissue, for each animal, the myelinated slices (10-11 DIV) on one membrane were left untreated (control), while the ones on the other membrane were treated with tetrodotoxin (TTX, 1 hour, 500 nM, Tocris) or apamin (1 hour,

500 nM, Sigma-Aldrich), to inhibit or activate neuronal activity respectively. Similarly, PSB0739 (4 hours, 1 µM, Tocris) or MRS2211 (4 hours, 50 µM, Tocris) were used to inhibit the microglial purinergic receptors P2Y12R and P2Y12R/P2Y13R respectively. Tetraethylammonium (TEA, 1 hour, 30 mM, Sigma) was used to inhibit potassium channels and tetrapentylammonium (TPA, 1 hour, 50 µM, Sigma) to inhibit the microglial THIK-1 channel. To study microglia-node interaction in remyelination, for each animal, the two membranes were demyelinated using LPC, and one of the demyelinated membranes was treated at 10-11 DIV with TEA (1h, 30 mM) or TPA (1 hour, 50 □M), while the other membrane was kept untreated as control.

To evaluate the functional impact of the perturbation of microglia-node interaction, demyelinated slices were treated at the very onset of remyelination (9.5 DIV) with 30 mM TEA or 50 µM TPA for 2 hours and fixed 2h or 15 h post-treatment (together with untreated demyelinated slices as control), to evaluate microglial phenotype and remyelination rate, respectively.

Antibodies

Primary antibodies: mouse IgG2a anti-AnkyrinG (clone N106/36; 1:100), mouse IgG2b anti-AnkyrinG (clone N106/65; 1:75) and mouse IgG1 anti-Caspr (1:100), all from Neuromab; mouse IgG1 anti-Pan Nav (clone K58/35; 1:150; Sigma); mouse anti-Calbindin (1:500; Sigma), rabbit anti-Calbindin (1:500; Swant), rabbit anti-Caspr (1:300; Abcam), rat anti-PLP (1:10; kindly provided by Dr. K. Ikenaka, Okasaki, Japan), mouse IgG2b anti-MBP (1:200; SMI99, Millipore), rabbit IgG anti-Iba1 (1:500; Wako), chicken anti-GFAP (1:500; Aves Labs), rat anti-PDGFrα (1:100; BD Biosciences), rabbit IgG anti-TMEM119 (1:100; Sigma), rabbit IgG anti-P2Y12r (1:300; Alomone), chicken anti-GFP (1:250; Millipore), mouse IgG2a anti-iNOS (1:100; BD Biosciences). Secondary antibodies corresponded to goat or donkey anti-chicken,

goat, mouse IgG2a, IgG2b, IgG1, rabbit and rat coupled to Alexa Fluor 488, 594, 647 or 405 from Invitrogen (1:500), or goat anti-mouse IgG1 DyLight from Jackson Immuno Research (1:600).

Live-Imaging

Live-imaging study ex vivo

Prior to imaging, the slices were mounted onto 35 mm glass-bottom dishes (Ibidi, BioValley) and incubated with a phenol-red free medium consisting of : 75% DMEM, 20% 1X HBSS, supplemented with HCO3- (0.075 g/L final), HEPES Buffer (10 mM final), GlutaMax (2 mM final), penicillin-streptomycin (100 IU/mL each), 5% heat-inactivated horse serum, all from Thermo Fischer Scientific, and D-Glucose (4.5 g/L final; Sigma). Imaging was performed using a Yokogawa CSU-X1 M Spinning Disk, on an inverted Leica DMi8 microscope, with a 40X NA 1.30 oil immersion objective, using the 488 nm and 561 nm laser lines and a Hamamatsu Flash 4 LT camera. Images were acquired at 37°C in a temperature-controlled chamber under 5% CO2 using Metamorph software (Molecular Devices), for periods of 10 min with a confocal Z-series stack of 10µm (921x1024 pixels, 177.8x197.7 µm) acquired for both GFP and mCherry every 30 seconds, using a Z-interval of 0.5µm between optical slices.

Longitudinal live imaging study in vivo

At 7 DPI (peak of demyelination) or 11 DPI (early phase of remyelination), the mice were anesthetized as described before and anesthesia was maintained by reinjection of Ketamin/Xylazin (respectively 11/2.5 mg/kg) when needed along the experiment. Imaging was performed in a heated chamber at 34°C using an upright 2-photon microscope Zeiss 710 NLO with a 20X water objective (NA 1,0) and a Coherent Vision II laser. Z-series stack (1024x1024 pixels, 170x170µm) were acquired with a Z-interval of 0.78 µm at an excitation wavelength of

940 nm every 10 or 30 minutes (15 to 20 images per stack). Focal lesions were identified by the visualization of microglial activation and acquisitions were made at lesion direct vicinity (less than 250 µm) at 7 DPI and in the remyelinating area at 11 DPI (nodal structures were selected within the lesion border). We selected nodes initially contacted by microglia for acquisitions and performed 1-hour movies (one stack every 10 minutes) and 3-hour movies (one stack every 30 minutes). Following imaging, the mice at 7 DPI were placed in a warming chamber until awaken and re-imaged at 11 DPI. Post-acquisition image processing was carried out using ImageJ (NIH, Bethesda, Maryland), Zen (Zeiss, 2010). Briefly, images were realigned using StackReg in ImageJ (http://bigwww.epfl.ch/thevenaz/stackreg/). Filter Median (3,0 X and Y) was used in Zen and Substract Background (100 pixels in green) in ImageJ.

Electron microscopy

Mice were transcardially perfused with PB 0.2M, 4% PFA, 0.5% glutaraldehyde (Electron Microscopy Services). Following 30 minutes post-fixation, the cerebellum was embedded in PB (0.2 M), 4% agarose (Sigma). Sagittal sections (50 µm thick) were generated using a VT1200S vibratome (Leica). The sections were then incubated in Ethanol 50% for 30 min, washed in PBS and incubated with anti-Iba1 antibody (1:1000; Wako), in PBS, 3% NGS, 0.05% Triton-X, for 48 hours on a rotating apparatus at room temperature (RT). The tissue was then washed in PBS and incubated for 1 hour in biotinylated anti-rabbit IgG (1:200; Vector Labs, Burlingame, CA, USA), rotating at RT, further washed in PBS and incubated for 1 hour in ABC (Vector Labs) solution, under rotation at RT. Following incubation, sections were washed 20 minutes with PBS and developed by incubating in 0.025% diamino-benzidine (DAB) and 0.002% hydrogen peroxide, in PBS. Sections were then processed for electron microscopy. Briefly, sections were post-fixed in 1% osmium tetroxide for 60 minutes and dehydrated by ethanol and acetone immersion. A flat-embedding procedure was used, after which a semi-thin

section was cut to find the area of interest and then ultrathin (60-80 nm) sections was cut with an ultramicrotome (Leica EM UC7, Wetzlar, Germany). The sections were stained with uranyl acetate and lead citrate to enhance contrast. Sections were examined with a Jeol Flash 1400 transmission electron microscope. Images of Iba1 immunolabeled microglial cells were captured with a Radius Morada digital camera. Once acquired, the brightness and contrast of the images were adjusted and structures of interest were highlighted using Photoshop software (Adobe, version CC).

Analysis

Quantification

For the *ex vivo* fixed slices, using ImageJ software, the brightness and contrast of the images were adjusted and the total number of nodal structures, as well as the number of nodal structures contacted by microglial cells were quantified per field using the middle plan of each Z-series, the rest of the series being used to confirm the nature of the contacted structure and exclude potential granule cell axon initial segment. A contact was defined by at least one positive pixel for the microglial marker juxtaposed to at least one pixel positive for the nodal marker. Three to five images were analyzed per animal with at least four animals per condition and the mean percentage of contacted nodes per condition was calculated by doing the mean of the mean percentage of contact per animal. To analyze the effect of TEA and TPA treatments on remyelination, five images of an entire folium were acquired per condition for each animal (1900x1900 pixels, approximately 550x550 µm). The myelination index was calculated semi-automatically using a custom written script on ImajeJ 71. Briefly, a region of interest including Purkinje cells axon (excluding soma and white matter tracks) was first selected. A mask for axonal area (Calbindin signal) and a mask for myelinated axonal area (PLP signal overlapping with Calbindin signal) were then generated, and the myelination index was calculated from the

quotient of the area of the two respective masks (myelin/axon). Myelinations indexes of the five images were averaged to give the mean myelination index per animal for each condition. The microglial phenotype was further analyzed by calculating the amount of Iba1+ cells expressing iNOS (pro-inflammatory microglia) on the total number of Iba1+ cells (using five images per condition for each animal, 1024x1024 pixels, 290.9x290.9 μm). For each experiment, at least six animals were analyzed, with paired control and treated slices from each animal.

For the *in vivo* fixed tissue study, imageJ software was used to adjust the brightness and contrast of the images and to quantify the total number of nodal structures and the number of structures contacted per field using the middle plan of each Z-series, the rest of the serie being used to confirm the nature or the contacted structure. A contact was defined by at least one positive pixel for the microglial marker juxtaposed to at least one pixel positive for the nodal marker. Three to five images were analyzed per animal with four animals per condition and the mean percentage of contact per condition was calculated by doing the mean of the mean percentage of contact per animal.

Time-lapse imaging analysis

For ex vivo time-lapse acquisitions, the field of interest was defined by selecting a node (i-e β1NavmCherry cluster along an axon) or an internodal area initially contacted by the tip of a microglial process. ImageJ software was used to adjust the brightness and contrast of the images of each movie and ImajeJ stabilizer Plugins was used to realign the different timeframes using the nodes as stationary reference (red channel) and subsequently applying the same corrections to the green channel (microglia, moving). For each timepoint, the contact was defined by at least one positive pixel for the microglial marker juxtaposed to at least one pixel positive for

the nodal marker. The percentage of frames with contact and the maximum number of consecutive frames with and without contact were then calculated.

To analyze the dynamics of microglial process tips initially contacting a node or not, the images were first realigned automatically, and the exact coordinates of the node (or original location of tips without contacts) were measured. For each movie, the microglial process tip contacting the node and of two non-contacting microglial process tips chosen randomly were tracked manually to get their coordinates at each timepoint. For each time point, the t0 coordinates were subtracted from the coordinates of the microglial process tips to get the coordinates relative to their initial position (fixed). Lastly, for each microglial tip independently, the position at t0 was set in Cartesian coordinates at (0, 0). Representation of the trajectories in Rose plots were generated using a custom written R script and the distance between two successive timepoints t_n and t_{n+1} in the Cartesian coordinates were calculated using the following formula:

$$t_{n+1}t_n = \sqrt{(x_{tn+1} - x_{tn})^2 + (y_{tn+1} - y_{tn})^2}$$

For the *in vivo* live-imaging study of the microglia-node contact in dorsal spinal cord, image fields were chosen where we had initially a clear contact between at least one node and one microglial cell. In case of multiple initial contacts between node(s) and microglia on the first timeframe, each microglia-node pair was considered independently. ImageJ software was used to adjust the brightness and contrast of the images for each movie. The Z-series were then used to assess whether the nodal structure(s) were contacted by the microglial cell(s) or not. A contact was defined when at least one pixel positive for a microglial signal was juxtaposed to at least one pixel positive for the nodal signal. Whether the contact was maintained or lost for each microglia-node pair was assessed along each movie and the percentages of timeframes with contact per movie, as well as the longest sequence of consecutive timepoints with contact, were calculated for each microglia-node pair.

Statistical analysis

All statistical analysis and data visualization were performed using Prism (GraphPad, version 7) and R (R Foundation for Statistical Computing, Vienna, Austria, 2005, http://www.r-project.org, version 3.5.2).

For all the experiments, the group size and statistical tests applied are indicated in the text or in the figure legends. Graphs and data are reported as the mean ± SEM. The level of statistical significance was set at $p < 0.05$ for all tests. Asterisk denote statistical significance as follow: *$p < 0.05$, **$p < 0.01$, ***$p < 0.001$, ****$p < 0.0001$, ns. indicates no significance.

For the fixed ex vivo cultured slices, the treated and untreated groups were compared using paired test. Parametric tests (paired Student's t tests) were used when n□6 and the distributions passed the normality test (Shapiro-Wilk test). Otherwise, non-parametric tests were applied (Wilcoxon matched pairs tests).

For ex vivo live-imaging, when measuring the percentage of frames in contact and the maximum consecutive frames with or without contact, Mann-Whitney tests were used.

The study of the dynamics of process tips contacting a nodal structure or without contact, involved repeated measure design. The statistical analysis was thus performed with linear mixed models using lmer function from lme4 package (R software). Significance of the main effect was evaluated with the Anova function using Type II Wald chi-square tests. When necessary, to better match the model assumptions (normality and constant variance of residuals), the data were square root transformed prior to modeling. For data representation, the estimated marginal means and model based standard errors were extracted for each condition using emmeans package (R software).

For the *in vivo* fixed tissue study regarding the percentage of nodes contacted, comparisons involving five conditions in a repeated measure design were conducted with linear mixed models using the lmer function in the lme4 package. Significance of the main effect was

evaluated with the Anova function in the car package in R using Type II Wald chi-square tests. Tukey's post-hoc pairwise comparisons were then performed using the emmeans and pairs functions in the emmeans package.

For the *in vivo* live-imaging studies, as the condition of normal distribution was not fulfilled within the groups, we used nonparametric tests. The differences between the groups were estimated using the nonparametric Kruskal-Wallis test followed by post hoc Dunn's test with further p-value adjustment by the Benjamini-Hochberg false discovery rate method.

Ackowledgments

We thank Prof P.J. Brophy, University of Edinburgh, UK and Prof S. Jung, Tel Aviv, Israel for kindly providing the Thy1-Nfasc186mCherry and the CX3CR1-GFP mouse line and Dr P. Ravassard for the gift of the pTrip-Syn plasmid. We thank Prof G. Rougon and Dr F. Debarbieux, INT, France, for the *in vivo* spinal cord window technique, and Dr Roberta Magliozzi, University of Verona, Italy, for the immunohistostaining technique on human post-mortem tissue. We thank Dr B. Zalc, Dr N. Sol-Foulon and Dr Bruno Stankoff for insights and fruitful discussions. We thank the MS Society Tissue Bank at Imperial College London and Dr. Gveric for the provision of the MS brain samples (supported by grant 007/14 from the UK MS Society). We thank the icm.Quant imaging platform, ICM biostatistics platform (iCONICS), CELIS, electrophysiology, histology, vectorology and genotyping ICM platforms, and PhenoICMice ICM facilities. All animal work was conducted at the PHENO-ICMice facility (supported by ANR-10- IAIHU-06 and ANR-11-INBS-0011-NeurATRIS and FRM). This work was funded by INSERM, ICM, ARSEP Grants (to C.L. and A.D.), FRM fellowships (SPF20110421435, to A.D. and FDT20170437332, to M.T.), APHP fellowship and ARSEP

travel grant to T.R., Prix Bouvet-Labruyère - Fondation de France (to A.D.), BBT (ICM; to A.D.), ANR JC (ANR-17-CE16-0005-01; to A.D.) and FRC (Espoir en tête, Rotary Club).

Contribution

AD, RR, TR and CL designed research. RR, TR, MSA and AD performed research and analyzed data. LR and JMV generated electron microscopy data. TR, RM and AD designed and performed the human study. FXL, RR, TR and AD designed and did the biostatistical analysis. MT and EM participated in project initiation and experimental design. AD, RR, TR and CL wrote the paper.

Conflict of interest:

The authors declare no conflict of interest.

Data and Code availability

Raw source data files and scripts for remyelination analysis (ImajeJ), data representation (R) and statistical analysis (R) are available upon request. Detailed plasmid description is available upon request.

References

1. Lawson, L. J., Perry, V. H., Dri, P. & Rlksn, S. G. Heterogeneity in the distribution and morphology of microglia in the normal adult mouse brain. Neuroscience 39, 151–170 (1990).

2. Colonna, M. & Butovsky, O. Microglia Function in the Central Nervous System During Health and Neurodegeneration. Annu. Rev. Immunol. 35, 441–468 (2017).

3. Thion, M. S., Ginhoux, F. & Garel, S. Microglia and early brain development: An intimate journey. Science (80-.). 362, 185–189 (2018).

4. Hammond, T. R., Robinton, D. & Stevens, B. Microglia and the Brain: Complementary Partners in Development and Disease. Annu. Rev. Cell Dev. Biol. 34, 523–544 (2018).

5. Davalos, D. et al. ATP mediates rapid microglial response to local brain injury in vivo. Nat. Neurosci. 8, 752–758 (2005).

6. Nimmerjahn, A., Kirchhoff, F. & Helmchen, F. Resting microglial cells are highly dynamic surveillants of brain parenchyma in vivo. Science (80-.). 308, 1314–1318 (2005).

7. Bernier, L. P. et al. Nanoscale Surveillance of the Brain by Microglia via cAMP-Regulated Filopodia. Cell Rep. 27, 2895-2908.e4 (2019).

8. Fontainhas, A. M. et al. Microglial Morphology and Dynamic Behavior Is Regulated by Ionotropic Glutamatergic and GABAergic Neurotransmission. PLoS One 6, e15973 (2011).

9. Stowell, R. D. et al. Noradrenergic signaling in the wakeful state inhibits microglial surveillance and synaptic plasticity in the mouse visual cortex. Nat. Neurosci. 22, 1782–1792 (2019).

10. Madry, C. et al. Microglial Ramification, Surveillance, and Interleukin-1β Release Are Regulated by the Two-Pore Domain K+ Channel THIK-1. Neuron 97, 299-312.e6 (2018).

11. Cserép, C. et al. Microglia monitor and protect neuronal function via specialized somatic purinergic junctions. Science (80-.). 4, eaax6752 (2019).

12. Szepesi, Z., Manouchehrian, O., Bachiller, S. & Deierborg, T. Bidirectional Microglia–Neuron Communication in Health and Disease. Front. Cell. Neurosci. 12, 1–26 (2018).

13. Voet, S., Prinz, M. & van Loo, G. Microglia in Central Nervous System Inflammation and Multiple Sclerosis Pathology. Trends Mol. Med. 25, 112–123 (2019).

14. Miron, V. E. et al. M2 microglia and macrophages drive oligodendrocyte differentiation during CNS remyelination. Nat. Neurosci. 16, 1211–1218 (2013).

15. Lloyd, A. F. & Miron, V. E. The pro-remyelination properties of microglia in the central nervous system. Nat. Rev. Neurol. 29–34 (2019). doi:10.1038/s41582-019-0184-2

16. Cunha, M. I. et al. Pro-inflammatory activation following demyelination is required for myelin clearance and oligodendrogenesis. J. Exp. Med. 217, (2020).

17. Ransohoff, R. M. A polarizing question: do M1 and M2 microglia exist? Nat. Neurosci. 19, 987–991 (2016).

18. Masuda, T. et al. Spatial and temporal heterogeneity of mouse and human microglia at single-cell resolution. Nature 566, 388–392 (2019).

19. Hammond, T. R. et al. Single-Cell RNA Sequencing of Microglia throughout the Mouse Lifespan and in the Injured Brain Reveals Complex Cell-State Changes. Immunity 50, 253-271.e6 (2019).

20. Wolf, S. A., Boddeke, H. W. G. M. & Kettenmann, H. Microglia in Physiology and Disease. Annu. Rev. Physiol. 79, 619–643 (2017).

21. El Behi, M. et al. Adaptive human immunity drives remyelination in a mouse model of demyelination. Brain 140, 967–980 (2017).

22. Butovsky, O. et al. Microglia activated by IL-4 or IFN-γ differentially induce neurogenesis and oligodendrogenesis from adult stem/progenitor cells. Mol. Cell. Neurosci. 31, 149–160 (2006).

23. Liu, Y. U. et al. Neuronal network activity controls microglial process surveillance in awake mice via norepinephrine signaling. Nat. Neurosci. 22, 1771–1781 (2019).

24. Nebeling, F. C. et al. Microglia motility depends on neuronal activity and promotes structural plasticity in the hippocampus. bioRxiv 515759 (2019). doi:10.1101/515759

25. Tremblay, M. Ě., Lowery, R. L. & Majewska, A. K. Microglial interactions with synapses are modulated by visual experience. PLoS Biol. 8, (2010).

26. Wake, H., Moorhouse, A. J., Jinno, S., Kohsaka, S. & Nabekura, J. Resting microglia directly monitor the functional state of synapses in vivo and determine the fate of ischemic terminals. J. Neurosci. 29, 3974–3980 (2009).

27. Paolicelli, R. C. et al. Synaptic Pruning by Microglia Is Necessary for Normal Brain Development. Science (80-.). 333, 1456–1458 (2011).

28. Li, Y., Du, X. F., Liu, C. S., Wen, Z. L. & Du, J. L. Reciprocal Regulation between Resting Microglial Dynamics and Neuronal Activity In Vivo. Dev. Cell 23, 1189–1202 (2012).

29. Hughes, A. N. & Appel, B. Microglia phagocytose myelin sheaths to modify developmental myelination. Nat. Neurosci. 215, 41–47 (2020).

30. Baalman, K. et al. Axon initial segment–associated microglia. J. Neurosci. 35, 2283–2292 (2015).

31. Clark, K. C. et al. Compromised axon initial segment integrity in EAE is preceded by microglial reactivity and contact. Glia 64, 1190–1209 (2016).

32. Lubetzki, C., Sol-Foulon, N. & Desmazières, A. Nodes of Ranvier during development and repair in the CNS. Nat. Rev. Neurol. 1871, (2020).

33. Zhang, J., Yang, X., Zhou, Y., Fox, H. & Xiong, H. Direct contacts of microglia on myelin sheath and Ranvier's node in the corpus callosum in rats. J. Biomed. Res. 33, 192–200 (2019).

34. Fenrich, K. K. et al. Long-term in vivo imaging of normal and pathological mouse spinal cord with subcellular resolution using implanted glass windows. J. Physiol. 590, 3665–3675 (2012).

35. Coman, I. et al. Nodal, paranodal and juxtaparanodal axonal proteins during demyelination and remyelination in multiple sclerosis. Brain 129, 3186–3195 (2006).

36. Birgbauer, E., Rao, T. S. & Webb, M. Lysolecithin induces demyelination in vitro in a cerebellar slice culture system. J. Neurosci. Res. 78, 157–166 (2004).

37. Thetiot, M., Ronzano, R., Aigrot, M. S., Lubetzki, C. & Desmazières, A. Preparation and Immunostaining of Myelinating Organotypic Cerebellar Slice Cultures. J. Vis. Exp. 1–7 (2019). doi:10.3791/59163

38. Paolicelli, R. C., Bisht, K. & Tremblay, M.-Ã. Fractalkine regulation of microglial physiology and consequences on the brain and behavior. Front. Cell. Neurosci. 8, (2014).

39. Kyrargyri, V. et al. P2Y 13 receptors regulate microglial morphology, surveillance, and resting levels of interleukin 1β release. Glia glia.23719 (2019). doi:10.1002/glia.23719

40. Zonouzi, M. et al. GABAergic regulation of cerebellar NG2 cell development is altered in perinatal white matter injury. Nat. Neurosci. 18, 674–682 (2015).

41. Demerens, C. et al. Induction of myelination in the central nervous system by electrical activity. Proc. Natl. Acad. Sci. U. S. A. 93, 9887–9892 (1996).

42. Madry, C. et al. Effects of the ecto-ATPase apyrase on microglial ramification and surveillance reflect cell depolarization, not ATP depletion. Proc. Natl. Acad. Sci. U. S. A. 115, E1608–E1617 (2018).

43. Bacmeister, C. M. et al. Motor learning promotes remyelination via new and surviving oligodendrocytes. Nat. Neurosci. (2020). doi:10.1038/s41593-020-0637-3

44. Gründemann, J. & Clark, B. A. Calcium-Activated Potassium Channels at Nodes of Ranvier Secure Axonal Spike Propagation. Cell Rep. 12, 1715–1722 (2015).

45. Brohawn, S. G. et al. The mechanosensitive ion channel TRAAK is localized to the mammalian node of Ranvier. Elife 8, (2019).

46. Kanda, H. et al. TREK-1 and TRAAK Are Principal K + Channels at the Nodes of Ranvier for Rapid Action Potential Conduction on Mammalian Myelinated Afferent Article TREK-1 and TRAAK Are Principal K + Channels at the Nodes of Ranvier for Rapid Action Potential Conduction on. Neuron 1–12 (2019). doi:10.1016/j.neuron.2019.08.042

47. Serwanski, D. R., Jukkola, P. & Nishiyama, A. Heterogeneity of astrocyte and NG2 cell insertion at the node of Ranvier. J. Comp. Neurol. 1–10 (2016). doi:10.1002/cne

48. Mount, C. W. & Monje, M. Wrapped to Adapt: Experience-Dependent Myelination. Neuron 95, 743–756 (2017).

49. Ronzano, R., Thetiot, M., Lubetzki, C. & Desmazieres, A. Myelin Plasticity and Repair: Neuro-Glial Choir Sets the Tuning. Front. Cell. Neurosci. 14, 1–11 (2020).

50. Maldonado, P. P., Vélez-Fort, M., Levavasseur, F. & Angulo, M. C. Oligodendrocyte precursor cells are accurate sensors of local K+ in mature gray matter. J. Neurosci. 33, 2432–2442 (2013).

51. Thetiot, M. et al. An alternative mechanism of early nodal clustering and myelination onset in GABAergic neurons of the central nervous system. Glia 68, 1891–1909 (2020).

52. Orthmann-Murphy, J. et al. Remyelination alters the pattern of myelin in the cerebral cortex. Elife 9, 1–61 (2020).

53. Black, J. A. & Waxman, S. G. The perinodal astrocyte. Glia 1, 169–183 (1988).

54. Dutta, D. J. et al. Regulation of myelin structure and conduction velocity by perinodal astrocytes. Proc. Natl. Acad. Sci. U. S. A. 115, 11832–11837 (2018).

55. Butovsky, O. et al. Identification of a unique TGF-β–dependent molecular and functional signature in microglia. Nat. Neurosci. 17, 131–143 (2014).

56. Howell, O. W. et al. Activated microglia mediate axoglial disruption that contributes to axonal injury in multiple sclerosis. J. Neuropathol. Exp. Neurol. 69, 1017–1033 (2010).

57. Nikić, I. et al. A reversible form of axon damage in experimental autoimmune encephalomyelitis and multiple sclerosis. Nat. Med. 17, 495–499 (2011).

58. Zrzavy, T. et al. Loss of 'homeostatic' microglia and patterns of their activation in active multiple sclerosis. Brain 140, 1900–1913 (2017).

59. Yamasaki, R. et al. Differential roles of microglia and monocytes in the inflamed central nervous system. J. Exp. Med. 211, 1533–1549 (2014).

60. Gautier, H. O. B. et al. Neuronal activity regulates remyelination via glutamate signalling to oligodendrocyte progenitors. Nat. Commun. 6, (2015).

61. Ortiz, F. C. et al. Neuronal activity in vivo enhances functional myelin repair. JCI Insight 4, (2019).

62. Iaccarino, H. F. et al. Gamma frequency entrainment attenuates amyloid load and modifies microglia. Nature 540, 230–235 (2016).

63. Umpierre, A. D. et al. Microglial calcium signaling is attuned to neuronal activity in awake mice. Elife 9, (2020).

64. Lloyd, A. F. et al. Central nervous system regeneration is driven by microglia necroptosis and repopulation. Nat. Neurosci. 22, 1046–1052 (2019).

65. Locatelli, G. et al. Mononuclear phagocytes locally specify and adapt their phenotype in a multiple sclerosis model. Nat. Neurosci. 21, 1196–1208 (2018).

66. Muñoz-Planillo, R. et al. K+ Efflux Is the Common Trigger of NLRP3 Inflammasome Activation by Bacterial Toxins and Particulate Matter. Immunity 38, 1142–1153 (2013).

67. Hamada, M. S. & Kole, M. H. P. Myelin Loss and Axonal Ion Channel Adaptations Associated with Gray Matter Neuronal Hyperexcitability. J. Neurosci. 35, 7272–7286 (2015).

68. Jäkel, S. et al. Altered human oligodendrocyte heterogeneity in multiple sclerosis. Nature 566, 543–547 (2019).

69. Lundgaard, I. et al. Neuregulin and BDNF Induce a Switch to NMDA Receptor-Dependent Myelination by Oligodendrocytes. PLoS Biol. 11, (2013).

70. Jung, S. et al. Analysis of Fractalkine Receptor CX3CR1 Function by Targeted Deletion and Green Fluorescent Protein Reporter Gene Insertion. Mol. Cell. Biol. 20, 4106–4114 (2000).

71. Zhang, H., Jarjour, A. A., Boyd, A. & Williams, A. Central nervous system remyelination in culture - A tool for multiple sclerosis research. Exp. Neurol. 230, 138–148 (2011).

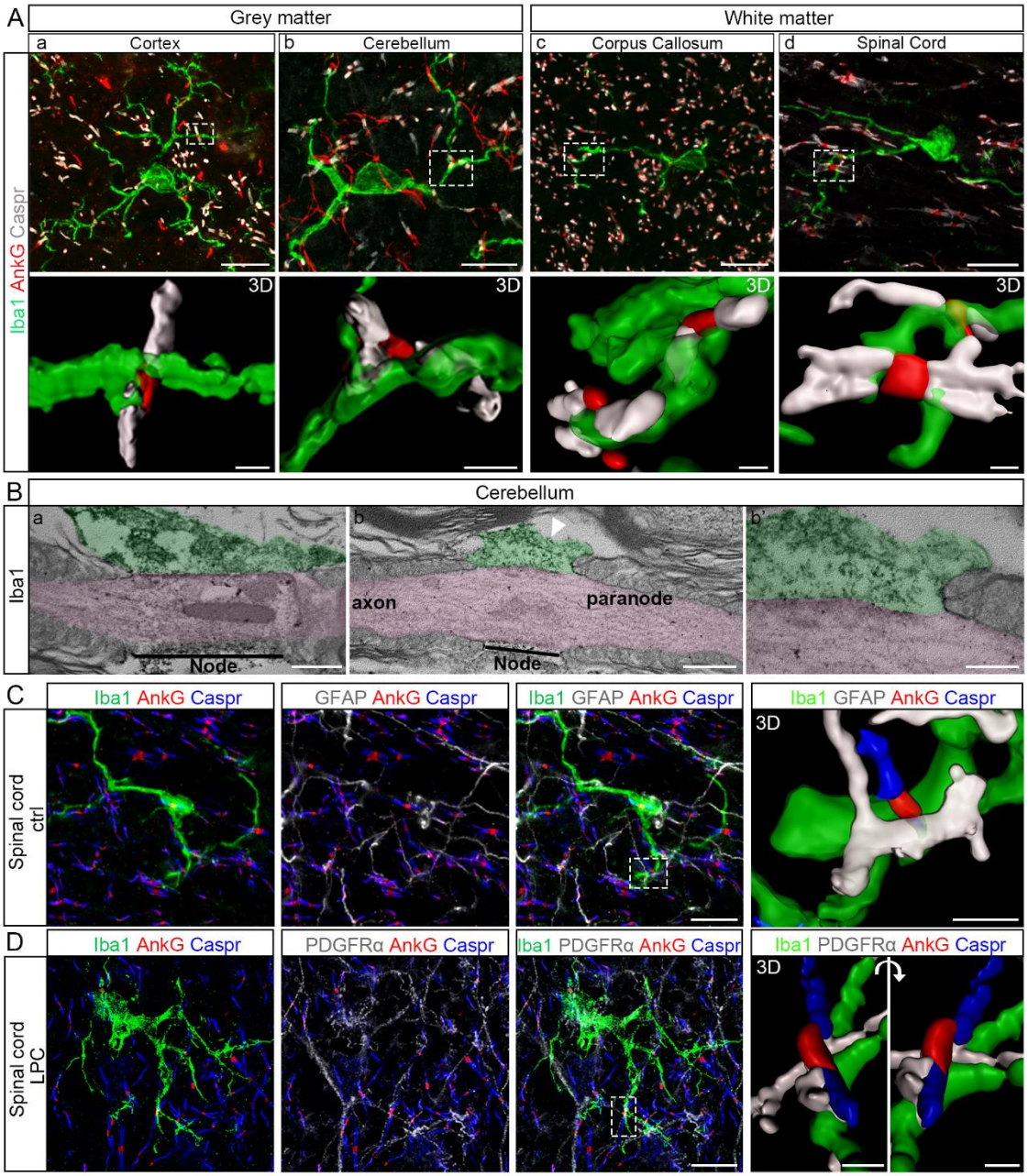
A
Grey matter
White matter
a Cortex
b Cerebellum
c Corpus Callosum
d Spinal Cord
Iba1 AnkG Caspr
3D
B
Cerebellum
Iba1
a
b
b'
axon
paranode
Node
Node
C
Spinal cord ctrl
Iba1 AnkG Caspr
GFAP AnkG Caspr
Iba1 GFAP AnkG Caspr
Iba1 GFAP AnkG Caspr
3D
D
Spinal cord LPC
Iba1 AnkG Caspr
PDGFRα AnkG Caspr
Iba1 PDGFRα AnkG Caspr
Iba1 PDGFRα AnkG Caspr
3D

Figure 1

Figure 1. Microglial cells contact nodes of Ranvier in mouse central nervous system.

In adult mouse nervous tissue, microglial cells (Iba1, green) contact nodes of Ranvier (AnkyrinG, indicated as AnkG in the figures, red) in grey (**a**, cortex and **b**, cerebellum) and white matter (**c**, corpus callosum and **d**, dorsal spinal cord, cortico-spinal tractus). (**a-d**) 3D reconstructions correspond to the boxed area. (**B**) Transmission electron micrographs showing microglial processes ($Iba1^+$, green) contacting directly the nodal axolemma (pink) in adult mouse cerebellum. (**b'**) Higher magnification of the micrograph (**b**), showing the interaction between the microglial process, the axolemma and first paranodal loop. (**C, D**) Immunohistostainings of adult mouse dorsal spinal cord showing nodes of Ranvier (AnkyrinG, red) contacted by both a microglial cell (Iba1, green) and an astrocyte (GFAP, white) in control condition (**C**) and a microglial cell (Iba1, green) and an oligodendrocyte progenitor cell (PDGFRα, white) in remyelinating condition (**D**). 3D reconstructions correspond to the boxed area. Scale bars: (**A, C, D**) 2D: 10μm; 3D: (**A**) 1μm, (**C-D**) 2μm; (**Bi-ii**) 500nm, (**Biii**) 200nm.

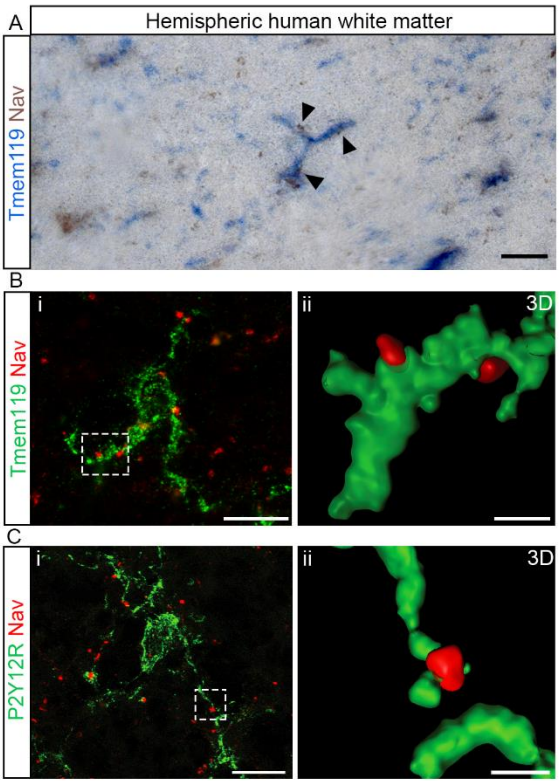
A
Hemispheric human white matter
Tmem119 Nav
B
i
ii
3D
Tmem119 Nav
C
i
ii
3D
P2Y12R Nav

Figure 2

Figure 2. Microglial cells contact nodes of Ranvier in human central nervous system.

(**A, B**) Immunohistostainings of post-mortem human hemispheric white matter tissue (healthy donor) showing microglial cells (blue, resident microglia, TMEM119) contacting nodes of Ranvier (Na_V, brown). (**C, D**) Immunofluorescent stainings of post-mortem human hemispheric white matter tissue (healthy donor) showing microglial cells (green; **C**, resident microglia, TMEM119, and **D**, homeostatic microglia, P2Y12R) contacting nodes of Ranvier (Na_V, red). (**Cii, Dii**) 3D reconstructions correspond to the boxed area in **Ci** and D**i** respectively. Scale bars: (2D) (**A, B, C, D**) 10μm; (3D) (**C, D**) 2μm.

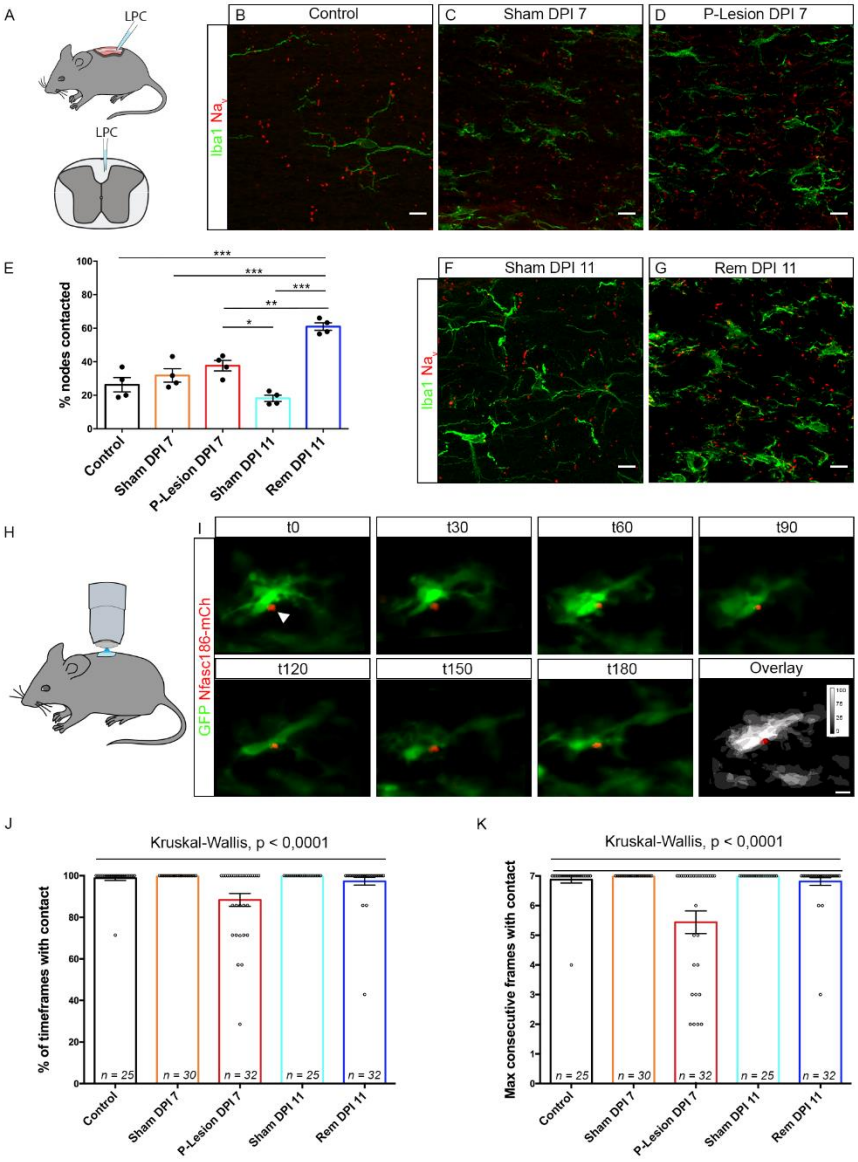
A
LPC
LPC
B Control
C Sham DPI 7
D P-Lesion DPI 7
Iba1 Nav
E
% nodes contacted
Control
Sham DPI 7
P-Lesion DPI 7
Sham DPI 11
Rem DPI 11
F Sham DPI 11
G Rem DPI 11
H
I
t0
t30
t60
t90
t120
t150
t180
Overlay
GFP Nfasc186-mCh
J
Kruskal-Wallis, p < 0,0001
% of timeframes with contact
n = 25
n = 30
n = 32
n = 25
n = 32
K
Kruskal-Wallis, p < 0,0001
Max consecutive frames with contact

Figure 3

Figure 3. Microglial cell contacts at nodes of Ranvier are stable *in vivo* and increase in remyelination.

(A) LPC injection in mouse spinal cord (cortico-spinal tractus). **(B-G)** Contacts are observed between nodes of Ranvier (Na_V, red) and microglia (Iba1, green) in control (without injection) **(B)**, Sham 7 and 11 days post-NaCl injection **(C and F,** respectively**),** in perilesional tissue 7 days post LPC injection **(D)** and in remyelinating tissue 11 days post-LPC injection **(G)**. **(E)** Corresponding quantifications of the percentage of nodes contacted (n=4 animals per condition; 4 to 6 areas per animal, 42 nodes minimum per area). **(H)** Glass-window system above dorsal spinal cord for 2-Photon live-imaging **(I)** Images from a 3 hour movie (Movie 1) from a CX3CR1-GFP/Thy1-Nfasc186mCherry mouse shows a stable interaction between a microglial cell (green) and a node of Ranvier (red) (arrow head). Scale bar: 10 µm. **(J)** Percentage of time in contact in 1 hour movies, with one acquisition every 10 minutes. **(K)** Longest sequence of consecutive timepoints with contact in 1 hour movies. Each dot is a microglia-node pair. The number of node-microglia pairs imaged is indicated on each bar. n=6 to 11 animals per condition. Scale bars: (**B**, **C**, **D**, **F**, **G**, **I**) 10 µm. (**E**) ANOVA with post-hoc Tukey test; (**J**, **K**) Kruskal-Wallis test. *P < 0.05, **P < 0.01, ***P < 0.001, ****P < 0.0001, ns: not significant. Bars and error bars represent the mean ± s.e.m. For detailed statistics, see Supplementary Table.

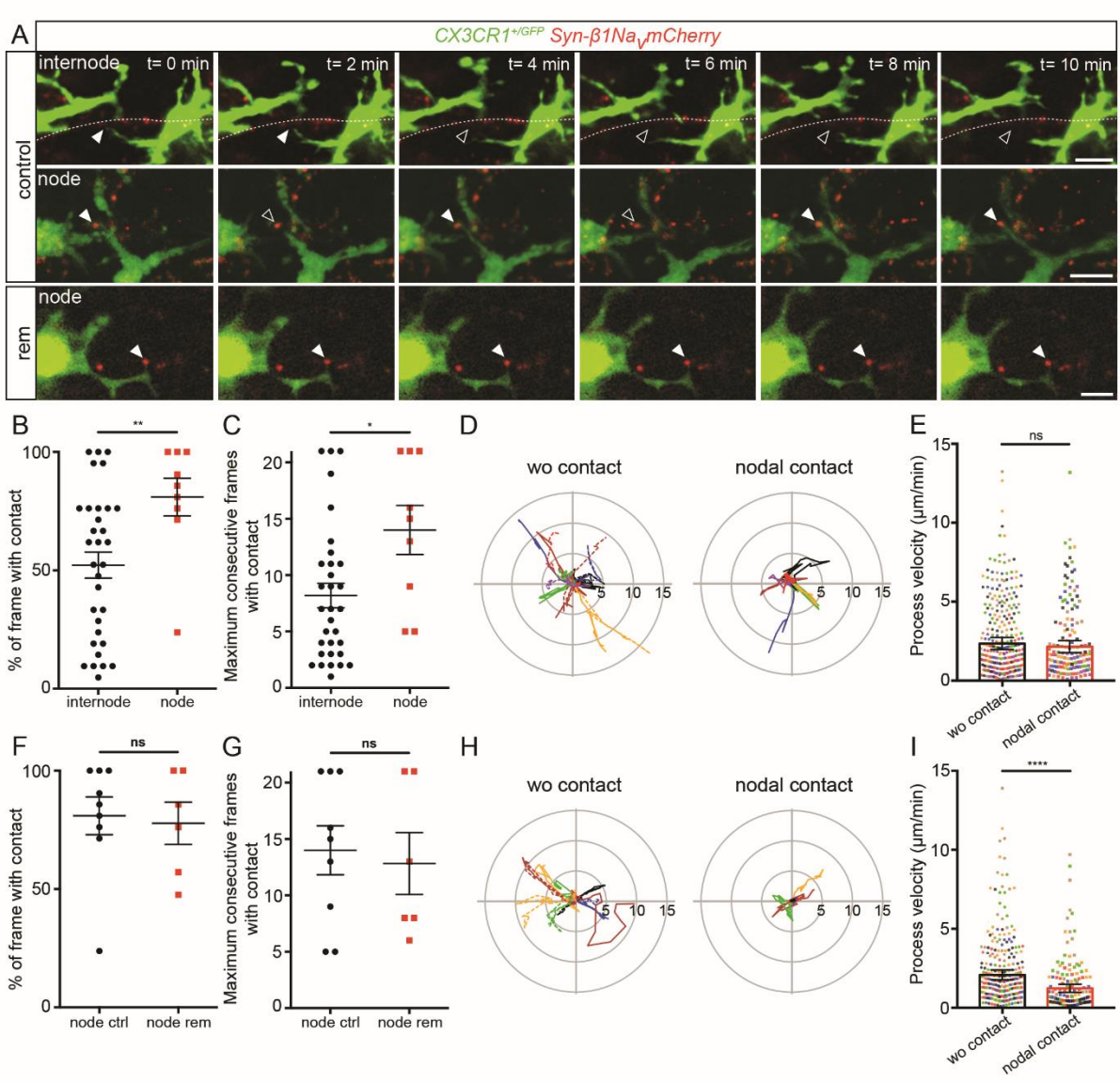
A
CX3CR1+/GFP Syn-β1NaVmCherry
internode
t= 0 min
t= 2 min
t= 4 min
t= 6 min
t= 8 min
t= 10 min
control
node
rem
node
B
**
% of frame with contact
internode
node
C
*
Maximum consecutive frames with contact
internode
node
D
wo contact
nodal contact
E
ns
Process velocity (µm/min)
wo contact
nodal contact
F
ns
% of frame with contact
node ctrl
node rem
G
ns
Maximum consecutive frames with contact
node ctrl
node rem
H
wo contact
nodal contact
I
****
Process velocity (µm/min)
wo contact
nodal contact

Figure 4

Figure 4. Microglia process dynamics are modified by nodal structure vicinity in myelinated and remyelinating cultured slices.

(A) Microglial cells (green) initially contacting an internode or a node (red) in myelinated slices, or a node in a remyelinating slice. Arrowheads show the initial contact position (filled: contact, empty: no contact). **(B-C)** Dynamics of microglial processes contacting an internode vs a node in myelinated slices (internode: n=32 contacts from 16 animals, node: n=9 contacts from 8 animals). **(D)** Trajectories (with t0 position as reference, distance in µm) of microglial process tips in myelinated slices, initially contacting a node (nodal contact) or not (wo contact). wo contact: n=14, nodal contact: n=7, from 7 color coded animals. (**E**) Instantaneous process velocity in myelinated slices. wo contact: 280 measures from 14 trajectories in 7 animals, nodal contact: 140 measures from 7 trajectories in 7 color coded animals. **(F-G)** Dynamics of microglial processes contacting a node in control or remyelinating slices. ctrl: n=9 contacts from 8 animals, rem: n=6 contacts from 6 animals. **(H)** Trajectories (with t0 position as reference, distance in µm) of microglial process tips in remyelinating slices, initially contacting a node or not. wo contact: n=12, nodal contact: n=6, in 6 color coded animal. (**I**) Instantaneous process velocity in remyelinating slices. wo contact: 240 measures from 12 trajectories in 6 animals, nodal contact: 120 measures from 6 trajectories in 6 color coded animals. Scale bars: (**A**) 10 µm**. (C**, **D**, **G**, **H)** Mann-Whitney tests, **(E, I)** Type II Wald chi-square tests. *P < 0.05, **P < 0.01, ***P < 0.001, ****P < 0.0001, ns: not significant; bars and error bars represent the mean ± s.e.m. For detailed statistics, see Supplementary Table.

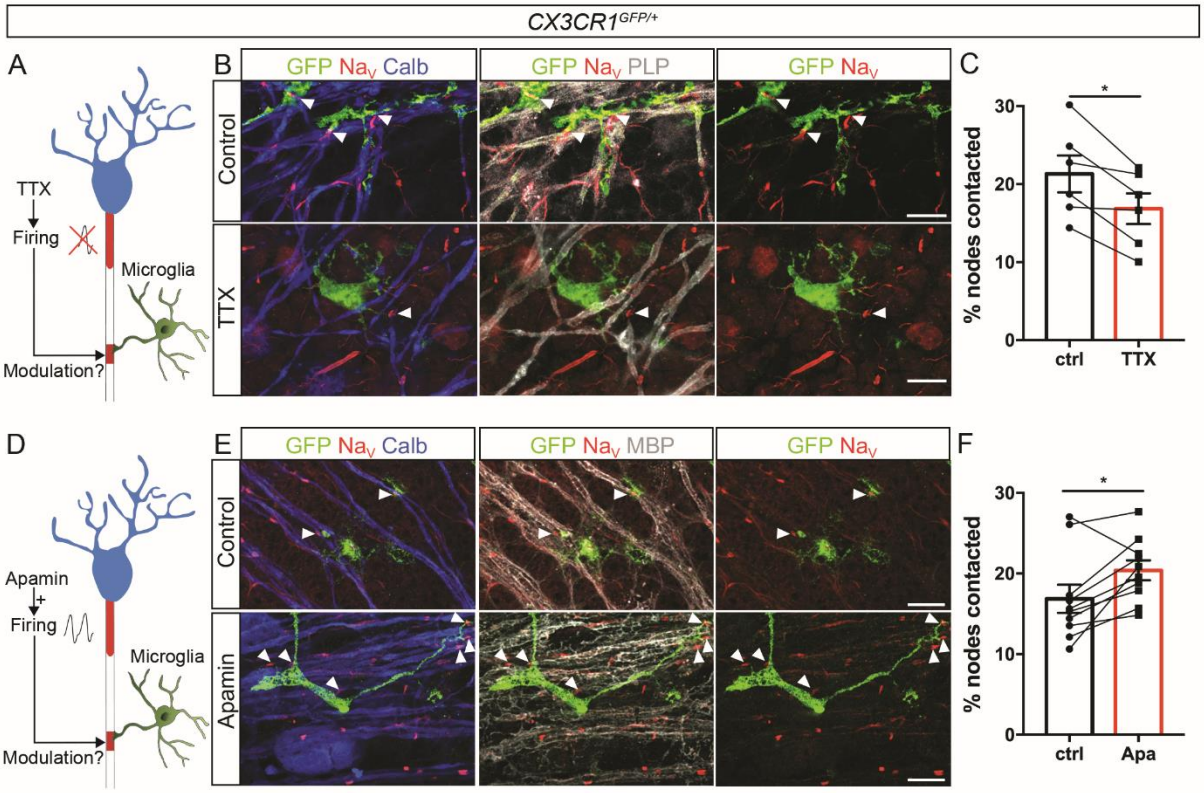
CX3CR1GFP/+
A
TTX
Firing
Microglia
Modulation?
B
GFP Nav Calb
GFP Nav PLP
GFP Nav
Control
TTX
C
% nodes contacted
30
20
10
0
ctrl
TTX
*
D
Apamin
+
Firing
Microglia
Modulation?
E
GFP Nav Calb
GFP Nav MBP
GFP Nav
Control
Apamin
F
% nodes contacted
30
20
10
0
ctrl
Apa
*

Figure 5

Figure 5. Neuronal activity modulates microglia-node of Ranvier interaction.

(A-D) Schematics of the experimental design. **(B-C)** In myelinated CX3CR1$^{GFP/+}$ cerebellar organotypic slices, microglia (GFP, green) contacts with nodes (Na_V, red) are reduced following electrical activity inhibition (TTX). **(E-F)** They are conversely increased following electrical activity activation (Apamin). Arrowheads show the nodes of Ranvier contacted by microglia. **(C, F)** Percentage of nodes of Ranvier contacted by microglial cells in control vs 1-hour treated slices from the same animal **(C)** TTX (500 nM, n=6 animals), **(F)** Apamine (500 nM, n=10 animals). Scale bars: (**B**, **E**) 10 µm**. (C)** Paired t-test; **(F)** Wilcoxon matched pairs test. *P < 0.05, **P < 0.01, ***P < 0.001, ****P < 0.0001, ns: not significant; bars and error bars represent the mean ± s.e.m. For detailed statistics, see Supplementary Table.

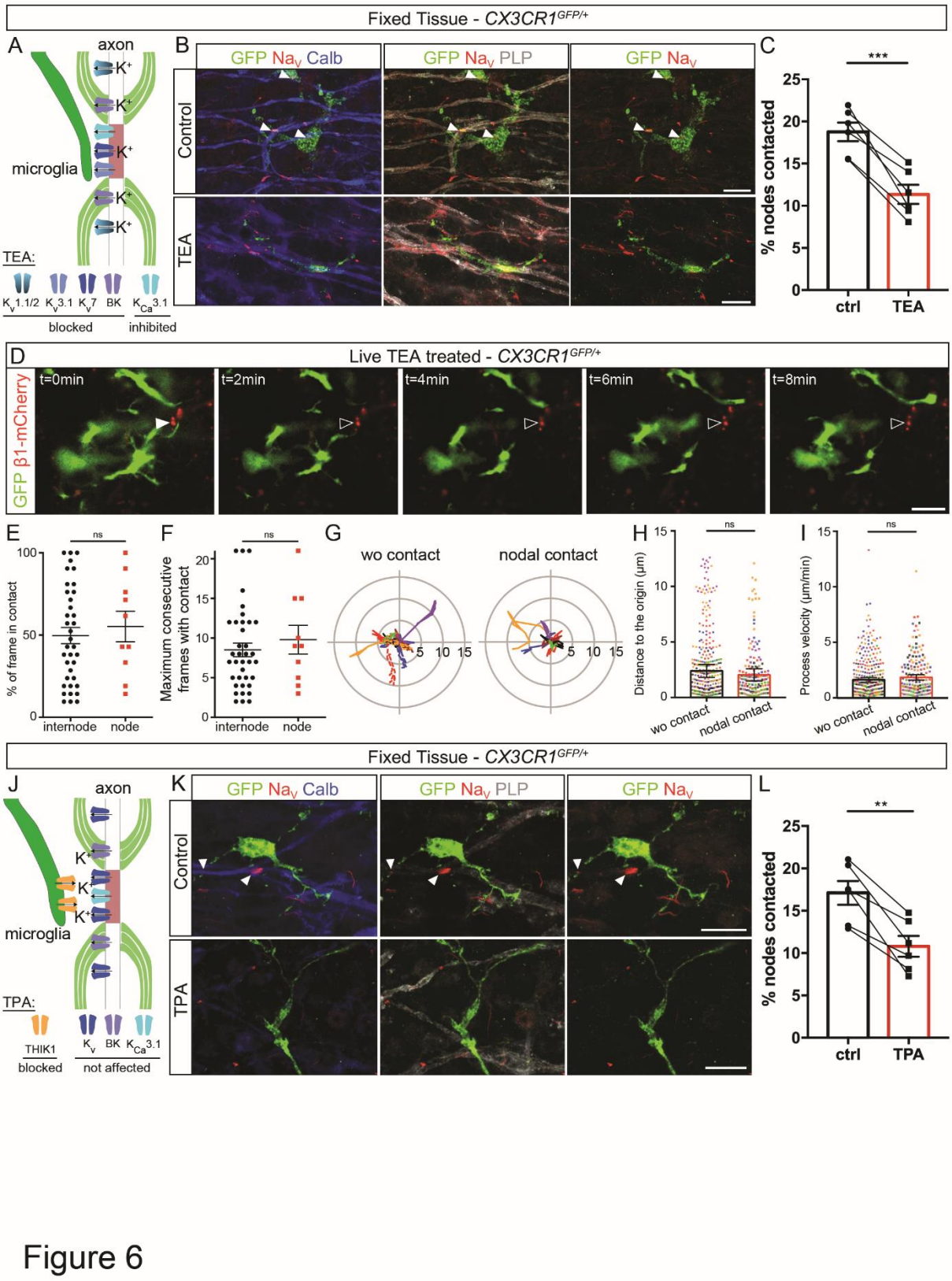
Fixed Tissue - CX3CR1GFP/+
A
axon
microglia
TEA:
Kv1.1/2 Kv3.1 Kv7 BK
blocked
KCa3.1
inhibited
B
GFP Nav Calb
GFP Nav PLP
GFP Nav
Control
TEA
C
***
% nodes contacted
ctrl
TEA
D
Live TEA treated - CX3CR1GFP/+
GFP β1-mCherry
t=0min
t=2min
t=4min
t=6min
t=8min
E
ns
% of frame in contact
internode
node
F
ns
Maximum consecutive frames with contact
internode
node
G
wo contact
nodal contact
H
ns
Distance to the origin (µm)
wo contact
nodal contact
I
ns
Process velocity (µm/min)
wo contact
nodal contact
Fixed Tissue - CX3CR1GFP/+
J
axon
microglia
TPA:
THIK1
blocked
Kv BK KCa3.1
not affected
K
GFP Nav Calb
GFP Nav PLP
GFP Nav
Control
TPA
L
**
% nodes contacted
ctrl
TPA

Figure 6

Figure 6. Microglia preferential contact with nodes depends on potassium fluxes.

(A) Experimental design. **(B)** In myelinated CX3CR1$^{GFP/+}$ cerebellar organotypic slices, microglia (GFP, green) contacts with nodes (Na_V, red) are reduced following potassium channel inhibition by TEA. Arrowheads indicate the nodes of Ranvier contacted. **(C)** Percentage of nodes of Ranvier contacted in control condition or following 1 hour TEA treatment (30 mM, n=6 animals). **(D)** Microglial cell (green) initially contacting a node (red) in a myelinated slice treated with TEA. Arrowheads show the initial contact position (filled: contact, empty: no contact). **(E-F)** Dynamics of microglial tips contacting an internode vs a node in myelinated slices treated with TEA (internode: n=37 contacts from 12 animals, node: n=10 contacts from 8 animals). **(G)** Trajectories (with t0 position as reference, distance in µm) of microglial process tips whether they were contacting a node (nodal contact) or not (wo contact) at t0 (wo contact: n=14; nodal contact: n=7; from 7 color coded movies from 6 animals). **(H)** Distance between the process tip and its position at t0 for each timepoint in myelinated slices treated with TEA (wo contact: 280 measures from 14 trajectories in 6 animals, nodal contact: 140 measures from 7 trajectories from 7 color coded movies in 6 animals). **(I)** Instantaneous process velocity in myelinated slices (wo contact: 280 measures from 14 trajectories in 7 animals; nodal contact: 140 measures from 7 trajectories in 7 color coded animals). **(J)** Schematic of the experimental design. **(K)** Microglia (GFP, green) contacts with nodes (Na_V, red) are importanlty reduced following THIK-1 inhibition by TPA. **(L)** Percentage of nodes of Ranvier contacted by microglial cells in control condition or following 1 hour TPA treatment (50 µM, n=6 animals). Scale bars: (**B**, **D**, **K**) 10 µm. **(C, L)** Paired t-test; **(E, F)** Mann-Whitney tests; **(H, I)** Type II Wald chi-square tests. *P < 0.05, **P < 0.01, ***P < 0.001, ****P < 0.0001, ns: not significant; bars and error bars represent the mean ± s.e.m. For detailed statistics, see Supplementary Table.

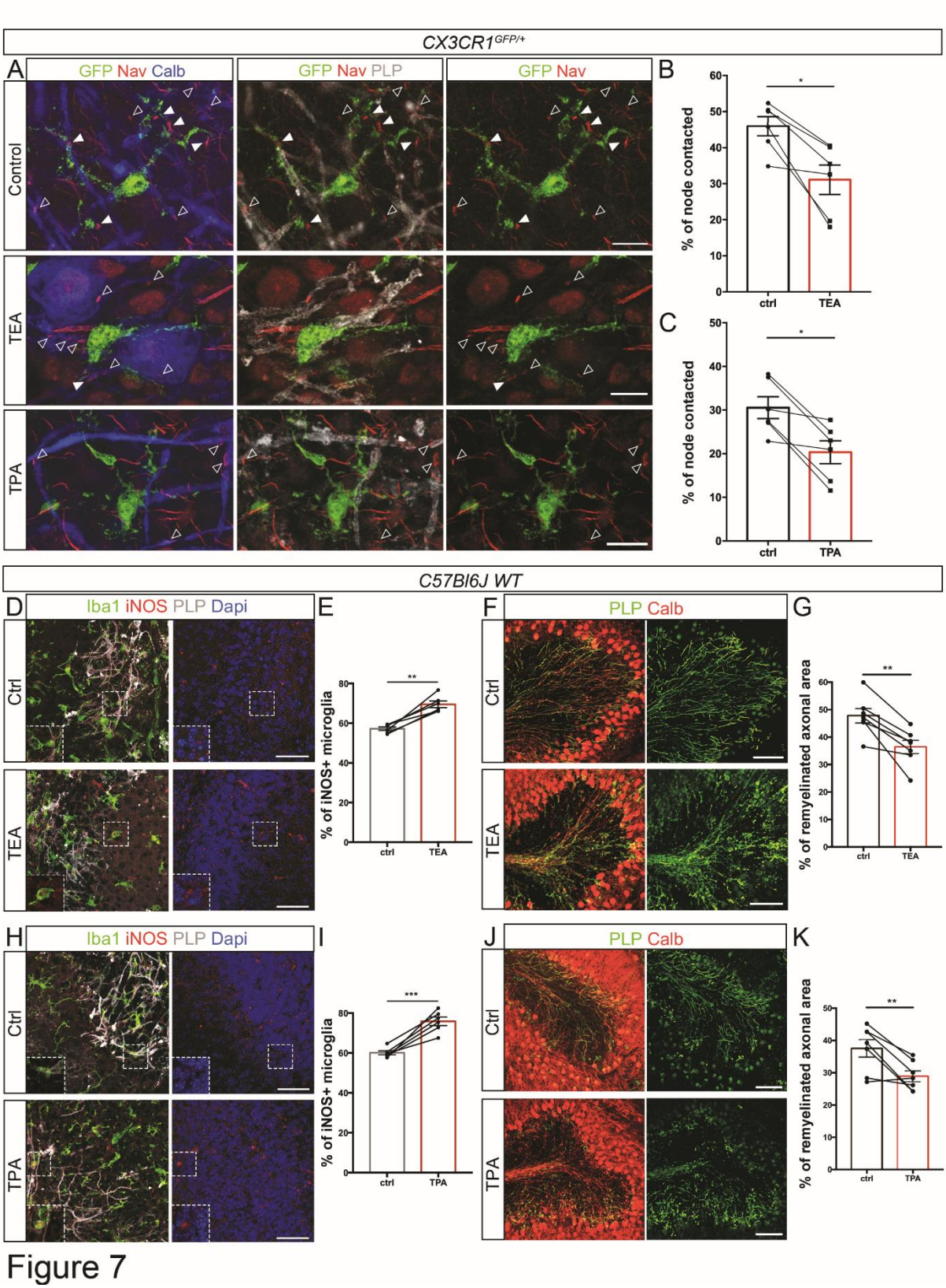
CX3CR1GFP/+
A
GFP Nav Calb
GFP Nav PLP
GFP Nav
Control
TEA
TPA
B
% of node contacted
ctrl
TEA
C
% of node contacted
ctrl
TPA
C57Bl6J WT
D
Iba1 iNOS PLP Dapi
Ctrl
TEA
E
% of iNOS+ microglia
ctrl
TEA
F
PLP Calb
Ctrl
TEA
G
% of remyelinated axonal area
ctrl
TEA
H
Iba1 iNOS PLP Dapi
Ctrl
TPA
I
% of iNOS+ microglia
ctrl
TPA
J
PLP Calb
Ctrl
TPA
K
% of remyelinated axonal area
ctrl
TPA

Figure 7

Figure 7. Altering K^+ fluxes increases pro-inflammatory microglial profile following demyelination and impairs remyelination.

(A) In remyelinating CX3CR1$^{GFP/+}$ cerebellar organotypic slices, microglia (GFP, green) contacts with nodes (Na_V, red) are importanlty reduced following potassium channels inhibition by TEA and TPA treatments. Arrowheads show the nodal structures (filled: contacted by microglia; empty: not contacted). **(B-C)** Percentage of nodal structures contacted by microglial cells in control remyelinating condition or following 1 hour TEA (B, 30 mM, n=6 animals) or TPA treatment (C, 50 μM, n=6 animals); the mean values per animal are individually plotted. **(D-H)** In remyelinating C57bl6/J cerebellar organotypic slices, microglial expression of iNOS is increased following potassium channel inhibition by TEA (D) or THIK-1 inhibition by TPA treatment (H). **(E-I)** Percentage of iNOS$^+$ microglial cells at remyelination onset, with no treatment (ctrl) or with TEA (E, 2 hours, 30 mM, n=7 animals) or TPA treatment (I, 2 hours, 50 μM, n=7 animals), the mean values per animal are individually plotted and paired with the corresponding control. **(F-J)** In remyelinating C57bl6 cerebellar organotypic slices, remyelination is reduced following TEA (F) or TPA (J) treatment. **(G-K)** Percentage of axonal area remyelinated in LPC-demyelinated slices without (ctrl) or with TEA (G, 2 hours, 30 mM, n=7 animals) or TPA treatment (K, 2 hours, 50 μM, n=7 animals). Scale bars: (**A**) 10 μm; (**D, H**) 50 μm; (**F, J**) 100 μm. (**B**, **C**, **E**, **G**, **I**, **K**) Paired t-test. *P < 0.05, **P < 0.01, ***P < 0.001, ****P < 0.0001, ns: not significant; bars and error bars represent the mean ± s.e.m. For detailed statistics, see Supplementary Table.

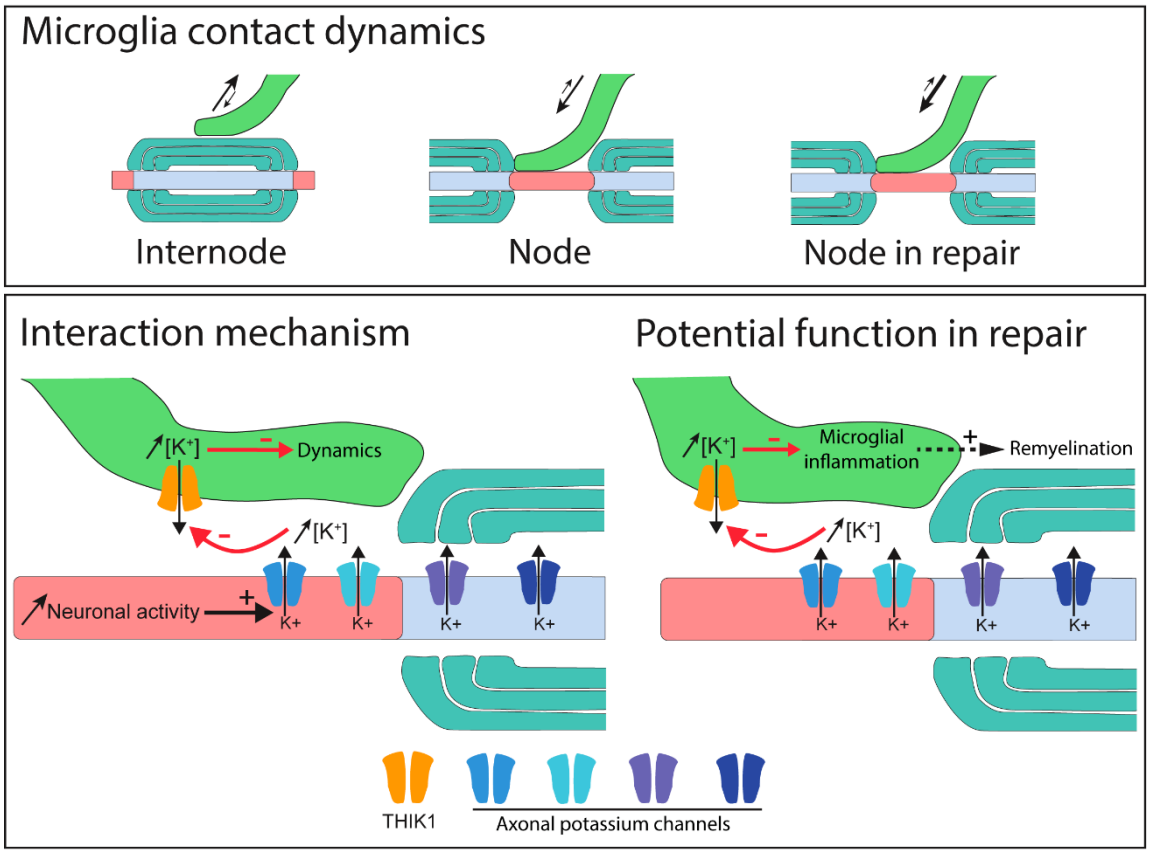
Microglia contact dynamics
Internode
Node
Node in repair
Interaction mechanism
Potential function in repair
[K+]
Dynamics
[K+]
Neuronal activity
K+
K+
K+
K+
[K+]
Microglial inflammation
Remyelination
[K+]
K+
K+
K+
K+
THIK1
Axonal potassium channels

Figure 8

Figure 8. Model for microglila interaction at nodes of Ranvier.

Microglial contact with nodes of Ranvier depends on the tissular context. The interaction is in particular reduced in perilesional area at the peak of demyelination, and increased in remyelination compared to healthy myelinated tissue. Neuronal activity and nodal K^+ efflux promote the interaction, with microglial read-out depending on THIK-1. Altering K^+ efflux or THIK-1 activity in remyelination correlates with more pro-inflammatory microglia and decreased remyelination.

SUPPLEMENTARY METHODS:

Tissue preparation

Ex vivo cerebellar slices

Cultured slices were fixed while attached to the membrane with either 4% or 1% paraformaldehyde (PFA) for 30 min at room temperature (RT) and washed with PBS.

In vivo mouse brain and spinal cord

For spinal cord preparation, the tissue was dissected following perfusion and post-fixed in PFA 2% for 30min, washed in PBS and incubated in PBS, 15% sucrose for 3 days at 4°C. Spinal cords were then embedded in PBS, 15% Sucrose, 4% gelatin and frozen in isopropanol onto carbonic ice.

For adult as well as P12 myelinating mouse brain tissue, animals were perfused with PFA 2% and the brain was dissected and post-fixed in PFA 2% for 30min, washed in PBS and incubated in PBS with successively 7, 15 and 30% sucrose for 3 days at 4°C for cryoprotection. The tissues were then embedded in O.C.T (Tissue-Tek, Sakura).

Tissue sectioning

Mouse spinal cords and brains were cut longitudinally and sagitally respectively. Human tissues (healthy donors, UK MS Society Tissue Bank at Imperial College, London, under ethical approval by the National Research Ethics Committee 08/MRE09/31) were obtained as snap frozen blocks. Sections were cut using a cryostat Leica CM 1950 (30 and 15 µm thick for mouse and human respectively), collected on Superfrost+ slides and stored at -80°C until used.

Immunhistostainings

Immunofluorescent stainings

Human sections were first fixed in 4% PFA for 5 minutes. For myelin protein staining, tissues were preincubated in absolute ethanol at -20°C for 20 min. Tissues were blocked in PBS, 5-10% Normal Goat Serum (50-062Z; Thermo Fisher Scientific), 0,2-0,4% Triton X-100 (RDTH), then incubated with primary antibodies in blocking solution overnight at room temperature, washed in PBS and incubated with secondary antibodies for 1-3 hours at RT in the dark. When applicable, tissues were immersed for 30s in Hoechst solution (10 µg/ml,

Euromedex). They were finally mounted under coverslip (VWR) with Fluoromount (Southern Biotech).

Chromogenic immunohistochemistry on post-mortem brain tissues

Snap frozen tissue blocks were rehydrated with PBS. Sections were then immersed in 4% PFA for 10 minutes before elimination of endogenous peroxidase activity with 0.1% H2O2 (Sigma Aldrich) in PBS for 20 minutes. Blocking was performed using 5% Normal Goat Serum before incubation with primary antibodies diluted in PBS containing 0.05% Triton 100-X and 5% sera. The biotinylated secondary antibody targeting one of the primary antibodies (Vector Laboratories) was visualized with the avidin-biotin horseradish peroxidase complex (Dako, Biotin Blocking System) followed by 3,3'-diamino-benzidine (DAB) (Vector Laboratories) as substrate. The second primary antibody was detected with the ABC-alkaline phosphatase detection system (Vector Laboratories), using Vector Blue as the substrate. Images were captured with a QICAM digital camera (QImaging Inc.).

Imaging

Confocal microscopy for ex vivo cultured slices

Confocal microscopy was performed using an FV-1200 Upright Confocal Microscope and a Leica inverted SP8 with 63x oil immersion objectives with 1.40 numerical aperture, using respectively metamorph and LasX software. For each acquisition, stacks of 1024x1024 pixel images (160.6 µm x 160.6 µm), including at least 10 Z-series with a z-step of 0.30 µm, were acquired using 405, 488, 552 and 638 laser lines or a white laser with optimized wavelengths at the peak of excitation for each fluorophore.

Confocal microscopy for in vivo tissue

Confocal microscopy was performed using an inverted Leica SP8 with 40x or 63x oil immersion objectives with 1.30 and 1.40 numerical aperture respectively, using LasX software. For quantification, 1024x1024 pixel images were acquired using a 40X oil-objective with a numerical zoom of 2, corresponding to a 211.0 µm x 211.0 µm final area, and 10 sections were acquired with a step of 0.30 µm. For 3D reconstruction, images were acquired using the 63x oil immersion objective, and a z-step of 0.20 µm. Deconvolution was carried out using Huygens

software (v.17.10). Following deconvolution, the surface of each structure was reconstructed in 3D using Imaris software (GraphPad, Bitplane, v.9.2).

Figures were made using Photoshop (Adobe, version CC).

Electrophysiology

Myelinated cultured slices (10-13 DIV) were transferred to a recording chamber and continuously superfused with oxygenated (95% O_2 and 5% CO_2) aCSF containing (in mM): 124 NaCl, 3 KCl, 1.25 NaH_2PO_4, 26 $NaHCO_3$, 1.3 $MgSO_4$, 2.5 $CaCl_2$, and 15 glucose (pH 7.4). Purkinje cells were visualized under differential interference contrast optics using a 63X N.A 1 water immersion objective. Loose patch voltage clamp recordings of the spontaneous firing activity was performed at 32-34°C with a borosilicate glass pipette filled with aCSF. Signals were amplified with a Multiclamp 700B amplifier (Molecular devices), sampled and filtered at 10 kHz with a Digidata 1550B (Molecular Devices). Data were acquired with the pClamp software (Molecular devices, version 10.4). To avoid any alteration of the spontaneous firing frequency of the cell by the patch procedure (Perkins, 2006), the holding membrane potential was set to the value at which zero current is injected by the amplifier. The resistance of the seal (R_{seal}) was controlled and calculated every minute from the current response to a voltage step (200 ms; -10 mV). Only recordings with a R_{seal} in the range of 10 to 200MΩ and stable during the all recording procedure were included in the analysis. Spontaneous activity was tested in control condition and consecutively in the presence of apamin (500 nM) and TTX (500 nM) applied by bath perfusion. The firing rate was analysed over a two minutes recording time window using a threshold crossing spike detection in Clampfit (Molecular devices, version 10.4) and calculated as the number of action potential current divided by the duration of the recording. The instantaneous frequency was calculated as the multiplicative inverse of the interspike interval.

Supplementary Figure and Movie legend

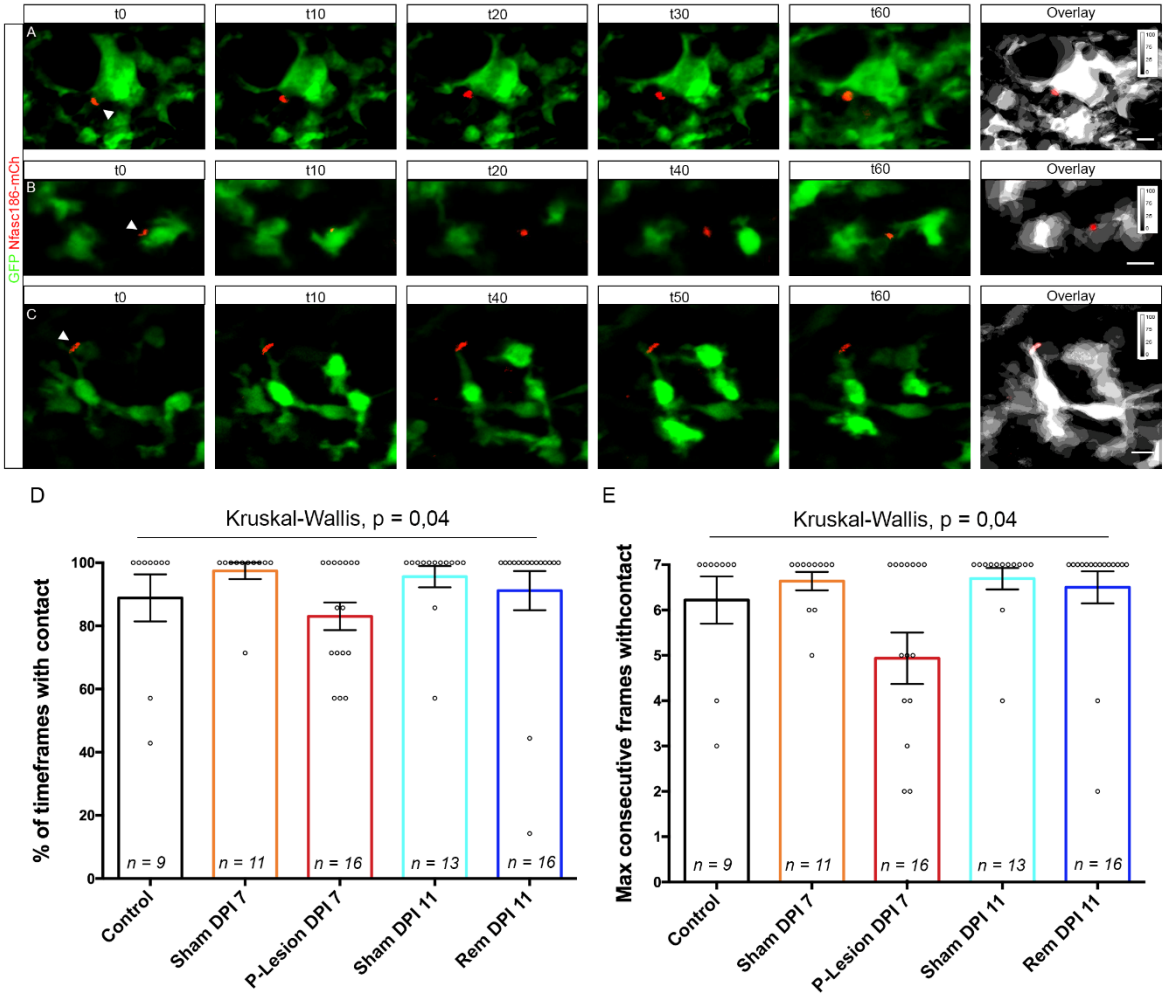

Figure S1

Figure S1. Microglial contacts with nodes of Ranvier are less stable during demyelination. **(A-C)** *In vivo* live-imaging from CX3CR1-GFP/Thy1-Nfasc186mCherry mouse dorsal spinal cord with an initial contact between microglia (green) and nodes of Ranvier (red, arrowheads); 1-hour movies with an acquisition every 10 minutes. **(A)** Sham animal (NaCl injection) imaging at 7 DPI (corresponding to Movie 2); **(B)** LPC-injected animal imaged at 7 DPI (demyelination, corresponding to Movie 3); **(C)** LPC-injected animal at 11 DPI (remyelination, corresponding to Movie 4). **(D)** Percentage of frames with microglia-node contact in 3-hour movies. **(E)** Longest sequence of consecutive timepoints with microglia-node contact in 3-hour movies. Each dot is a microglia-node pair. The number of microglia-node pairs imaged is indicated on each bar (n=4 to 7 animals per condition). (**A**, **B**, **C**) Scale bar 10 µm. (**D**, **E)** Kruskal-Wallis test. Bars and error bars represent the mean ± s.e.m. For detailed statistics, see Supplementary Table.

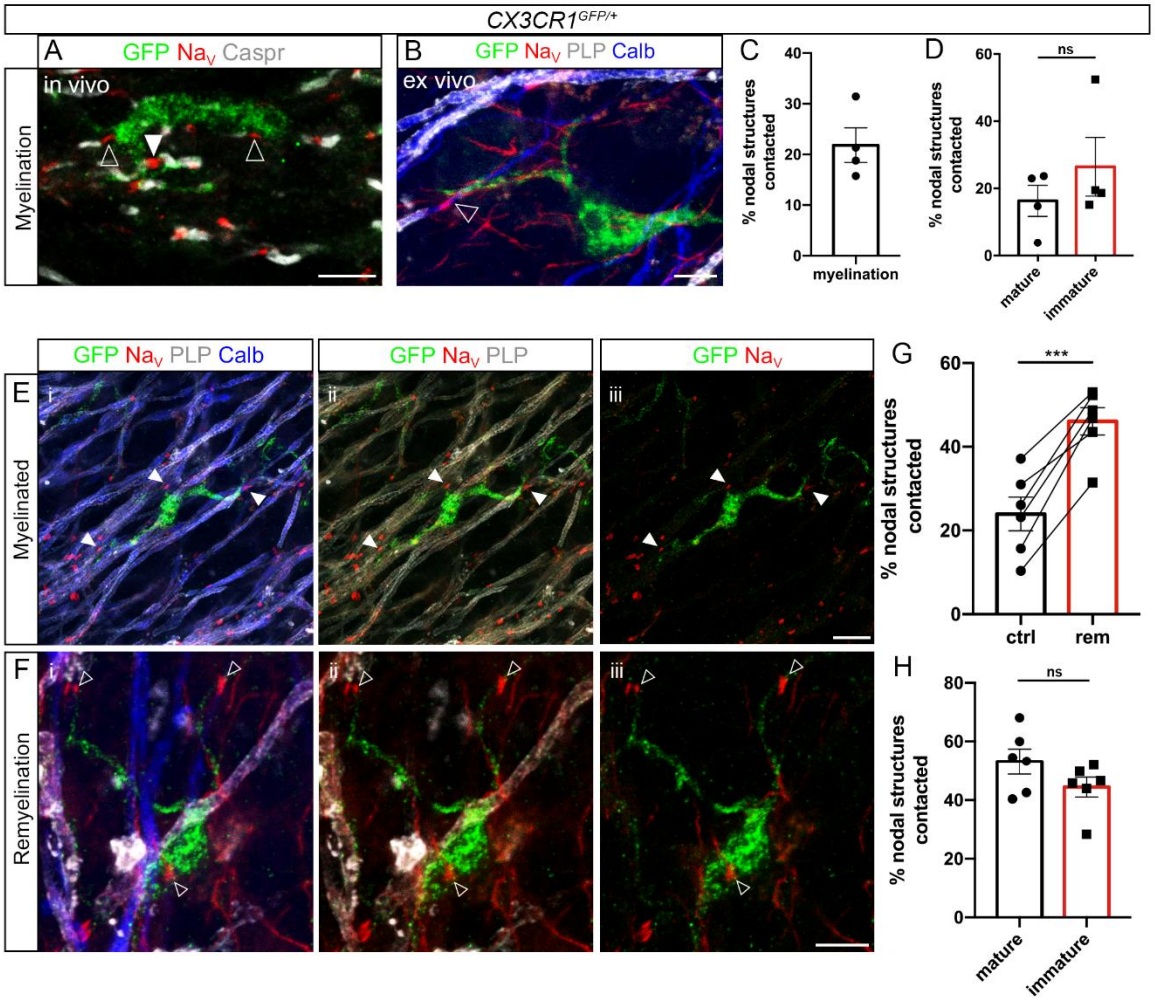
CX3CR1GFP/+
A
GFP Nav Caspr
in vivo
Myelination
B
GFP Nav PLP Calb
ex vivo
C
% nodal structures contacted
myelination
D
ns
% nodal structures contacted
mature
immature
E
GFP Nav PLP Calb
GFP Nav PLP
GFP Nav
Myelinated
i
ii
iii
G
***
% nodal structures contacted
ctrl
rem
F
Remyelination
H
ns
% nodal structures contacted
mature
immature

Figure S2

Figure S2. Microglial cells contact nodal structures in *ex vivo* organotypic cerebellar slice culture. (A, B) Microglia contact nodal structures during myelination in CX3CR1$^{GFP/+}$ mouse cerebellum *in vivo* (**A**, P12) and *ex vivo* (**B**, 4 DIV). Both mature nodes of Ranvier (filled arrowheads) and immature nodal structures (node-like clusters and heminodes, empty arrowheads) are contacted. **(C)** Percentage of nodal structures contacted by microglia in myelinating slices *ex vivo* (n=4 animals). **(D)** Percentage of mature and immature nodal structures contacted in myelinating condition *ex vivo* (n=4 animals per condition). **(E, F)** Microglia also contact nodal structures in myelinated **(E)** and remyelinating slices **(F)** *ex vivo* (11 DIV). Arrowheads indicate the nodes of Ranvier contacted by microglia. **(G)** Percentage of nodal structures contacted by microglia in myelinated (ctrl) vs remyelinating (rem) slices, (n=6 animals per condition). **(H)** Percentage of mature and immature nodal structures contacted in remyelinating condition (n=6 animals per condition). Scale bars: **(A, B)** 5µm, **(E, F, I, J)** 10 µm. **(D)** Wilcoxon matched pairs test; **(G, H)** Paired t-test. *P < 0.05, **P < 0.01, ***P < 0.001, ****P < 0.0001, ns: not significant; bars and error bars represent the mean ± s.e.m. For detailed statistics, see Supplementary Table.

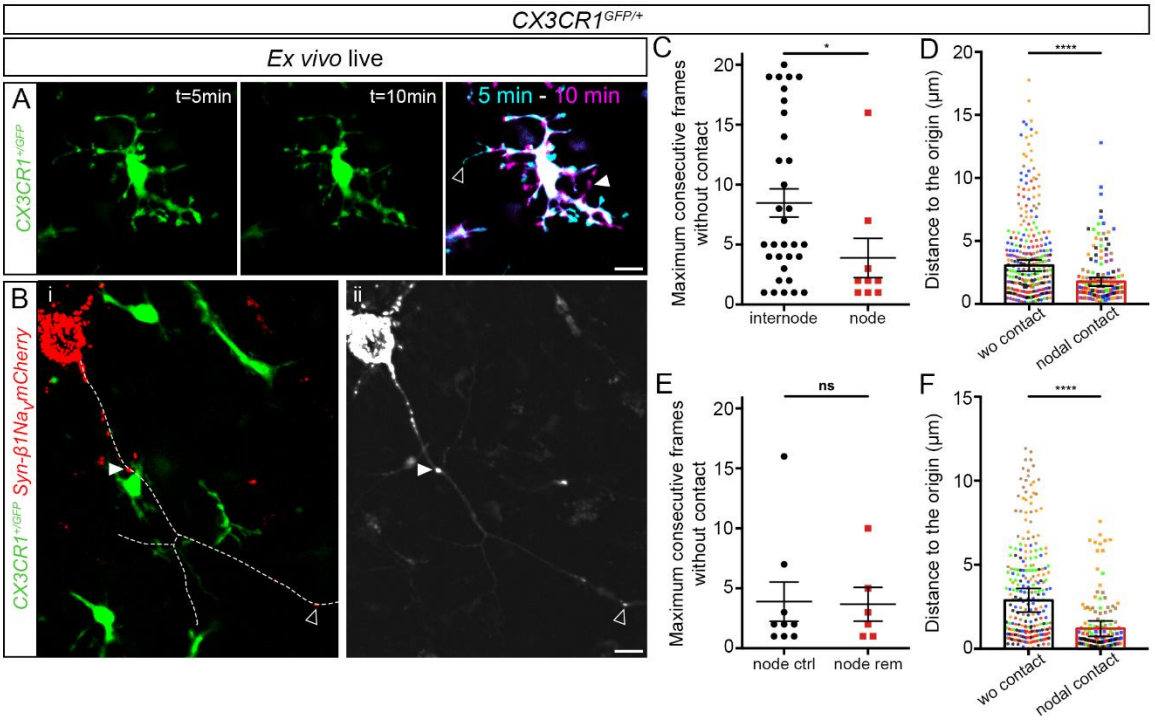
CX3CR1GFP/+
Ex vivo live
A
CX3CR1+/GFP
t=5min
t=10min
5 min - 10 min
B
CX3CR1+/GFP Syn-β1Nav.mCherry
i
ii
C
Maximum consecutive frames without contact
internode
node
*
D
Distance to the origin (µm)
wo contact
nodal contact
****
E
Maximum consecutive frames without contact
node ctrl
node rem
ns
F
Distance to the origin (µm)
wo contact
nodal contact
****

Figure S3. Live-imaging of microglia-node contact in organotypic cerebellar slice culture. (A) Live images of a microglial cell (GFP^+) at two different timepoints, and the corresponding overlay showing the dynamics of the microglial cell, with extending (pink) and retracting (cyan) processes (arrowheads: most dynamic processes). **(B)** Myelinated $CX3CR1^{GFP/+}$ cerebellar slice with a Purkinje cell expressing β1Na_VmCherry following lentiviral transduction. (i) Live-image showing a node ($mCherry^+$, filled arrowhead) contacted by a microglial cell, and a non-contacted node (empty arrowhead). (ii) Summed projection of the movie showing the axon trajectory. **(C)** Maximum duration without contact between a microglial process and an internode or a node in myelinated slices (10 minutes acquisition, internode: n=32 contacts from 16 animals, node: n=9 contacts from 8 animals). **(D)** Distance between the process tip and its position at t0 for each frame, whether the process was initially contacting a node (nodal contact) or without contact (myelinated slices; wo contact: 280 measures from 14 trajectories, n=7 animals; nodal contact: 140 measures from 7 trajectories, n=7 color coded animals). **(E)** Maximum duration without contact between the tip of a microglial process and the node in myelinated vs remyelinating slices (10 minutes acquisition, ctrl: n=9 contacts from 8 animals, rem: n=6 contacts from 6 color coded animals). **(F)** Distance between the process tip and its position at t0 for each frame (remyelinating slices; wo contact: 240 measures from 12 trajectories, n=6 animals, nodal contact: 120 measures from 6 trajectories, n=6 animals). (**A**, **B)** Scale bars: 10 µm **(C, E)** Mann-Whitney test; **(D, F)** Type II Wald chi-square test. *P < 0.05, **P < 0.01, ***P < 0.001, ****P < 0.0001, ns: not significant; bars and error bars represent the mean ± s.e.m. For detailed statistics, see Supplementary Table.

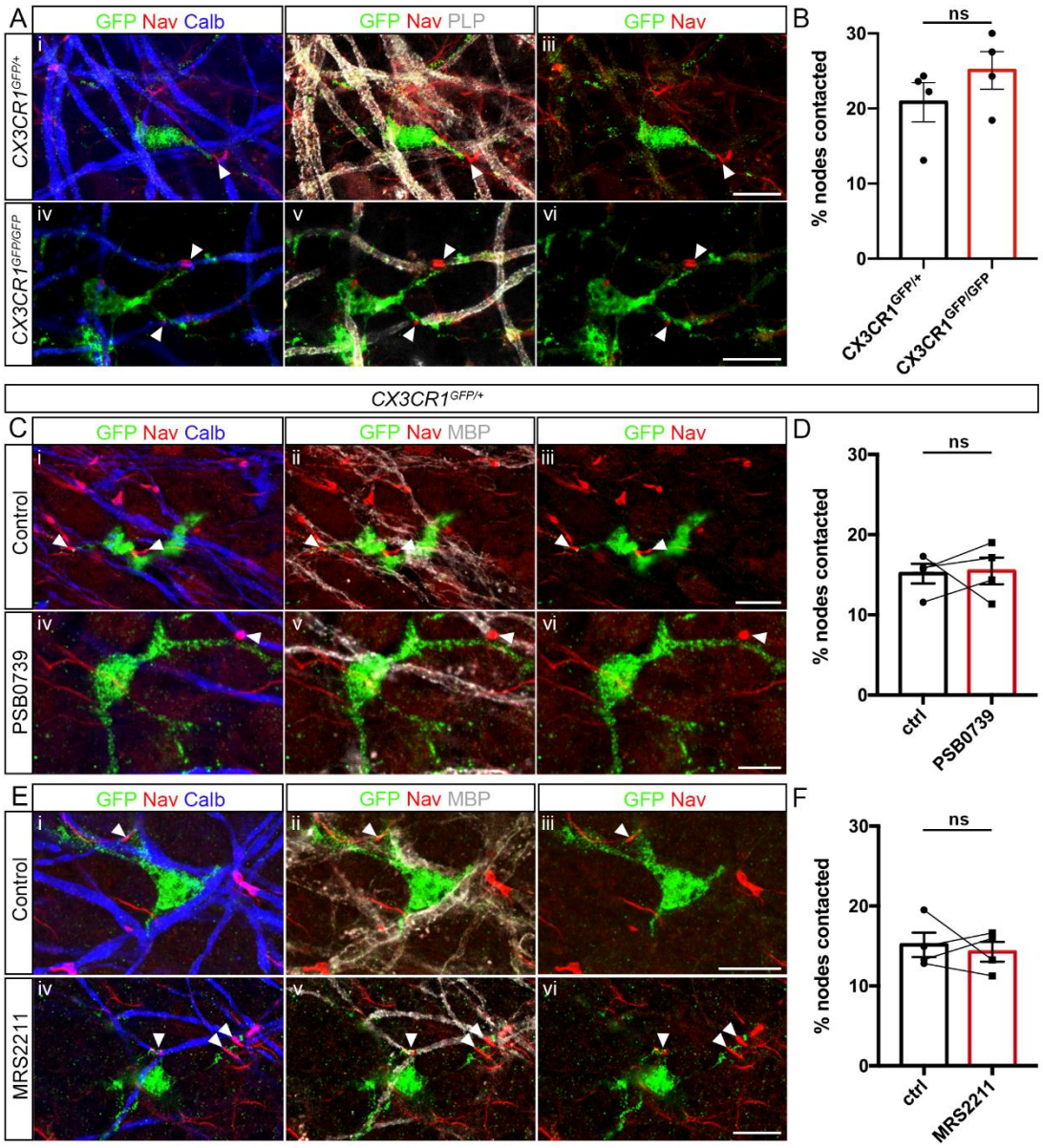
A
GFP Nav Calb
GFP Nav PLP
GFP Nav
CX3CR1GFP/+
CX3CR1GFP/GFP
i
ii
iii
iv
v
vi
B
ns
% nodes contacted
30
20
10
0
CX3CR1GFP/+
CX3CR1GFP/GFP
CX3CR1GFP/+
C
GFP Nav Calb
GFP Nav MBP
GFP Nav
Control
PSB0739
D
ns
% nodes contacted
ctrl
PSB0739
E
GFP Nav Calb
GFP Nav MBP
GFP Nav
Control
MRS2211
F
ns
% nodes contacted
ctrl
MRS2211

Figure S4

Figure S4. The microglial receptors CX3CR1, P2Y12R and P2Y13R are not required for microglia-node interaction. (A) Microglia (GFP, in green) contact nodes (Na_V, in red) both in *CX3CR1*$^{GFP/+}$ and *CX3CR1*$^{GFP/GFP}$ myelinated cerebellar slices. **(B)** Percentage of nodes of Ranvier contacted by microglia in *CX3CR1*$^{GFP/+}$ vs *CX3CR1*$^{GFP/GFP}$ littermate slices (n=4 animals per condition). **(C, E)** Illustration of microglia-node contacts in myelinated slices treated with PSB0739 (**C**, P2Y12R inhibitor, 1 µM, 4-hour treatment) or MRS2211 (**E**, P2Y12R/P2Y13R inhibitor 50 µM, 4-hour treatment). **(D, F)** Percentage of nodes contacted by microglial cells in *CX3CR1*$^{GFP/+}$ myelinated slices in control vs treated condition, with PSB0739 (**D**, 1 µM) or MRS2211 (**F**, 50 µM), n=4 animals per condition. Arrowheads show the nodes of Ranvier contacted by microglial cells. Scale bars: **(A, Ciii, E)** 10 µm, **(Cvi)** 5 µm. **(B)** Mann-Whitney rank test, **(D, F)** Wilcoxon matched pairs test. *P < 0.05, **P < 0.01, ***P < 0.001, ****P < 0.0001, ns: not significant; bars and error bars represent the mean ± s.e.m. For detailed statistics, see Supplementary Table.

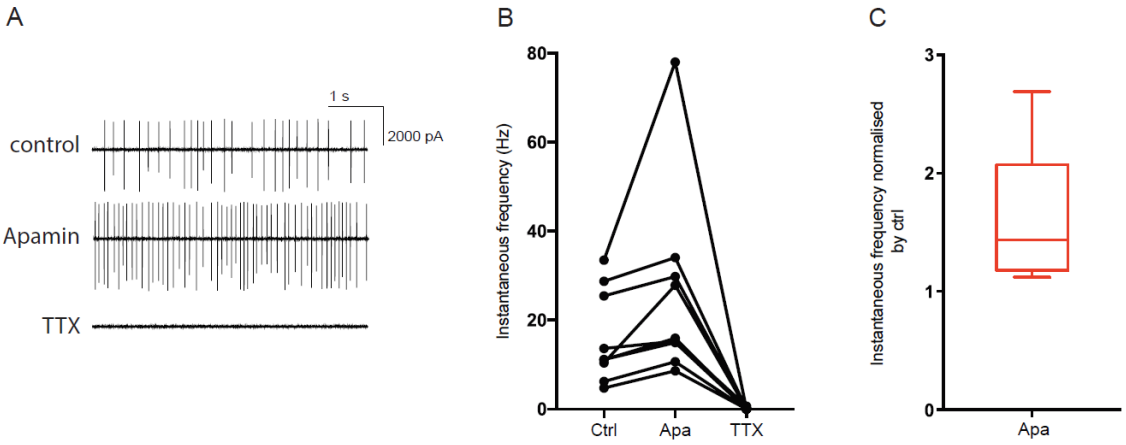
A
1 s
2000 pA
control
Apamin
TTX
B
Instantaneous frequency (Hz)
80
60
40
20
0
Ctrl
Apa
TTX
C
Instantaneous frequency normalised by ctrl
3
2
1
0
Apa

Figure S5. Purkinje cells present spontaneous activity in myelinated organotypic cerebellar slices. (A) Representative example of loose-cell attached recordings on a Purkinje cell, in control condition followed by Apamin (500 nM) and TTX (500 nM) consecutive treatments. **(B)** Instantaneous firing frequencies recorded in Purkinje cells of myelinated cerebellar organotypic slices (n=9 cells, n=7 animals, $p<0.0001$, Friedman test). **(C)** Instantaneous firing frequencies recorded in Purkinje cells in myelinated cerebellar organotypic slices after Apamin treatment, normalized by their matching control. The increased ratio of instantaneous frequencies ranges from 1.12 to 2.69 (n=9 cells, n=7 animals; center line, median; box limits, upper and lower quartiles; whiskers, min and max). *P < 0.05, **P < 0.01, ***P < 0.001, ****P < 0.0001, ns: not significant; bars and error bars represent the mean ± s.e.m. For detailed statistics, see Supplementary Table.

Movie 1 (associated to Figure 2). Stable interaction between a node and a microglial cell along time.

Representative example of a 3-hour movie from a CX3CR1-GFP/Thy1-Nfasc186mCherry mouse showing a stable interaction between a microglial cell (green) and a node of Ranvier (red). Acquisitions every 30 minutes. Sham animal (NaCl injection) DPI 11. Filled arrowheads indicate contact, empty arrowheads an absence of contact. Scale bar: 10µm.

Movie 2 (associated to Figure S1). Stable interaction between a node and a microglial cell in control condition. Representative example of a 1-hour movie from a CX3CR1-GFP/Thy1-Nfasc186mCherry mouse allowing to observe interactions between microglia in green and nodes of Ranvier in red. Acquisitions every 10 minutes. Sham animal (NaCl injection) DPI 7. Filled arrowheads indicate contact, empty arrowheads an absence of contact. Scale bar: 10µm.

Movie 3 (associated to Figure S1). Unstable interaction between a node and a microglial cell in the perilesional tissue in demyelinating context. Representative example of a 1-hour movie from a CX3CR1-GFP/Thy1-Nfasc186mCherry mouse allowing to observe the intermittent interaction between microglia in green and nodes of Ranvier in red. Acquisitions every 10 minutes. LPC injection DPI 7 (perilesional area, peak of demyelination). Filled arrowheads indicate contact, empty arrowheads an absence of contact. Scale bar: 10µm.

Movie 4 (associated to Figure S1). Stable interaction between a node and a microglial cell during remyelination. Representative example of a one-hour movie from a CX3CR1-GFP/Thy1-Nfasc186mCherry mouse allowing to observe stable interactions between microglia in green and nodes of Ranvier in red. Acquisitions every 10 minutes. LPC injection DPI 11 (remyelination). Filled arrowheads indicate contact, empty arrowheads an absence of contact. Scale bar: 10µm.

Movie 5 (associated to Figure 4). A microglial process tip contacting an internode in a myelinated slice. Representative example showing a microglial cell (green) initially contacting an internode (red) in a myelinated slice. Filled arrowheads indicate a contact, and empty arrowheads an absence of contact. The dashed line represents the axon. Scale bar: 5µm.

Movie 6 (associated to Figure 4). A microglia process tip contacting a node in a myelinated slice. Representative example showing a microglial cell (green) initially contacting a node (red)

in a myelinated slice. Filled arrowheads indicate a contact, empty arrowheads an absence of contact. The dashed line represents the axon. Scale bar: 5µm.

Movie 7 (associated to Figure 4). A microglia process tip contacting a node in a remyelinating slice. Representative example showing a microglial cell (green) initially contacting a node (red) in a remyelinating slice. Filled arrowheads indicate a contact, empty arrowheads an absence of contact. The dashed line represents the axon. Scale bar: 5µm.

Movie 8 (associated to Figure 6). Microglia process tip contacting a node in a myelinated slice treated with TEA. Representative example showing a microglial cell (green) initially contacting a node (red) in a myelinated slice treated with TEA. Filled arrowheads indicate a contact, empty arrowheads an absence of contact. The dashed line represents the axon. Scale bar: 5µm.

NODE-MICROGLIA INTERACTION IN MS TISSUE

I. Introduction

In the first part of my thesis, we characterized, using experimental models, the existence of an interaction between microglia and nodes of Ranvier, the mechanisms underlying this interaction and its potential role in repair. We highlighted a correlation between this interaction and a microglial switch towards a pro-regenerative phenotype. Others have shown a role of this switch in remyelination (Miron et al., 2013) and deciphered how this switch is modulated by adaptative immune cues (El Behi et al., 2017). However, to our knowledge, the relationship between microglia contacts at the nodes and microglial phenotypes has not been studied in human tissue. Yet, deciphering these interactions in healthy and MS contexts could pave the way to new therapeutical strategies for repair.

First, the ability to distinguish in the brain, microglia, the CNS resident immune cells, from monocyte-derived macrophages is quite recent. Previously non-specific markers were used such as MHCII or CD68, that were unable to distinguish the two types of cells. Transmembrane protein 119 (TMEM119), a cell-surface protein, was found to be specific to microglia (i.e. derived from the yolk sac) (Bennett et al., 2016; Butovsky et al., 2014; Satoh et al., 2016). Then, P2Y12r, a metabotropic purinergic receptor (Hollopeter et al., 2001), was used to identify homeostatic microglia (M0) (Mildner et al., 2017). Thus, these two markers recently expanded our ability to study specifically microglial phenotypes in human tissues. As already reported above, Zrazvy at al. (Zrzavy et al., 2017) showed that homeostatic microglia stained with P2Y12r antibodies was significantly reduced in NAWM compared to controls and completely lost in active and chronic active lesions. Analysis of TMEM119, demonstrated that on average 45% of the macrophage-like cells in active lesions were derived from the microglial pool. These results demonstrate the loss of the homeostatic microglial signature in active multiple sclerosis. Yet, such a study in shadow plaques has not been performed. We were interested by two related questions : i) Is resident microglia present in shadow plaques and in such a case, which are the predominant phenotypes? ii) Is microglia-node interaction taking place in MS human tissues as in experiental model of MS? And in line with this second question, does frequency of nodes contacted depends on the lesional context?

To address these questions, we first analyzed microglial phenotypes in shadow plaques in comparison with controls, NAWM or (chronic) active lesions. We further studied node-microglia interaction depending on microglial phenotypes and lesion types, in particular at the

vicinity of active lesions or mixed active/inactive lesions (rim) and in shadow plaques, compared to NAWM or tissues from healthy donors.

II. Materials & methods

Tissue preparation

Human tissues (UK MS Society Tissue Bank at Imperial College, London, under ethical approval by the National Research Ethics Committee 08/MRE09/31) were obtained as snap frozen blocks. MS and control cases characterization is presented in Table 1. Sections were cut using a cryostat Leica CM 1950 (15 µm thick), collected on Superfrost+ slides and stored at -80°C until used.

Chromogenic immunohistochemistry

Snap frozen tissue blocks were rehydrated with PBS. Sections were then immersed in 4% PFA for 10 minutes before elimination of endogenous peroxidase activity with 0.1% H2O2 (Sigma Aldrich) in PBS for 20 minutes. Blocking was performed using 5% Normal Goat Serum before incubation with primary antibodies diluted in PBS containing 0.05% Triton 100-X and 5% sera. The biotinylated secondary antibody targeting one of the primary antibodies (Vector Laboratories) was visualized with the avidin-biotin horseradish peroxidase complex (Dako, Biotin Blocking System) followed by 3,3'-diamino-benzidine (DAB) (Vector Laboratories) as substrate. All sections were counterstained with haematoxylin. Images were captured with a slide scanner nanozoomer (Hamamatsu).

Fluorescent immunostainings

Human sections were first fixed in 4% PFA for 5 minutes. For myelin protein staining, tissues were preincubated in absolute ethanol at -20°C for 20 min. Tissues were blocked in PBS, 5-10% Normal Goat Serum (50-062Z; Thermo Fisher Scientific), 0,2-0,4% Triton X-100 (RDTH), then incubated with primary antibodies in blocking solution overnight at room temperature, washed in PBS and incubated with secondary antibodies for 1-3 hours at RT in the dark. When applicable, tissues were immersed for 30s in Hoechst solution (10 µg/ml, Euromedex). They were finally mounted under coverslip (VWR) with Fluoromount (Southern Biotech). Primary antibodies used are in Table 2.

Imaging

Confocal microscopy was performed using an inverted Leica SP8 with 40x or 63x oil immersion objectives with 1.30 and 1.40 numerical aperture respectively, using LasX software. For quantification, 1024x1024 pixel images were acquired using a 40X oil-objective with a

numerical zoom of 2, corresponding to a 211.0 µm x 211.0 µm final area, and 10 sections were acquired with a step of 0.30 µm. Figures were made using Photoshop (Adobe, version CC).

Analysis

For quantifications of the percentage of nodes contacted, imageJ software was used to adjust the brightness and contrast of the images and to quantify the total number of nodal structures and the number of structures contacted per field using the middle plan of each Z-series, the rest of the series being used to confirm the nature of the contacted structure. Evaluations were made blind for condition. A contact was defined by at least one positive pixel for the microglial marker juxtaposed to at least one pixel positive for the nodal marker. Three images were analyzed per lesion with four to six lesions per condition and the mean percentage of contact per condition was calculated by doing the mean of the mean percentage of contact per lesion.

Statistical analysis

Statistical analysis was performed with Prism (GraphPad, version 7). Graphs and data are reported as the mean ± SEM. The level of statistical significance was set at $p < 0.05$ for all tests. Asterisks denote statistical significance as follow: *$p < 0.05$, **$p < 0.01$, ***$p < 0.001$, ****$p < 0.0001$, ns. indicates no significance. Significance of the main effect was evaluated with the Anova function. Post-hoc multiple comparisons tests used Tukey's test.

Table 1: MS and control cases summary

	Sex	Age	Death to tissue preservation (hours)	Disease course	Disease duration (years)	Lesion types
MS160	F	44	18h	SP	16	A, I, S
MS166	F	52	7h	SP	36	N, A, S
MS179	F	70	20h	SP	>21	N, CA, S
MS180	F	44	9h	SP	>10	A
MS187	F	57	13h	SP	>27	N, I, S
MS207	F	46	10h	SP	25	N, A, CA, I, S
MS275	F	63	11h	SP	34	S
MS317	F	48	21h	SP	29	N, A, CA, S
C028	F	60	13h	-	-	-
C049	M	85	23h	-	-	-
C054	M	66	16h	-	-	-
C064	F	63	21h	-	-	-
C074	F	84	22h	-	-	-

N: NAWM; A: Active lesion; I: Inactive lesion; CA: Chronic Active lesion; S: Shadow plaque

Table 2: Antibodies used

Antibody	Origin	Target	Dilution	Source
α-Nav	Mouse, IgG1	α-subunits of Nav channels	1:400	Sigma, Clone K58/35
AnkG	Mouse, IgG2b	AnkyrinG	1:100	Neuromab, clone N106/65
TMEM119	Rabbit, polyclonal	Transmembrane protein 119	1:100	Sigma, HPA051870
P2Y12r	Rabbit, polyclonal	Purinergic receptor	1:300	Alomone
p22phox	Mouse, IgG1	NADPH oxidase protein	1:100	Santa Cruz, sc-130551
MHCII	Mouse, IgG1	MHC Class II antigen	1:100	Dako, clone CR3/43

III. Results

Tissue characterization

To classify the lesions, we used two consecutive slides for each block: one slide was stained with MOG antibodies for myelin, the other with MHCII antibodies for macrophages/microglia (Fig.1). Active lesions were defined by the absence of MOG staining and an intense invasion of foamy macrophages inside the lesion. Mixed active/inactive lesions were defined by the presence of a rim of macrophages at the lesion edge. Shadow plaques were defined by the presence of a pale MOG staining compared to normally myelinated areas (NAWM). The mean age of our controls (5 cases) was 71.6+/-5.4 versus 53+/-3.4 for MS cases (8 cases) (Table 1). MS cases were all women and SPMS. We studied, in our 8 MS cases, 5 active lesions, 6 shadow plaques and 3 chronic active lesions.

Characterization of microglia in shadow plaques

We first verified the presence of resident microglia (TMEM119+) in shadow plaques (Fig.2A). We further confirmed the presence of homeostatic microglia (P2Y12r+) (Fig.2B). Next, we performed a microglial double staining for P2Y12r and MHCII (Fig.3C). This latter marker is for activated microglia or MD-macrophages without specificity. Most cells were P2Y12r+/MHCII+, whereas P2Y12r+/MHCII- corresponded to 21+/-4% of stained cells in shadow plaques, showing the reappearance of homeostatic cells in this tissue (Fig.3C-D). Interestingly, MHCII+/P2Y12r- cells were scarce (<1%) (Fig.3D). To further confirm the activated signature of microglial cells in shadow plaques, we asked whether TMEM119+ resident microglia could express p22phox, a pro-inflammatory marker. We show that most resident microglial cells (TMEM119+) express p22phox suggesting a sustained inflammatory activity in remyelinating(ed) areas (Fig.4C).

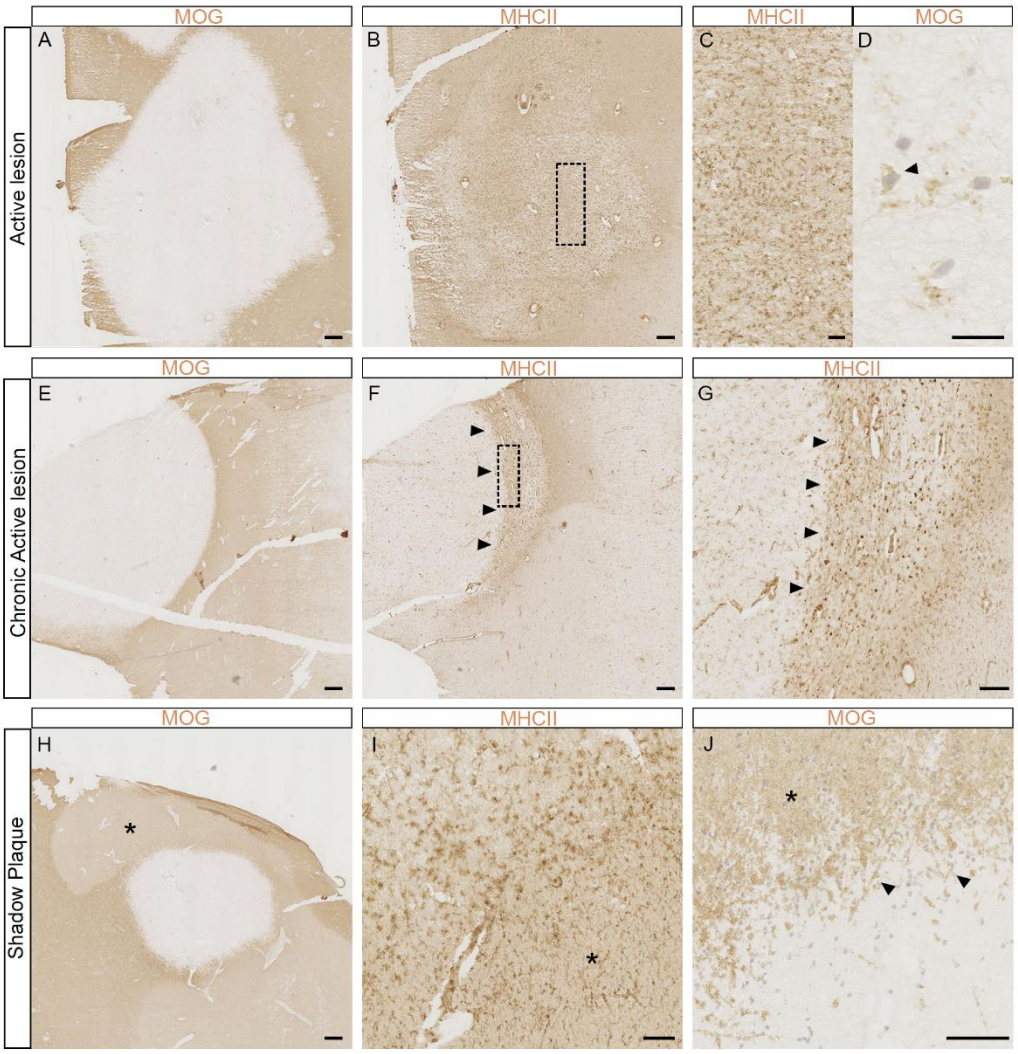

Figure 1. Classification of MS lesions

(A-J) MOG or MHCII staining associated with hematoxylin coloration (A-D) Active lesion: (A) Complete demyelination with sharp limit of lesion; (B) High density of foamy macrophages inside the lesion; (C) Zoom corresponding to the boxed area in (B); (D) Macrophages inside the lesion with cytoplasmic myelin debris (arrowhead). (E-G) Chronic Active lesion: (E) Complete demyelination with sharp limit of lesion; (F) Moderate density of macrophages inside the lesion and rim of macrophages at the lesion edge (arrowheads); (G) Zoom on the rim of macrophages (arrowheads) corresponding to the boxed area in (F). (H-J) Shadow plaque (asterisk) in the vicinity of an active lesion: (H) area with a pale MOG staining characteristic of a shadow plaque (asterisk); (I) Moderate density of ramified macrophages (asterisk) compared to active lesion beside; (J) shadow plaque edge (asterisk) showing ongoing remyelination (arrowhead). Scale bars: (A-B; E-F; H) 500 µm; (G) 200 µm; (C; I-J) 100 µm; (D) 25 µm.

Resident microglia contact nodes of Ranvier

We previously observed microglial contacts at nodes of Ranvier in human control tissues, and thus wanted to address whether this was still the case in MS context. To answer this question, we performed TMEM119 and P2Y12r staining in consecutive slides associated with a nodal staining (Nav) in controls, NAWM and shadow plaques (Fig.2). In controls, 28.6+/-3.3% of nodes were contacted by P2Y12r+ cells and 19.61+/-3.0% by TMEM 119+ cells. These percentages of interaction are relatively similar to what we observed in our experimental models in control condition. Surprisingly, nodes are significantly more contacted by P2Y12r+ cells than TMEM119+ cells ($p=0.041$), while the mean microglial density was similar for both staining (3.6+/0.3 and 3.6+/-0.4 respectively per area). These results confirm that resident microglia, especially homeostatic microglia, interact with axons at nodes of Ranvier.

We then studied NAWM and shadow plaques and detected microglia-node contacts in both conditions. Interestingly, regarding P2Y12r cells, the percentage of contacted nodes decreased in NAWM compared to controls (15.7+/-1.5% vs. 28.6+/-3.3% respectively, $p=0.002$). On the contrary, in shadow plaques, the percentage of nodes contacted was similar to controls (25.62+/-1.2% vs. 28.62+/-3.3%, ns), underlying a potential role of node-microglia interaction during repair. To exclude that this difference might simply reflect a variable density of P2Y12r+ cells, we measured the density of P2Y12r+ cells in all three conditions without observing statistical differences (Fig.3D). We also checked the node of Ranvier density which was similar between control and NAWM (mean of 233+/-16 vs. 256+/-29 nodes) and slightly decreased in shadow plaques (mean of 189+/-13 nodes, ns). This latter result could partly participate to the higher percentage of nodes contacted in shadow plaques compared to NAWM. With TMEM119+ cells, we observed the same tendency without statistical significance (19.61+/-3.0% in controls vs. 15.73+/-1.5% in NAWM vs. 25.43+/-0.7% in shadow plaques, ns). These results suggest an impaired interaction in NAWM compared to control tissue, and a restored interaction in shadow plaques.

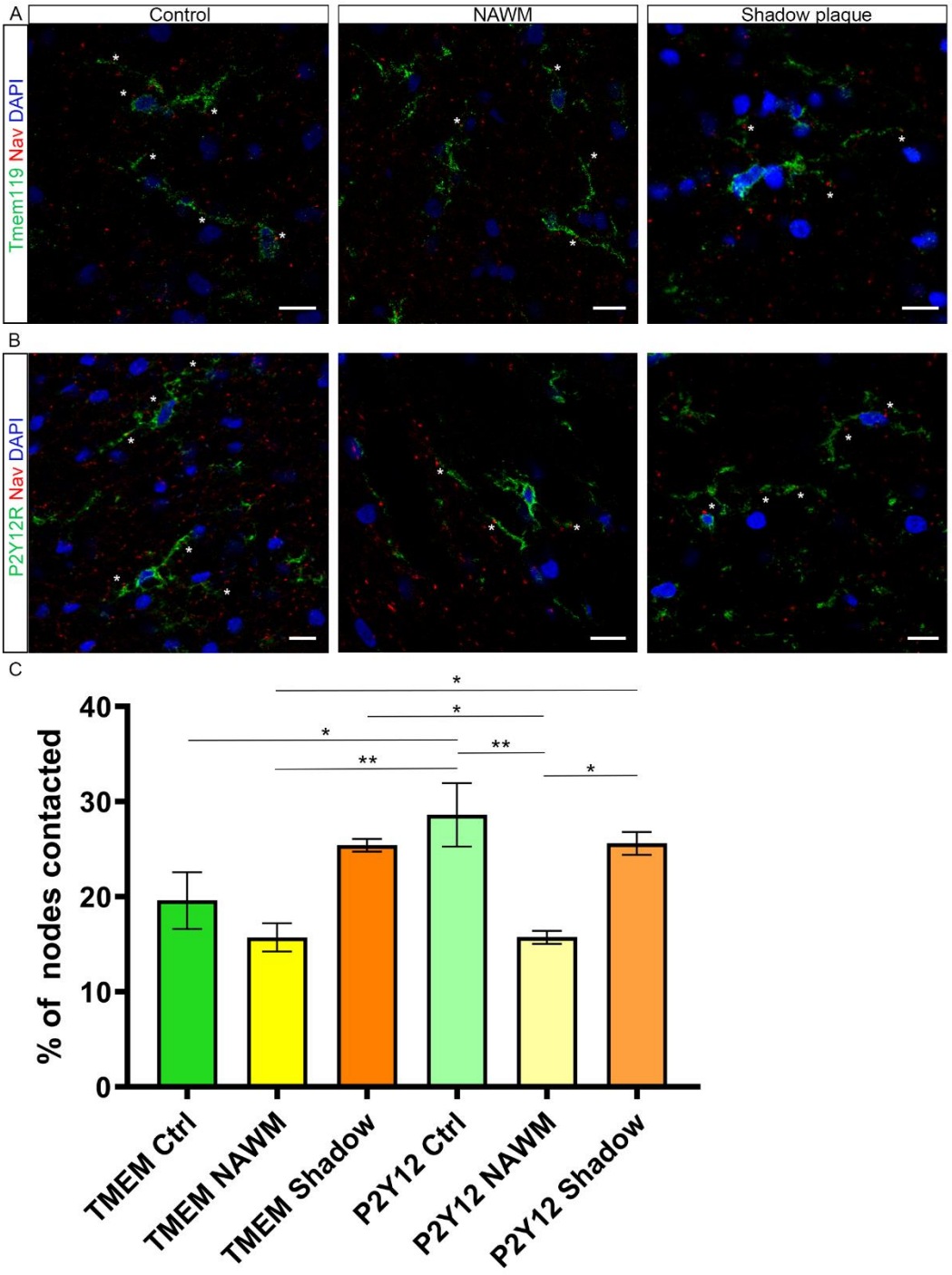

Figure 2. Resident microglia contact nodes of Ranvier in MS

(A) Resident microglial cells (TMEM119+; green) contact nodes of Ranvier (Nav, red) in control, NAWM and shadow plaques (asterisks). (B) Homeostatic microglial cells (P2Y12r+; green) contact nodes of Ranvier (Nav, red) in control, NAWM and shadow plaques (asterisks). (A-B) Scale bars 10 µm. (C) Diagram showing the percentage of contacted nodes of Ranvier for each condition, one-way ANOVA with Tukey's post-hoc comparison tests, * $p<0.05$, ** $p<0.01$, ***$p<0.001$. NAWM=normal appearing white matter.

Interactions are observed with various microglial phenotypes

We further performed a double staining for P2Y12r and MHCII, together with AnkyrinG to visualize the nodes of Ranvier, to address whether activated microglia also contacted nodes of Ranvier (Fig.3). Surprisingly, P2Y12r+/MHCII- (dark arrowhead) cells represent only about 11.8 and 11.3% of stained cells in controls and NAWM respectively, with the majority being double positive P2Y12r+/MHCII+ cells, therefore corresponding to activated microglia (Fig.3D). All the stained cells contact nodes regardless of the tissue condition (control, NAWM or shadow plaque; Fig.3D). This suggests that in human tissues, activated microglia indeed contact nodes of Ranvier.

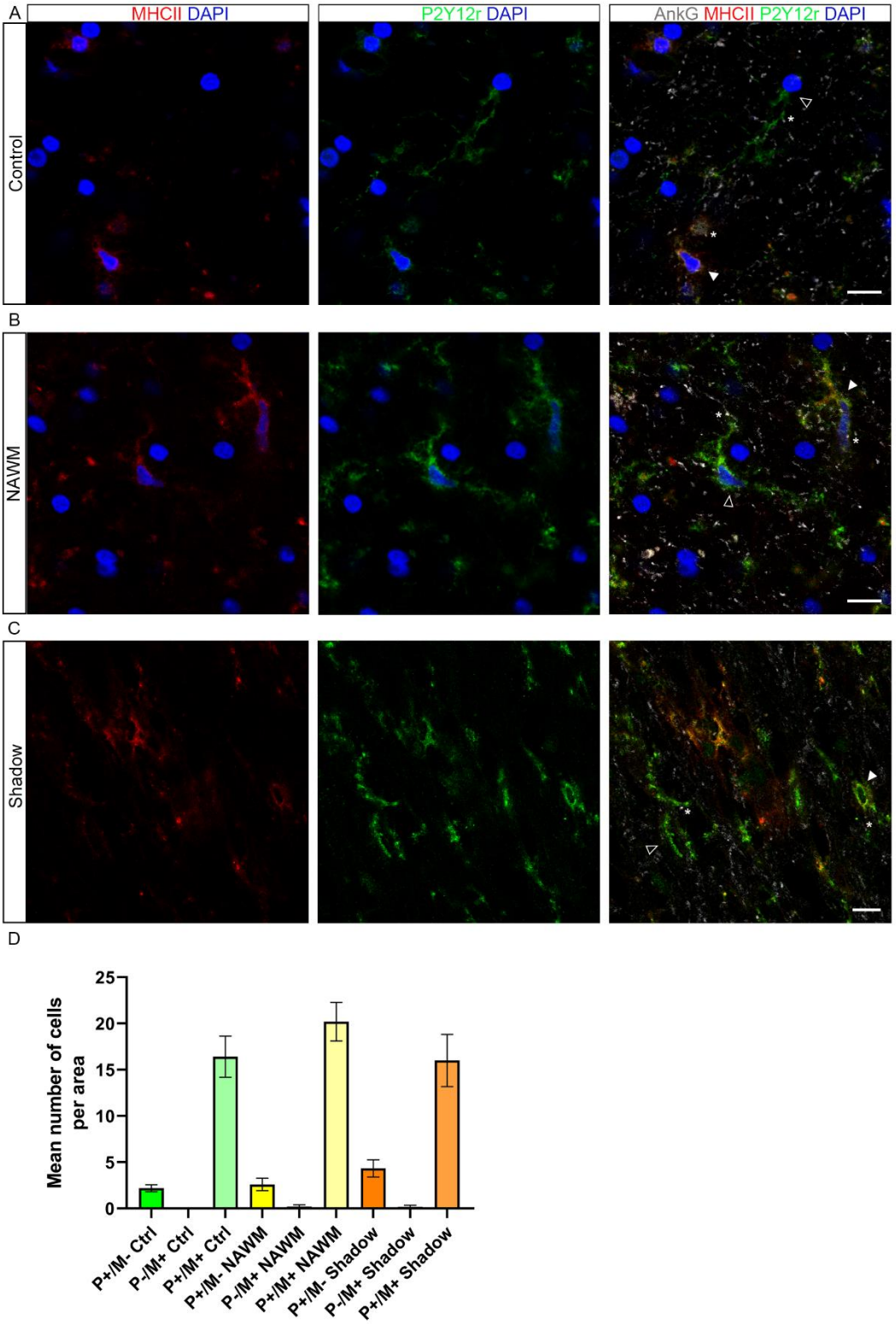

Figure 3. Microglia express the homeostatic marker P2Y12R in shadow plaques as in control or NAWM

(A-C) P2Y12r+/MHCII+ cells (white arrowheads) and P2Y12r+/MHCII- cells (dark arrowheads) contact nodes of Ranvier (AnkyrinG, white) (asterisks) in control (A), NAWM (B), and shadow plaques (C). (C) Most of MHCII+ cells are expressing P2Y12r in shadow plaques. (D) Expression profile of microglial cells. Mean cell number per area. Ctrl: control; NAWM: normal appearing white matter; Shadow: shadow plaque; P: P2Y12r; M: MHCII. Scale bars 10 µm.

Interactions are observed at the vicinity of various types of lesions including in inflammatory areas (Fig.4)

We next addressed whether microglia-node contact was altered in perilesional tissue, using p22phox (for inflammatory microglia) and TMEM119 (for resident microglia) double staining in (chronic) active lesions. First, we confirmed previously published results (Zrzavy et al., 2017) showing that TMEM119 positive cells are present in periplaque white matter (PPWM) and in the rim of chronic active lesions (Fig.4A-B). In these conditions, we focused on p22phox+ cells, a pro-inflammatory marker. As expected, some of these cells concomitantly expressed TMEM119, thus confirming that resident microglia and blood-derived macrophages can adopt a pro-inflammatory phenotype in this context. Interestingly, we observed that all p22phox+/TMEM119+ were contacting nodes of Ranvier, confirming that pro-inflammatory microglia can interact with nodes of Ranvier and that this interaction could also have a role during inflammation.

Finally, we focused on shadow plaques. Similarly, all p22phox+/TMEM119+ cells contacted nodes of Ranvier (Fig.4C). Taken together, these results show that microglial cells contact nodes of Ranvier in human tissue independently of the pathological context and their activation status.

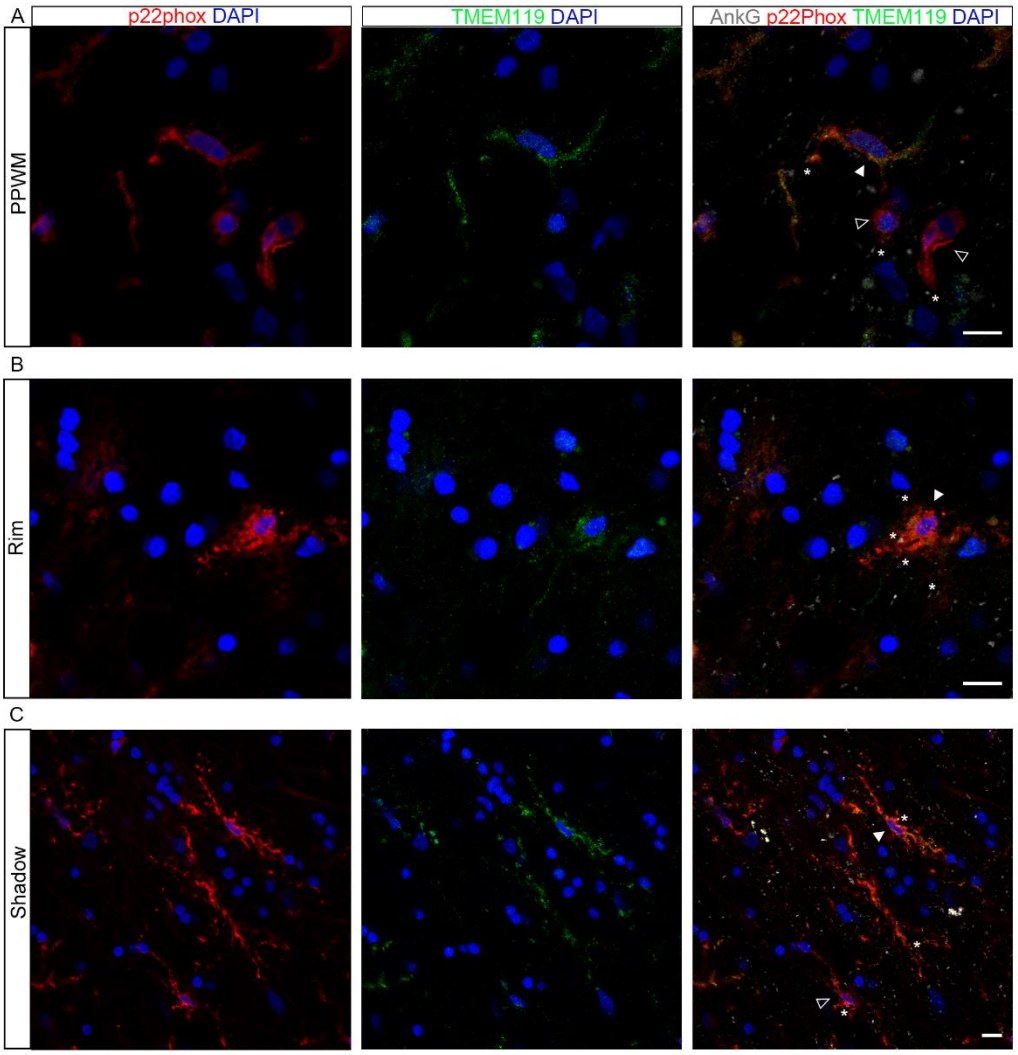

Figure 4. Pro-inflammatory microglia participate in node-microglia interactions in MS including in remyelinating areas.
(A-C) p22phox+/TMEM119+ cells (white arrowheads) and p22phox+/TMEM119- cells (dark arrowheads) contact nodes of Ranvier (AnkyrinG, white) (asterisks) in PPWM of active lesion (A), in the rim of chronic active lesion (B), and in shadow plaques (C). (C) Multiple p22phox+ cells are present in shadow plaques and most of TMEM119+ cells express p22phox. Scale bars: 10 µm. PPWM=peri-plaque white matter.

IV. Discussion

Reduced microglia-node interaction in NAWM compared to controls

Here, we show that resident microglia can contact nodes of Ranvier in control as well as in MS human tissue. Furthermore, using P2Y12r antibody, we showed a significant decrease of the percentage of nodes contacted by homeostatic microglia in NAWM compared to controls. We checked whether it could have been due to a difference in the nodal or microglial density, which is not the case. The constant density of homeostatic microglia that we detected is contradicting the results obtained by, Zrzavy et al., who reported a decrease of P2Y12r+ cells in NAWM compared to controls (Zrzavy et al., 2017). This could be due to the nature of the samples used (71,6 years old in our case vs. 61,3 years old in Zravy et al., SPMS in our study vs RRMS and SPMS cases in Zravy's study), as it is known that microglia tend to become activated with age (Griffin et al., 2006; Letiembre et al., 2007; Perry et al., 1993).

Surprisingly, we found that most of P2Y12r+ cells in controls and NAWM also expressed MHC-II (about 90%). Zrzavy et al. previously showed similar results without reaching this proportion (Zrzavy et al., 2017). However, their quantifications were not performed using double staining. Furthermore, these discrepancies could be due to the MHCII we used which differs from theirs, or the characteristics of the samples we used described above. Moreover, Locatelli et al. showed that very different microglial populations (according to their metabolic profile, identified through RNA-sequencing) could have very similar cytokine and activation marker expression profile. This "mixed" microglial profile could be due to a real co-expression of the markers, or to a slow turn-over of one of the markers considered, whereas corresponding genes are no longer expressed. Post-translational modifications or localization of these markers within the cells could also temper with the functional properties of the microglial cells co-expressing them.

Node-microglia interaction is preserved near active lesions

Interestingly, using an *in vivo* live-imaging approach in a mouse experimental model we showed that in the vicinity of a demyelinating lesion, microglia interactions at nodes are less stable, though the frequency of node contacted was similar to controls. Here, we showed that in post-mortem MS tissue, TMEM119/p22phox double-positive cells interact with nodes near (chronic) active lesions. Conclusions regarding the stability of these latter interactions

are however difficult to draw from post-mortem human tissue. To determine whether these interactions are positive or deleterious in an inflammatory context, we could characterize axonal health status to search for a correlation with the microglial profile contacting nodes in a given area.

Node-microglia interaction restored in shadow plaques

Regarding shadow plaques, we observed a similar percentage of nodes contacted by microglia compared to controls, suggesting a restored interaction following nodal reclustering and myelin repair. In mouse tissue, this percentage of interaction was higher in remyelinated areas, and the contacts more stable than in control condition, suggesting an even reinforced interaction.

Next, using a co-staining with MHCII (activated microglia or macrophages) and P2Y12r (homeostatic resident microglia) we observed that 20% of cells in shadow plaques were P2Y12r positive and MHCII negative. Zrzavy et al. showed previously that P2Y12r cells were absent of active lesions (Zrzavy et al., 2017). Thus, our results suggest that homeostatic microglia are reinstalled in remyelinating(ed) areas. Whether it is consecutive to a switch from former active microglia or to homeostatic cells re-entering in shadow plaques remain to be deciphered.

Finally, we surprisingly observed that most of TMEM119+ cells in shadow plaques expressed p22phox suggesting that inflammation is still at play. We know that pro-inflammatory microglia play a role in repair (Cunha et al., 2020; Miron et al., 2013). Here, however we do not know whether the studied shadow plaques are remyelinating or fully remyelinated. Discriminating with accuracy these different remyelinating stages could be of interest to more precisely decipher the role of p22phox+/TMEM119+ cells in repair, and to see whether they are transient or persistent within shadow plaques. To do so, RNA-sequencing of OLs allowing to define specific subclusters according to lesion type is a promising avenue (Jäkel et al., 2019).

Future perspectives

Our next step will be to better characterize microglia phenotype in shadow plaques using "pro-regenerative" markers as CCL22, CD206 or CD163. Indeed, knowing that p22phox positive cells are extensively present in shadow plaques, can they cohabit with "pro-regenerative" cells? Could these latter cells contact nodes of Ranvier? It would be also helpful to use other pro-inflammatory markers such as CD68 for phagocytosis or iNOS for nitric oxide radical production as our results could suggest p22phox is not that specific of inflammation. These future observations would be valuable to decipher repair mechanisms through node-microglia interactions.

To go further, it will be of interest to repeat this study in different CNS areas such as spinal cord or cerebellum, two areas with bad prognosis following demyelination, as they poorly remyelinate (Goldschmidt et al., 2009). Could node-microglia interaction correlate with these different evolutions? In case all microglial cells contact nodes regardless of the CNS area or the lesion type, one can hypothesize that the neuronal status will then influence microglial behavior.

To conclude, node-microglia interaction takes place in control and MS human tissues and is altered in NAWM. Homeostatic microglia reappear in shadow plaques despite the persistence of inflammatory microglia and node-microglia interaction is restored following nodal reclustering in these areas. Our team has previously shown reclustering of nodal proteins prior to (re)myelination in some neuronal populations, both in experimental models and in shadow plaques in MS tissues (Coman et al., 2006; Freeman et al., 2015; Lubetzki et al., 2020). Thus, it could be interesting to address whether microglia can contact these node-like clusters in human remyelinating tissues, and in which proportion, to highlight a potential early role in repair.

Our present results confirm and expand our previous data, highlighting node-microglia interaction as a potential player in neuro-glial crosstalk during health and repair in human CNS tissue.

GENERAL DISCUSSION

Multiple sclerosis is a CNS inflammatory demyelinating pathology. It is also a neurodegenerative disease, without available treatments able to slow progression of disability. Thus, new treatments enhancing repair and neuroprotection are an unmet need. To better decipher repair mechanisms following a demyelinating insult is a crucial step towards this goal. Here we propose new insights in the microglial-neuron crosstalk participating in remyelination processes.

During my PhD, I showed a stable interaction between nodes of Ranvier and microglia in various mice CNS areas and in human tissues. We demonstrated that this interaction is observed whatever the tissue status (i.e. control, demyelinating area or remyelinating area) or the microglial phenotype, with a decreased stability in demyelinating conditions in mice and a decrease of contact frequency in NAWM of MS tissues. Our results provide further evidence for a role of microglia-node contact in microglial switch toward a pro-repair phenotype during remyelination and suggest that this interaction plays a role in the remyelination process.

I. Characteristics of node-microglia interaction in control tissue

We first showed that multiple contacts are present between microglia and nodes of Ranvier in various areas of the mouse CNS. We showed that the percentage of contacted nodes is around 20-25% in all control tissues considered in our study i.e. *in vivo* mice spinal cord, *ex vivo* organotypic cerebellar slice culture or human hemispheric white matter. We did not find a variation in this percentage depending on the different tissues we considered or accounted for by microglial density variations, suggesting an independent underlying mechanism regulating this interaction. Nonetheless, it will be interesting to quantify the percentage of nodes contacted in other areas of the brain such as hippocampus, corpus callosum or pons to search for spatial differences. We could also search for differences between neuronal populations like it has been showed with AIS-microglia interactions (Baalman et al., 2015). A variable percentage of nodes contacted in some CNS areas could depend on neuronal subtypes, neuronal activity pattern, or different microglial subtypes (Colonna and Butovsky, 2017; Mosser and Edwards, 2008; Silvin and Ginhoux, 2018).

We further demonstrated the stability of this interaction using live-imaging techniques, suggesting it may have a functional role. Zhang et al. previously observed interactions between nodes and microglia, as well as microglial contacts on myelin, in rat corpus callosum by

immunohistochemistry and electronic microscopy (Zhang et al., 2019). However, microglia are highly motile cells and these observations could have corresponded to random interactions (Davalos et al., 2005; Nimmerjahn et al., 2005). Our live-imaging approach allowed us to demonstrate that node-microglia interaction is stable and reinforced compared to internodal contacts, suggesting it is not due to random microglial surveying, but is rather mediated by neuronal signalling. Furthermore, others previously showed interactions between microglia and neuronal soma or synapses (Cserép et al., 2019; Gehrmann et al., 1992; Hughes and Appel, 2020; Trapp et al., 2007). Microglia processes have been shown to contact neuronal soma through purinergic signals mediate by P2Y12r allowing a microglia-induced neuroprotection (Cserép et al., 2019). The fractalkine/CX3CR1 pathway is also classically associated to neuron-microglia dialog especially during pruning of dendritic spines (Bertollini et al., 2006; Hoshiko et al., 2012; Paolicelli and Gross, 2011; Paolicelli et al., 2011; Ragozzino et al., 2006; Ransohoff et al., 2007). Baalman et al., who showed interactions between microglia and AIS only showed that AnkyrinG presence, with preserved AIS structure is necessary for the interaction (Baalman et al., 2015).

We thus investigated the nature of the signal mediating node-microglia interaction. We first showed that neither ATP signaling, nor fractalkine pathway were required for microglia-node interaction. Further experiments demonstrated that node-microglia interaction depends on neuronal activity, and more precisely on potassium release from the axon. We also proposed that microglial read-out is mediated through THIK-1, a two-pore domain channel recently identified as the main K+ channel expressed in microglia (Madry et al., 2018). Madry et al. showed that THIK-1 maintains the microglial resting potential through an inward potassium influx. They demonstrated its role in microglia ramification and surveillance. Interestingly blocking THIK-1 did not impair process outgrowth towards damaged tissue suggesting two distinct mechanisms. Whether neuronal activity and K+ efflux could be implicated in other interactions between neurons and microglia as well is currently unknown.

We observed that microglial contact at nodes can be mediated both by microglial soma and processes, with the somatic contact being very stable: whether it implicates different functions is unknown.

Our 3D reconstruction of confocal acquisitions showed that some microglial processes extend to the junction between node and paranode. D'este et al. studied the ultrastructural anatomy of nodes of Ranvier using STED microscopy (D'Este et al., 2017). They found a periodical distribution of Nav and Kv channels without showing an accumulation of Kv channels at the

junction between nodes and paranodes. However, they did not look at KCa3.1 specific to Purkinje cells (Gründemann and Clark, 2015) or the recently described TRAAK and TREK (Brohawn, Kanda) precise organization. It would be interesting to better localize these channels at nodes. Furthermore, Kv1.1 and 1.2 are clustered at the juxtaparanodes (Rasband, 2010; Wang et al., 1993) and BK/Slo1 channels have been identified at paranodes of Purkinje cells playing a role in high-frequency conduction (Hirono et al., 2015). Knowing that potassium can leak through the axoglial junction (Hodgkin and Huxley, 1952), it is possible that these fluxes explain the affinity of microglial processes towards the first paranodal loops. Trying to better isolate the main channels involved in K+ signaling mediating node-microglia interaction could help to decipher more precisely the nature of this signal.

II. Characteristics of node-microglia interaction in pathological states

Perilesional areas are characterized by a high macrophagic activity (Zrzavy et al., 2017), and perinodal abnormalities (Howell et al., 2006). We observed, using *in vivo* live-imaging of mouse dorsal spinal cord, that the stability of node-microglia interaction is decreased near a demyelinating area, suggesting an impaired neuron-microglia dialog. Baalman et al showed that AIS-microglia interaction was reduced after injury, which is in accordance with our findings (Baalman et al., 2015). We could hypothesize that upon injury, the neuronal cues needed to maintain the interaction, such as adequate neuronal activity (Li et al., 2012; Tremblay et al., 2010; Wake et al., 2009), are lost or that inhibitory cues are expressed by the axon (Charles et al., 2002b) or by other glial cells in its direct environment (Syed et al., 2011). It could also be that inflammatory cues in the area of the lesion overcome node-microglia interaction signalling. The frequency of contacts in perilesional areas was however preserved in our mice model, which could be linked to an increase of microglial cell number in these areas. Accordingly, in human MS tissue, inflammatory microglia/MD-macrophages in the vicinity of active lesions in MS keep contacting nodes. Whether it is deleterious or enhancing onset of repair is unknown. It appears however that in EAE at onset of demyelination, the cells actively attacking nodal domains are rather monocyte derived macrophages than microglial cells (Yamasaki et al., 2014). Moreover, given our results, microglial contact at nodes seems to be beneficial at the onset of remyelination, as when this contact is inhibited, the switch towards pro-regenerative microglia and the remyelination rate are reduced.

Furthermore, we observed in MS tissues a decrease of contacted nodes in NAWM suggesting that node-microglia interaction could be altered even far from the lesions, or prior to any visible demyelination. As we know that microglial play a role in neuronal support (Hagemeyer et al., 2017; Torres et al., 2016; Wlodarczyk et al., 2017), we could hypothesize that neuronal function might be impacted and that this could contribute to the disease. The mechanisms involved in this decreased interaction remain unknown, but it could be due to similar processes as the ones discussed above regarding reduced stability.

Microglia are known for their surveillance role, and able to extend their processes towards the lesion in case of injury (Nimmerjahn et al., 2005). One hypothesis is that microglia could act as a sensor of health status during demyelination and during early steps of repair. They could assess the capacity of each axon to remyelinate and survive properly. Thus, it will be interesting to see whether the contacts and the phenotype of contacting microglia correlates with the axon health status in MS tissues, using APP or neurofilament markers.

However, how do microglial cells integrate information about neuronal status is still under debate (Tvrdik and Kalani, 2017). Many microglial responses are thought to be mediated by intracellular Ca2+ signals (Färber and Kettenmann, 2006). Transient microglial Ca2+ loads have been visualized *in vivo* (Eichhoff et al., 2011). Interestingly in this seminal observation, the rarity of spontaneous Ca2+ transients observed in physiological context makes this technique a very interesting candidate to study microglial response when environment is altered. Thus, we could propose to use a GCaMP Calcium indicator, specifically expressed in microglia, as it has been done in rat astrocytes (Gee et al., 2015) and follow Ca2+ transients when neuronal activity varies or following demyelination.

On the other hand, quantifications of the percentage of contacted nodes in fixed mouse spinal cord tissue showed an increased percentage during remyelination after LPC-induced focal demyelination suggesting that microglia-node interaction could play a role in repair. Moreover, the stability of the contacts is similar or even increased compared to control during remyelination, suggesting that the dialog could be strengthened during remyelination. We showed during myelination *ex vivo,* that immature nodal structures (node-like clusters and heminodes) are equally contacted than mature nodes. This suggests that microglia-node interaction could happen early in the (re)myelination process. If remyelination recapitulates myelination (Franklin and Hinks, 1999), we could indeed hypothesize that a similar process occurs in remyelinating tissues. Supporting this idea, we also found similar percentages of immature nodal structures and mature nodes contacted in remyelinating slices. This reinforced

attraction/stability could be linked to increased potassium release at the sites where nodal structures reaggregate compared to surrounding denuded axonal areas or to increased microglial sensitivity to this K+ signal in a remyelinating condition. Indeed, this pathway and other(s) could synergize, such as the P2Y12r pathway, which is known to potentiate THIK-1 (Madry et al., 2018).

Other environmental cues could also modulate node-microglia interaction. Among them, adaptative immune cues could participate. Yet, the LPC model allows to study demyelination without the adaptative inflammation counterpart known in MS. Thus, repeating our experiments in EAE model will be interesting to better decipher how the mechanisms we described could be affected.

Whether frequency of nodal contacts depends on the neuronal subtype is unknown. Repeating our experiments in other brain areas with a differentiation between neuronal subtype will easily answer this question. It is known that some CNS areas, such as spinal cord or cerebellum (Goldschmidt et al., 2009) remyelinate poorly compared to others. Thus, if as we hypothesize, microglia-node interaction is a key player in repair, different crosstalk depending on neuronal subtypes could impact remyelination efficiency. Indeed, we showed that interaction is mediated through K+ efflux, and we also know that K+ channels present at nodes of Ranvier could vary from one neuronal subtype to another (Brohawn et al., 2019; Devaux et al., 2004; Lien and Jonas, 2003). Moreover, THIK-1 expression may vary between microglia in different CNS areas as it has been shown that resting potential of microglia could vary according to different brain areas (De Biase et al., 2017). Thus, we could hypothesize a modulation of the signals according to the neuronal population.

The neuronal activity pattern could also be at play. It has been shown that microglia exert an acute and highly localized neuroprotective action under conditions of neuronal hyperactivity. Microglial processes migrated towards swollen axons in a mechanism involving both ATP and glutamate release via volume-activated anion channels (Kato et al., 2016). Moreover, intracellular K+ decrease has been associated with microglial inflammasome expression (Madry et al., 2018). The axonal K+ locally released at nodal structures when they reassemble could thus contribute to modulate microglial K+ homeostasis and subsequently limit inflammasome expression in the microglial cells at the direct vicinity of nodal areas. Conversely, the restoration of stable microglial contacts at nodal structures could allow for microglia to buffer reassembled nodal area and modulate activity at nodes, as neurons may be transiently hyperexcitable at onset of remyelination. Several studies have already shown that

neuronal activity can guide microglial processes to highly active neurons in larval zebrafish (Li et al., 2012; Tremblay et al., 2010; Wake et al., 2009). Interestingly, others showed that reciprocally, microglia contacting neurons reduced their electrical activity suggesting a homeostatic regulation on neuronal activity (Eyo et al., 2014; Kato et al., 2016; Li et al., 2012; Szalay et al., 2016).

As discussed in the introduction, finding the reasons why remyelination fails is one of the main goals to identify new therapeutic targets in MS (Franklin and ffrench-Constant, 2017). After deciphering how node-microglia interaction (or more broadly node-glial interactions) participate in repair, we could enhance or facilitate the mechanisms involved to increase remyelination and thus neuroprotection. As we showed that microglia-node interaction depends on neuronal activity through potassium fluxes, acting on THIK-1 channels to enhance microglial potassium read-out could be one lead to facilitate the dialog and thus remyelination.

III. Node-microglia interaction could participate in the microglial switch in repair

Here we showed that node-microglia interaction can influence microglia phenotype towards a more pro-regenerative state. Our results showed, using THIK-1 blockers, a decrease of the percentage of contacted nodes along with increase of pro-inflammatory markers in microglial cells. This hypothesis is further supported by our observation that, in remyelinating mouse dorsal spinal cord lesion following LPC-induced focal demyelination, microglia contacting nodal structures have a more pro-regenerative phenotype. We showed that during remyelination, contacting microglial cells showed a 31% increase in IGF1+ pro-regenerative cells and a 35% decrease in iNOS+ pro-inflammatory cells compared to non-contacting microglial cells (Fig.20). Others have shown that a microglial switch to pro-repair phenotypes is essential to remyelination (Lloyd et al., 2019; Locatelli et al., 2018; Miron et al., 2013). Taken together, these results suggest that neuronal crosstalk at nodes of Ranvier might be one of the key players of microglial phenotype switch during the evolution of a demyelinating lesion.

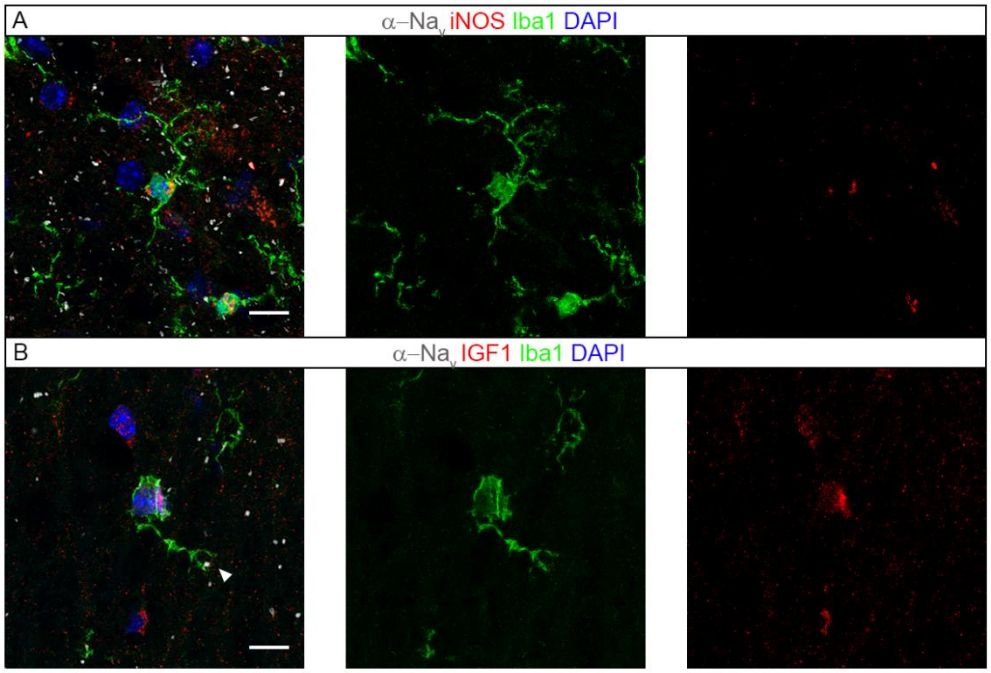

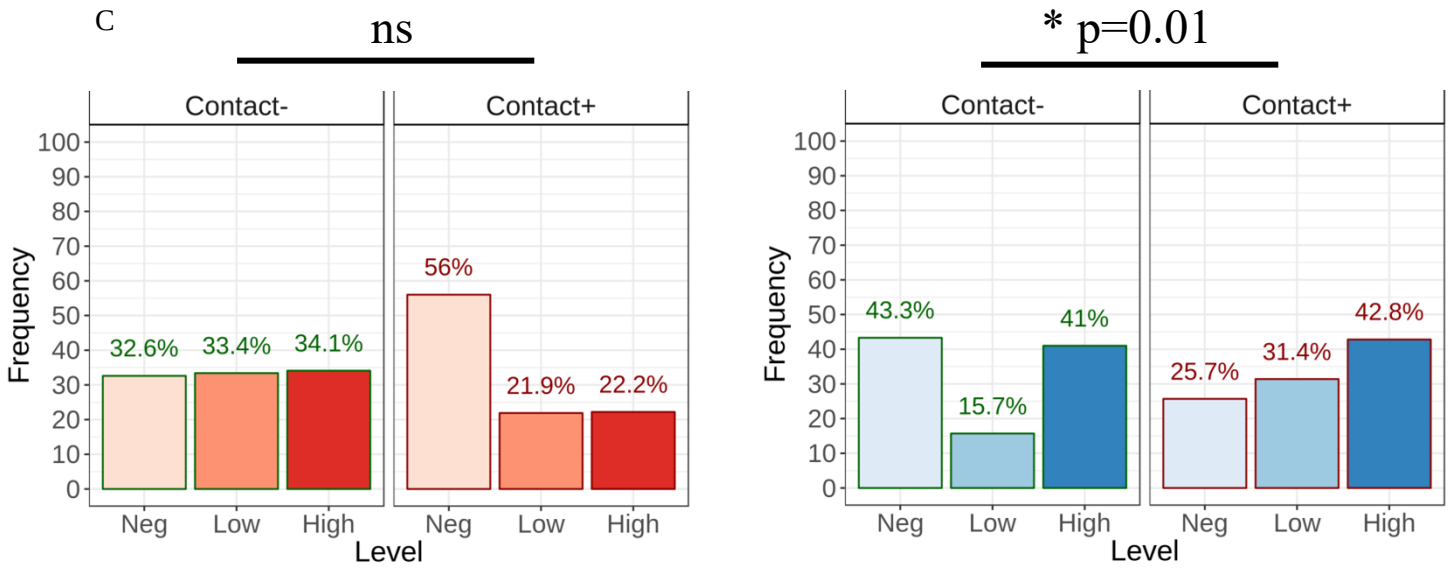

Fig.21/ Contacting microglial cells in remyelinating areas have a more pro-regenerative phenotype.
(A-B) Remyelinating areas after focal LPC-induced demyelination in mice spinal cord, scale bar=10µm; (A) A microglial cell (Iba1, green) expressing iNOS marker (red) and contacting nodes of Ranvier (Nav, white); (B) A microglial cell (Iba1, green) expressing IGF1 marker (red) and contacting nodes of Ranvier (Nav, white) (arrowhead); (C) Percentage of expressing cells (iNOS in red, IGFA in blue) according to contacting or non-contacting cells. Compute Cochran-Mantel-Haenszel chi-squared test *p < 0.05, **p < 0.01, ***p < 0.001, ****p < 0.0001, ns. indicates no significance.

Major related questions remain: what is the timing of this switch, why at this particular period, and finally how to enhance this microglial switch at the right time to favour repair? Could neuronal activity be a key in this process? Moreover, recent works showed a spatial and temporal distribution of various microglial phenotypes in particular during myelination (Hammond et al., 2019). It is very probable that the same is occurring during repair with a succession of different phenotypes along repair processes which might vary given the brain area considered.

Locatelli et al. employed the iNOS-tdTomato-Cre mouse line, which expresses a red fluorescent protein (tdTomato, as well as the Cre recombinase) under the control of the iNOS promoter, and the Arginase-YFP mouse line, which expresses YFP under the control of the arginase promoter (Locatelli et al., 2018). Interestingly, they showed that no reporter expression was observed in microglial cells in the healthy CNS, as analysed by flow cytometry, immunofluorescence, or in vivo imaging suggesting resting cells. These results contrast with what is seen in normal white matter of control human tissues where microglia exhibit a pre-activated phenotype (Zrzavy et al., 2017). It could be due to the fact that tissues are post-mortem with a delay prior to fixation. Nonetheless, these diverging results illustrate the differences between experimental models and MS. Moreover, authors also showed that the switch of macrophages from a pro-inflammatory state (iNOS+) to a pro-repair state (Arginase+) is influenced by CNS environment. They showed that the switch occurred in the presence of isolated CNS astrocytes. Taken together with our results, this suggests that multiple glial partners are likely to play a role in the switch at onset of repair, implying a multipartite dialog.Taken together, our study suggests that microglial phenotype can be modulated by direct neuronal interaction at nodes of Ranvier, leading to remyelination regulation and potentially neuronal survival.

IV. Microglial profiles observed in human tissues

For many years, distinguishing blood derived macrophages from resident microglia was impossible using immunochemistry. Then, specific markers as TMEM119 or P2Y12r were found (Butovsky et al., 2014; Mildner et al., 2017). In our study of human tissues, we were surprised by the high level of co-stained cells with a marker of activation (MHCII) and the homeostasic marker P2Y12r in controls, but microglial expression profile appears to be a continuum (Kigerl et al., 2009; Mantovani et al., 2007; Mosser and Edwards, 2008). This result

could be linked also to the fact that delays on collecting and processing post-mortem tissues could probably favour microglial activation. Moreover, the mean age corresponding to our control samples was 71.6+/-5.4 and microglia is known to adopt a more activated phenotype with age (Griffin et al., 2006; Letiembre et al., 2007; Perry et al., 1993).

In MS tissues, we showed that node-microglia interactions were similar to controls in remyelinating(ed) areas. We also showed that P2Y12r+ cells absent from active lesions can be present in shadow plaques. Taken together these observations suggest that microglia in remyelinating(ed) areas can re-adopt a surveilling profile as in control conditions. However, we also showed that most of resident microglial cells in remyelinating(ed) areas express the pro-inflammatory marker p22phox mainly associated to (chronic) active lesions (Zrzavy et al., 2017). Several studies emphasize the role of inflammatory microglial phenotypes in repair (Kotter et al., 2001; Li et al., 2005; Miron et al., 2013). They are required for myelin clearance, or OLs migration and proliferation (Cunha et al., 2020). But a deleterious role of these cells remains hypothetical once the tissue is remyelinated. Moreover, we showed that all these cells were contacting nodes of Ranvier suggesting that inflammatory status is not a brake for this dialog.

As classically done in the literature, we used a myelin staining (MOG) and a macrophage marker (MHC-II) in our study to classify our lesions (Lucchinetti et al., 2000). Shadow plaques are defined by a pale myelin staining attributed to thinner myelin sheaths after remyelination (Franklin, 2002). Shadow plaques are also known to contain active microglia by contrast with inactive lesions for example (Patrikios et al., 2006). However, the distinction between ongoing remyelination lesions or ongoing demyelination can be difficult. Some authors suggest looking at macrophage cytoplasms (Kuhlmann et al., 2017; Patrikios et al., 2006). If myelin degradation products are seen, it is in favour of an active lesion with ongoing demyelination. A better lesion classification is needed to investigate accurately differences between lesion types. To do so, RNA-sequencing of OLs allowing to define specific subclusters according to lesion type is a promising avenue (Jäkel et al., 2019). Thus, a better classification will probably need the association of specific markers from different glial cells.

The “mixed” microglial profile we observed could be due to a real co-expression of markers, or to a slow turn-over of one of the markers considered, whereas corresponding genes are no longer expressed. Post-translational modifications or localization of these markers within the cells could also temper with the functional properties of the microglial cells co-expressing them.

However, Locatelli et al. suggest that very different microglial populations (according to their metabolic profile, identified through RNA-sequencing) could have very similar cytokinin and activation marker expression profile (Locatelli et al., 2018).

Strikingly, we observed in our study that microglial cells contact nodes of Ranvier regardless their phenotype in different lesions including shadow plaques. In these latter, we could hypothesize that microglial cells, favored by their interaction with nodes of Ranvier, are shifting towards a more pro-regenerative state as shown in experimental models (Lloyd et al., 2019; Locatelli et al., 2018). On the other hand, the persistence of inflammatory microglial phenotypes contacting nodes could be deleterious for axons.

V. Nodes of Ranvier as a glial-communication hub

Other glial contacts have been identified at nodes of Ranvier (Black and Waxman, 1988; Ffrench-Constant et al., 1986; Sims et al., 1985). Astrocytes can interact with nodes as well as NG2 positive OPCs (Butt et al., 1999; Serwanski et al., 2017). We also showed that simultaneous interaction between a node and two glial cells exists: astrocyte and microglia or OPC and microglia. Serwanski et al. previously showed that similar multiple interactions at nodes exist with NG2 positive OPCs and astrocytes. Taken together these results suggest that the node of Ranvier might be a putative area of communication between the axon and its glial environment. It could be a key area for neuron-glial, as well as glial-glial crosstalk, as it allows for a direct access to the axon along myelinated fibres and for the presence of multiple glial cell processes simultaneously (Lubetzki et al., 2020). To further explore this idea, it would be interesting to achieve 4-color immunostaining: three colours for each glial cell and one for nodal or paranodal markers to investigate whether the three different glial cells can interact with a same node at the same time and how they are spatially organized. Indeed, Serwansky et al. showed that NG2 cells extend fine finger-like projections that often contact both the nodal axolemma and outermost paranodal myelin loops, while astrocytes extend broader processes covering the entire nodal gap, suggesting different interaction mechanisms and/or role at the node. Our observations showed that microglia can interact as NG2 cells with a fine finger-like projections but also with their soma or “en passant”. Moreover, Serwanski et al. showed extensive intertwining of the processes of astrocytes and NG2 cells suggesting that the two cells could communicate also one with another. We also demonstrated such glial-glial interactions with microglia. Taken together, these results suggest that various cues and signals should be at

play to orchestrate the different interactions between all these cellular actors and the role they are playing.

It has been shown that oligodendroglia lineage cells can sense neuronal activity which modulate their proliferation and differentiation (Barres and Raff, 1993). This suggests that both OPCs and microglia could have a read-out of neuronal activity at nodes through similar signalling pathways. The preferential site of interaction between NG2 cells and nodes at the junction of nodes and paranodes (Serwanski et al., 2017), like we observed with microglia, is the perfect area to sense myelin modulations and modulate myelination if needed. Furthermore, electrophysiological paired recordings show that OPCs adjacent to neurons can sense their discharge, and extracellular stimulation induces slow K+ currents in OPCs, showing they could sense K+ variations linked with activity (Maldonado et al., 2013). Altogether, this suggest OPCs and microglia could rely on similar mechanisms to contact node.

Finally, regarding astrocytes, one of their function is to clear neurotransmitters and K+ released during synaptic transmission (Kimelberg and Nedergaard, 2010), and they can buffer K+ at the nodes (Black and Waxman, 1988). Thus, it is tempting to hypothesize a modulation of microglial K+ read-out by astrocytes. Moreover, the ablation of reactive astrocytes in cuprizone-treated mice impairs recruitment of microglia to the demyelinating lesion (Skripuletz et al., 2013) suggesting they modulate microglial behaviour. Several studies suggested a synergic effect of microglia and astrocytes during repair. Recently Zamora et al. used a knock-out mouse for the Cav1.2 α subunit in GFAP-positive astrocytes, and induced demyelination using the cuprizone mice model. In this model, they observed a reduced microglial activation and an increased remyelination. Similar results were obtained using nimodipine, a Cav1.2 Ca2+ inhibitor (Zamora et al., 2020). Moreover, the proinflammatory cytokine tumour necrosis factor-a (TNF-a), secreted by microglia/macrophages as well as astrocytes in mouse cuprizone-induced lesions, promotes OPC expansion and remyelination through TNF receptor 2 (TNFR2) on NG2 positive cells (Arnett et al., 2001; Voss et al., 2012). Interleukin-1b (IL-1b), also secreted by microglia/macrophages (Madry et al., 2018) and astrocytes, is important for remyelination potentially by controlling oligodendrocyte lineage cells survival by stimulating IGF-1 secretion from microglia/macrophages in cuprizone-treated mice (Mason et al., 2001).

It would be interesting to perform some further experiments with the OL lineage and astrocytes to study the characteristics of their interaction with nodes and with microglia, and the functional impact it can have on repair. This could allow to better understand how the crosstalk between these different players are integrated to promote myelin repair.

CONCLUSION

In myelinated fibres, the clustering of voltage-gated sodium channels at the nodes of Ranvier supports the rapid propagation of action potentials by saltatory conduction. Nodes of Ranvier are known as a preferential target during demyelination. Furthermore, previous results showed that an early clustering of nodal proteins occur before remyelination. This suggests that the nodes may not only play a crucial role in physiological context, but also in disease. Microglia, the resident immune cells of the CNS, have been implicated in repair in various ways, by promoting OPCs differentiation and myelination, as well as neuronal survival. But their interaction with axons has been little studied in normal and pathological contexts.

We show that, at the axon, microglia interact preferentially with nodes of Ranvier by sensing neuronal activity. This interaction may modulate microglial phenotype towards a pro-regenerative state, thus its function, at the onset of remyelination. We also propose the node of Ranvier as a glial communication hub, as other glial cells can be present simultaneously. We further observed the interaction between nodes of Ranvier and microglia in human control and MS tissues. We observed a decreased node-microglia interaction in NAWM and a restored interaction in remyelinating(ed) areas. Furthermore, we observed a sustained inflammatory microglial phenotype in shadow plaques, supporting a dual role of pro-inflammatory microglia in MS, but suggesting shadow plaques could be more prone to successive alterations if these cells persist. Altogether, our results uncover a new way for microglia to interact with neurons and glial cells in health and repair and confirm microglia as a potential target for new therapeutics in MS.

REFERENCES

Absinta, M., Sati, P., Schindler, M., Leibovitch, E.C., Ohayon, J., Wu, T., Meani, A., Filippi, M., Jacobson, S., Cortese, I.C.M., et al. (2016). Persistent 7-tesla phase rim predicts poor outcome in new multiple sclerosis patient lesions. J Clin Invest *126*, 2597–2609.

Aggarwal, S., Yurlova, L., and Simons, M. (2011). Central nervous system myelin: structure, synthesis and assembly. Trends in Cell Biology *21*, 585–593.

Airas, L., Nylund, M., and Rissanen, E. (2018). Evaluation of Microglial Activation in Multiple Sclerosis Patients Using Positron Emission Tomography. Front Neurol *9*, 181.

Ajami, B., Bennett, J.L., Krieger, C., Tetzlaff, W., and Rossi, F.M.V. (2007). Local self-renewal can sustain CNS microglia maintenance and function throughout adult life. Nat Neurosci *10*, 1538–1543.

Arancibia-Cárcamo, I.L., Ford, M.C., Cossell, L., Ishida, K., Tohyama, K., and Attwell, D. (2017). Node of Ranvier length as a potential regulator of myelinated axon conduction speed. Elife *6*.

Arnett, H.A., Mason, J., Marino, M., Suzuki, K., Matsushima, G.K., and Ting, J.P. (2001). TNF alpha promotes proliferation of oligodendrocyte progenitors and remyelination. Nat Neurosci *4*, 1116–1122.

Arroyo, E.J., Xu, T., Grinspan, J., Lambert, S., Levinson, S.R., Brophy, P.J., Peles, E., and Scherer, S.S. (2002). Genetic dysmyelination alters the molecular architecture of the nodal region. J Neurosci *22*, 1726–1737.

Auer, F., Vagionitis, S., and Czopka, T. (2018). Evidence for Myelin Sheath Remodeling in the CNS Revealed by In Vivo Imaging. Curr Biol *28*, 549-559.e3.

Baalman, K., Marin, M.A., Ho, T.S.-Y., Godoy, M., Cherian, L., Robertson, C., and Rasband, M.N. (2015). Axon Initial Segment-Associated Microglia. Journal of Neuroscience *35*, 2283–2292.

Bakiri, Y., Káradóttir, R., Cossell, L., and Attwell, D. (2011). Morphological and electrical properties of oligodendrocytes in the white matter of the corpus callosum and cerebellum. J Physiol *589*, 559–573.

Bar, E., and Barak, B. (2019). Microglia roles in synaptic plasticity and myelination in homeostatic conditions and neurodevelopmental disorders. Glia *67*, 2125–2141.

Baraban, M., Koudelka, S., and Lyons, D.A. (2018). Ca2+ activity signatures of myelin sheath formation and growth in vivo. Nat Neurosci *21*, 19–23.

Barres, B.A., and Raff, M.C. (1993). Proliferation of oligodendrocyte precursor cells depends on electrical activity in axons. Nature *361*, 258–260.

Barry, J., Gu, Y., Jukkola, P., O'Neill, B., Gu, H., Mohler, P.J., Rajamani, K.T., and Gu, C. (2014). Ankyrin-G Directly Binds to Kinesin-1 to Transport Voltage-Gated Na+ Channels into Axons. Developmental Cell *28*, 117–131.

Battefeld, A., Tran, B.T., Gavrilis, J., Cooper, E.C., and Kole, M.H.P. (2014). Heteromeric Kv7.2/7.3 channels differentially regulate action potential initiation and conduction in neocortical myelinated axons. J Neurosci *34*, 3719–3732.

Bauer, N.G., Richter-Landsberg, C., and Ffrench-Constant, C. (2009). Role of the oligodendroglial cytoskeleton in differentiation and myelination. Glia *57*, 1691–1705.

Baumann, N., and Pham-Dinh, D. (2001). Biology of Oligodendrocyte and Myelin in the Mammalian Central Nervous System. Physiological Reviews *81*, 871–927.

Baumgartner, S., Littleton, J.T., Broadie, K., Bhat, M.A., Harbecke, R., Lengyel, J.A., Chiquet-Ehrismann, R., Prokop, A., and Bellen, H.J. (1996). A Drosophila neurexin is required for septate junction and blood-nerve barrier formation and function. Cell *87*, 1059–1068.

Bechler, M.E., Byrne, L., and Ffrench-Constant, C. (2015). CNS Myelin Sheath Lengths Are an Intrinsic Property of Oligodendrocytes. Curr Biol *25*, 2411–2416.

Bekku, Y., Rauch, U., Ninomiya, Y., and Oohashi, T. (2009). Brevican distinctively assembles extracellular components at the large diameter nodes of Ranvier in the CNS. J Neurochem *108*, 1266–1276.

Bengtsson, S.L., Nagy, Z., Skare, S., Forsman, L., Forssberg, H., and Ullén, F. (2005). Extensive piano practicing has regionally specific effects on white matter development. Nat Neurosci *8*, 1148–1150.

Bennett, M.L., Bennett, F.C., Liddelow, S.A., Ajami, B., Zamanian, J.L., Fernhoff, N.B., Mulinyawe, S.B., Bohlen, C.J., Adil, A., Tucker, A., et al. (2016). New tools for studying microglia in the mouse and human CNS. Proc Natl Acad Sci USA *113*, E1738–E1746.

Berghs, S., Aggujaro, D., Dirkx, R., Maksimova, E., Stabach, P., Hermel, J.M., Zhang, J.P., Philbrick, W., Slepnev, V., Ort, T., et al. (2000). betaIV spectrin, a new spectrin localized at axon initial segments and nodes of ranvier in the central and peripheral nervous system. J Cell Biol *151*, 985–1002.

Bertollini, C., Ragozzino, D., Gross, C., Limatola, C., and Eusebi, F. (2006). Fractalkine/CX3CL1 depresses central synaptic transmission in mouse hippocampal slices. Neuropharmacology *51*, 816–821.

Bhasin, M., Wu, M., and Tsirka, S.E. (2007). Modulation of microglial/macrophage activation by macrophage inhibitory factor (TKP) or tuftsin (TKPR) attenuates the disease course of experimental autoimmune encephalomyelitis. BMC Immunol *8*, 10.

Bieber, A.J., Kerr, S., and Rodriguez, M. (2003). Efficient central nervous system remyelination requires T cells. Ann Neurol *53*, 680–684.

Bitsch, A., Kuhlmann, T., Da Costa, C., Bunkowski, S., Polak, T., and Brück, W. (2000). Tumour necrosis factor alpha mRNA expression in early multiple sclerosis lesions: correlation with demyelinating activity and oligodendrocyte pathology. Glia *29*, 366–375.

Black, J.A., and Waxman, S.G. (1988). The perinodal astrocyte. Glia *1*, 169–183.

Black, J.A., Dib-Hajj, S., Baker, D., Newcombe, J., Cuzner, M.L., and Waxman, S.G. (2000). Sensory neuron-specific sodium channel SNS is abnormally expressed in the brains of mice with experimental allergic encephalomyelitis and humans with multiple sclerosis. Proc Natl Acad Sci U S A *97*, 11598–11602.

Blackwood W, Corsellis JAN, and (Prénom) (1976). Normal structure and general pathology of the nerve cell and neuroglia. In Greenfield's Neuropathology, p. Pp. 1-42.

Bodini, B., Veronese, M., García-Lorenzo, D., Battaglini, M., Poirion, E., Chardain, A., Freeman, L., Louapre, C., Tchikviladze, M., Papeix, C., et al. (2016). Dynamic Imaging of Individual Remyelination Profiles in Multiple Sclerosis: Imaging Remyelination in Multiple Sclerosis. Ann Neurol. *79*, 726–738.

Bogie, J.F.J., Stinissen, P., and Hendriks, J.J.A. (2014). Macrophage subsets and microglia in multiple sclerosis. Acta Neuropathol *128*, 191–213.

Boiko, T., Rasband, M.N., Levinson, S.R., Caldwell, J.H., Mandel, G., Trimmer, J.S., and Matthews, G. (2001). Compact myelin dictates the differential targeting of two sodium channel isoforms in the same axon. Neuron *30*, 91–104.

Boyd, A., Zhang, H., and Williams, A. (2013). Insufficient OPC migration into demyelinated lesions is a cause of poor remyelination in MS and mouse models. Acta Neuropathol *125*, 841–859.

Bramow, S., Frischer, J.M., Lassmann, H., Koch-Henriksen, N., Lucchinetti, C.F., Sørensen, P.S., and Laursen, H. (2010). Demyelination versus remyelination in progressive multiple sclerosis. Brain *133*, 2983–2998.

Brill, M.H., Waxman, S.G., Moore, J.W., and Joyner, R.W. (1977). Conduction velocity and spike configuration in myelinated fibres: computed dependence on internode distance. J Neurol Neurosurg Psychiatry *40*, 769–774.

Brohawn, S.G., Wang, W., Handler, A., Campbell, E.B., Schwarz, J.R., and MacKinnon, R. (2019). The mechanosensitive ion channel TRAAK is localized to the mammalian node of Ranvier. ELife *8*, e50403.

Brown, R.A., Narayanan, S., and Arnold, D.L. (2014). Imaging of repeated episodes of demyelination and remyelination in multiple sclerosis. Neuroimage Clin *6*, 20–25.

Bunge, M.B., Bunge, R.P., and Ris, H. (1961). Ultrastructural study of remyelination in an experimental lesion in adult cat spinal cord. J Biophys Biochem Cytol *10*, 67–94.

Butovsky, O., Landa, G., Kunis, G., Ziv, Y., Avidan, H., Greenberg, N., Schwartz, A., Smirnov, I., Pollack, A., Jung, S., et al. (2006). Induction and blockage of oligodendrogenesis by differently activated microglia in an animal model of multiple sclerosis. J Clin Invest *116*, 905–915.

Butovsky, O., Jedrychowski, M.P., Moore, C.S., Cialic, R., Lanser, A.J., Gabriely, G., Koeglsperger, T., Dake, B., Wu, P.M., Doykan, C.E., et al. (2014). Identification of a unique TGF-β–dependent molecular and functional signature in microglia. Nat Neurosci *17*, 131–143.

Butt, A.M., Duncan, A., Hornby, M.F., Kirvell, S.L., Hunter, A., Levine, J.M., and Berry, M. (1999). Cells expressing the NG2 antigen contact nodes of Ranvier in adult CNS white matter. 8.

Calaora, V., Rogister, B., Bismuth, K., Murray, K., Brandt, H., Leprince, P., Marchionni, M., and Dubois-Dalcq, M. (2001). Neuregulin signaling regulates neural precursor growth and the generation of oligodendrocytes in vitro. J Neurosci *21*, 4740–4751.

Campbell, Z., Sahm, D., Donohue, K., Jamison, J., Davis, M., Pellicano, C., Auh, S., Ohayon, J., Frank, J.A., Richert, N., et al. (2012). Characterizing contrast-enhancing and re-enhancing lesions in multiple sclerosis. Neurology *78*, 1493–1499.

Canoll, P.D., Musacchio, J.M., Hardy, R., Reynolds, R., Marchionni, M.A., and Salzer, J.L. (1996). GGF/neuregulin is a neuronal signal that promotes the proliferation and survival and inhibits the differentiation of oligodendrocyte progenitors. Neuron *17*, 229–243.

Casaccia-Bonnefil, P., Tikoo, R., Kiyokawa, H., Friedrich, V., Chao, M.V., and Koff, A. (1997). Oligodendrocyte precursor differentiation is perturbed in the absence of the cyclin-dependent kinase inhibitor p27Kip1. Genes Dev *11*, 2335–2346.

Catterall, W.A. (2000). From ionic currents to molecular mechanisms: the structure and function of

voltage-gated sodium channels. Neuron *26*, 13–25.

Chan, J.R., Watkins, T.A., Cosgaya, J.M., Zhang, C., Chen, L., Reichardt, L.F., Shooter, E.M., and Barres, B.A. (2004). NGF controls axonal receptivity to myelination by Schwann cells or oligodendrocytes. Neuron *43*, 183–191.

Charles, P., Tait, S., Faivre-Sarrailh, C., Barbin, G., Gunn-Moore, F., Denisenko-Nehrbass, N., Guennoc, A.-M., Girault, J.-A., Brophy, P.J., and Lubetzki, C. (2002a). Neurofascin is a glial receptor for the paranodin/Caspr-contactin axonal complex at the axoglial junction. Curr Biol *12*, 217–220.

Charles, P., Reynolds, R., Seilhean, D., Rougon, G., Aigrot, M.S., Niezgoda, A., Zalc, B., and Lubetzki, C. (2002b). Re-expression of PSA-NCAM by demyelinated axons: an inhibitor of remyelination in multiple sclerosis? Brain *125*, 1972–1979.

Clark, K.C., Josephson, A., Benusa, S.D., Hartley, R.K., Baer, M., Thummala, S., Joslyn, M., Sword, B.A., Elford, H., Oh, U., et al. (2016). Compromised axon initial segment integrity in EAE is preceded by microglial reactivity and contact: AIS Disruption in EAE. Glia *64*, 1190–1209.

Colonna, M., and Butovsky, O. (2017). Microglia Function in the Central Nervous System During Health and Neurodegeneration. Annu. Rev. Immunol. *35*, 441–468.

Coman, I., Aigrot, M.S., Seilhean, D., Reynolds, R., Girault, J.A., Zalc, B., and Lubetzki, C. (2006). Nodal, paranodal and juxtaparanodal axonal proteins during demyelination and remyelination in multiple sclerosis. Brain *129*, 3186–3195.

Compston, A., and Coles, A. (2002). Multiple sclerosis. Lancet *359*, 1221–1231.

Craner, M.J., Lo, A.C., Black, J.A., and Waxman, S.G. (2003). Abnormal sodium channel distribution in optic nerve axons in a model of inflammatory demyelination. Brain *126*, 1552–1561.

Craner, M.J., Hains, B.C., Lo, A.C., Black, J.A., and Waxman, S.G. (2004a). Co-localization of sodium channel Nav1.6 and the sodium-calcium exchanger at sites of axonal injury in the spinal cord in EAE. Brain *127*, 294–303.

Craner, M.J., Newcombe, J., Black, J.A., Hartle, C., Cuzner, M.L., and Waxman, S.G. (2004b). Molecular changes in neurons in multiple sclerosis: altered axonal expression of Nav1.2 and Nav1.6 sodium channels and Na+/Ca2+ exchanger. Proc Natl Acad Sci U S A *101*, 8168–8173.

Crawford, A.H., Tripathi, R.B., Foerster, S., McKenzie, I., Kougioumtzidou, E., Grist, M., Richardson, W.D., and Franklin, R.J.M. (2016). Pre-Existing Mature Oligodendrocytes Do Not Contribute to Remyelination following Toxin-Induced Spinal Cord Demyelination. Am J Pathol *186*, 511–516.

Cree, B.A.C., Mares, J., and Hartung, H.-P. (2019). Current therapeutic landscape in multiple sclerosis: an evolving treatment paradigm. Current Opinion in Neurology *32*, 365–377.

Cserép, C., Pósfai, B., Orsolits, B., Molnár, G., Heindl, S., Lénárt, N., Fekete, R., László, Z.I., Lele, Z., Schwarcz, A.D., et al. (2019). Microglia monitor and protect neuronal function via specialized somatic purinergic junctions (Neuroscience).

Cunha, M.I., Su, M., Cantuti-Castelvetri, L., Müller, S.A., Schifferer, M., Djannatian, M., Alexopoulos, I., van der Meer, F., Winkler, A., van Ham, T.J., et al. (2020). Pro-inflammatory activation following demyelination is required for myelin clearance and oligodendrogenesis. Journal of Experimental Medicine *217*, e20191390.

Czopka, T., Ffrench-Constant, C., and Lyons, D.A. (2013). Individual oligodendrocytes have only a

few hours in which to generate new myelin sheaths in vivo. Dev Cell *25*, 599–609.

Dal-Bianco, A., Grabner, G., Kronnerwetter, C., Weber, M., Höftberger, R., Berger, T., Auff, E., Leutmezer, F., Trattnig, S., Lassmann, H., et al. (2017). Slow expansion of multiple sclerosis iron rim lesions: pathology and 7 T magnetic resonance imaging. Acta Neuropathol *133*, 25–42.

Davalos, D., Grutzendler, J., Yang, G., Kim, J.V., Zuo, Y., Jung, S., Littman, D.R., Dustin, M.L., and Gan, W.-B. (2005). ATP mediates rapid microglial response to local brain injury in vivo. Nat Neurosci *8*, 752–758.

De Biase, L.M., Schuebel, K.E., Fusfeld, Z.H., Jair, K., Hawes, I.A., Cimbro, R., Zhang, H.-Y., Liu, Q.-R., Shen, H., Xi, Z.-X., et al. (2017). Local Cues Establish and Maintain Region-Specific Phenotypes of Basal Ganglia Microglia. Neuron *95*, 341-356.e6.

De Groot, C.J., Bergers, E., Kamphorst, W., Ravid, R., Polman, C.H., Barkhof, F., and van der Valk, P. (2001). Post-mortem MRI-guided sampling of multiple sclerosis brain lesions: increased yield of active demyelinating and (p)reactive lesions. Brain *124*, 1635–1645.

Demerens, C., Stankoff, B., Logak, M., Anglade, P., Allinquant, B., Couraud, F., Zalc, B., and Lubetzki, C. (1996). Induction of myelination in the central nervous system by electrical activity. Proceedings of the National Academy of Sciences *93*, 9887–9892.

Denisenko-Nehrbass, N., Oguievetskaia, K., Goutebroze, L., Galvez, T., Yamakawa, H., Ohara, O., Carnaud, M., and Girault, J.-A. (2003). Protein 4.1B associates with both Caspr/paranodin and Caspr2 at paranodes and juxtaparanodes of myelinated fibres. Eur J Neurosci *17*, 411–416.

D'Este, E., Kamin, D., Balzarotti, F., and Hell, S.W. (2017). Ultrastructural anatomy of nodes of Ranvier in the peripheral nervous system as revealed by STED microscopy. Proc Natl Acad Sci U S A *114*, E191–E199.

Devaux, J.J., Kleopa, K.A., Cooper, E.C., and Scherer, S.S. (2004). KCNQ2 is a nodal K+ channel. J Neurosci *24*, 1236–1244.

Dubessy, A., Mazuir, E., Rappeneau, Q., Ou, S., Abi Ghanem, C., Piquand, K., Aigrot, M., Thétiot, M., Desmazières, A., Chan, E., et al. (2019). Role of a Contactin multi-molecular complex secreted by oligodendrocytes in nodal protein clustering in the CNS. Glia *67*, 2248–2263.

Dubessy, A.-L., Zujovic, V., Papeix, C., and Stankoff, B. (2014). Biotherapies in multiple sclerosis: a step toward remyelination and neuroprotection? Rev Neurol (Paris) *170*, 770–778.

Duncan, D. (1934). A determination of the number of nerve fibers in the eighth thoracic and the largest lumbar ventral roots of the albino rat. J. Comp. Neurol. *59*, 47–60.

Duncan, I.D., Radcliff, A.B., Heidari, M., Kidd, G., August, B.K., and Wierenga, L.A. (2018). The adult oligodendrocyte can participate in remyelination. Proc Natl Acad Sci U S A *115*, E11807–E11816.

Dutta, D.J., Woo, D.H., Lee, P.R., Pajevic, S., Bukalo, O., Huffman, W.C., Wake, H., Basser, P.J., SheikhBahaei, S., Lazarevic, V., et al. (2018). Regulation of myelin structure and conduction velocity by perinodal astrocytes. Proc Natl Acad Sci USA *115*, 11832–11837.

Eichhoff, G., Brawek, B., and Garaschuk, O. (2011). Microglial calcium signal acts as a rapid sensor of single neuron damage in vivo. Biochim Biophys Acta *1813*, 1014–1024.

Einheber, S., Zanazzi, G., Ching, W., Scherer, S., Milner, T.A., Peles, E., and Salzer, J.L. (1997). The axonal membrane protein Caspr, a homologue of neurexin IV, is a component of the septate-like

paranodal junctions that assemble during myelination. J Cell Biol *139*, 1495–1506.

El Behi, M., Sanson, C., Bachelin, C., Guillot-Noël, L., Fransson, J., Stankoff, B., Maillart, E., Sarrazin, N., Guillemot, V., Abdi, H., et al. (2017). Adaptive human immunity drives remyelination in a mouse model of demyelination. Brain *140*, 967–980.

Etxeberria, A., Mangin, J.-M., Aguirre, A., and Gallo, V. (2010). Adult-born SVZ progenitors receive transient synapses during remyelination in corpus callosum. Nat Neurosci *13*, 287–289.

Eyo, U.B., Peng, J., Swiatkowski, P., Mukherjee, A., Bispo, A., and Wu, L.-J. (2014). Neuronal hyperactivity recruits microglial processes via neuronal NMDA receptors and microglial P2Y12 receptors after status epilepticus. J Neurosci *34*, 10528–10540.

Faivre-Sarrailh, C., and Devaux, J.J. (2013). Neuro-glial interactions at the nodes of Ranvier: implication in health and diseases. Front. Cell. Neurosci. *7*.

Faivre-Sarrailh, C., Gauthier, F., Denisenko-Nehrbass, N., Le Bivic, A., Rougon, G., and Girault, J.A. (2000). The glycosylphosphatidyl inositol-anchored adhesion molecule F3/contactin is required for surface transport of paranodin/contactin-associated protein (caspr). J Cell Biol *149*, 491–502.

Fancy, S.P.J., Baranzini, S.E., Zhao, C., Yuk, D.-I., Irvine, K.-A., Kaing, S., Sanai, N., Franklin, R.J.M., and Rowitch, D.H. (2009). Dysregulation of the Wnt pathway inhibits timely myelination and remyelination in the mammalian CNS. Genes Dev *23*, 1571–1585.

Färber, K., and Kettenmann, H. (2006). Functional role of calcium signals for microglial function. Glia *54*, 656–665.

Ffrench-Constant, C., Miller, R.H., Kruse, J., Schachner, M., and Raff, M.C. (1986). Molecular specialization of astrocyte processes at nodes of Ranvier in rat optic nerve. J Cell Biol *102*, 844–852.

Foote, A.K., and Blakemore, W.F. (2005). Inflammation stimulates remyelination in areas of chronic demyelination. Brain *128*, 528–539.

Ford, M.C., Alexandrova, O., Cossell, L., Stange-Marten, A., Sinclair, J., Kopp-Scheinpflug, C., Pecka, M., Attwell, D., and Grothe, B. (2015). Tuning of Ranvier node and internode properties in myelinated axons to adjust action potential timing. Nat Commun *6*, 8073.

Franklin, R.J.M. (2002). Why does remyelination fail in multiple sclerosis? Nat Rev Neurosci *3*, 705–714.

Franklin, R.J., and Hinks, G.L. (1999). Understanding CNS remyelination: clues from developmental and regeneration biology. J Neurosci Res *58*, 207–213.

Franklin, R.J.M., and ffrench-Constant, C. (2017). Regenerating CNS myelin — from mechanisms to experimental medicines. Nat Rev Neurosci *18*, 753–769.

Franklin, R.J.M., and Goldman, S.A. (2015). Glia Disease and Repair-Remyelination. Cold Spring Harb Perspect Biol *7*, a020594.

Franklin, R.J., Crang, A.J., and Blakemore, W.F. (1991). Transplanted type-1 astrocytes facilitate repair of demyelinating lesions by host oligodendrocytes in adult rat spinal cord. J Neurocytol *20*, 420–430.

Freeman, S.A., Desmazières, A., Simonnet, J., Gatta, M., Pfeiffer, F., Aigrot, M.S., Rappeneau, Q., Guerreiro, S., Michel, P.P., Yanagawa, Y., et al. (2015). Acceleration of conduction velocity linked to clustering of nodal components precedes myelination. Proc Natl Acad Sci USA *112*, E321–E328.

Freeman, S.A., Desmazières, A., Fricker, D., Lubetzki, C., and Sol-Foulon, N. (2016). Mechanisms of sodium channel clustering and its influence on axonal impulse conduction. Cell Mol Life Sci *73*, 723–735.

Frischer, J.M., Weigand, S.D., Guo, Y., Kale, N., Parisi, J.E., Pirko, I., Mandrekar, J., Bramow, S., Metz, I., Brück, W., et al. (2015). Clinical and pathological insights into the dynamic nature of the white matter multiple sclerosis plaque: Dynamic Nature of MS Plaque. Ann Neurol. *78*, 710–721.

Fünfschilling, U., Supplie, L.M., Mahad, D., Boretius, S., Saab, A.S., Edgar, J., Brinkmann, B.G., Kassmann, C.M., Tzvetanova, I.D., Möbius, W., et al. (2012). Glycolytic oligodendrocytes maintain myelin and long-term axonal integrity. Nature *485*, 517–521.

Garrido, J.J., Giraud, P., Carlier, E., Fernandes, F., Moussif, A., Fache, M.-P., Debanne, D., and Dargent, B. (2003). A targeting motif involved in sodium channel clustering at the axonal initial segment. Science *300*, 2091–2094.

Gasser, A., Ho, T.S.-Y., Cheng, X., Chang, K.-J., Waxman, S.G., Rasband, M.N., and Dib-Hajj, S.D. (2012). An ankyrinG-binding motif is necessary and sufficient for targeting Nav1.6 sodium channels to axon initial segments and nodes of Ranvier. J Neurosci *32*, 7232–7243.

Gautier, H.O.B., Evans, K.A., Volbracht, K., James, R., Sitnikov, S., Lundgaard, I., James, F., Lao-Peregrin, C., Reynolds, R., Franklin, R.J.M., et al. (2015). Neuronal activity regulates remyelination via glutamate signalling to oligodendrocyte progenitors. Nat Commun *6*, 8518.

GBD 2015 Neurological Disorders Collaborator Group (2017). Global, regional, and national burden of neurological disorders during 1990-2015: a systematic analysis for the Global Burden of Disease Study 2015. Lancet Neurol *16*, 877–897.

Gee, J.M., Gibbons, M.B., Taheri, M., Palumbos, S., Morris, S.C., Smeal, R.M., Flynn, K.F., Economo, M.N., Cizek, C.G., Capecchi, M.R., et al. (2015). Imaging activity in astrocytes and neurons with genetically encoded calcium indicators following in utero electroporation. Front Mol Neurosci *8*, 10.

Gehrmann, J., Gold, R., Linington, C., Lannes-Vieira, J., Wekerle, H., and Kreutzberg, G.W. (1992). Spinal cord microglia in experimental allergic neuritis. Evidence for fast and remote activation. Lab Invest *67*, 100–113.

Gensert, J.M., and Goldman, J.E. (1997). Endogenous progenitors remyelinate demyelinated axons in the adult CNS. Neuron *19*, 197–203.

Gibson, E.M., Purger, D., Mount, C.W., Goldstein, A.K., Lin, G.L., Wood, L.S., Inema, I., Miller, S.E., Bieri, G., Zuchero, J.B., et al. (2014). Neuronal activity promotes oligodendrogenesis and adaptive myelination in the mammalian brain. Science *344*, 1252304.

Giera, S., Luo, R., Ying, Y., Ackerman, S.D., Jeong, S.-J., Stoveken, H.M., Folts, C.J., Welsh, C.A., Tall, G.G., Stevens, B., et al. (2018). Microglial transglutaminase-2 drives myelination and myelin repair via GPR56/ADGRG1 in oligodendrocyte precursor cells. ELife *7*, e33385.

Ginhoux, F., Greter, M., Leboeuf, M., Nandi, S., See, P., Gokhan, S., Mehler, M.F., Conway, S.J., Ng, L.G., Stanley, E.R., et al. (2010). Fate mapping analysis reveals that adult microglia derive from primitive macrophages. Science *330*, 841–845.

Goldschmidt, T., Antel, J., König, F.B., Brück, W., and Kuhlmann, T. (2009). Remyelination capacity of the MS brain decreases with disease chronicity. Neurology *72*, 1914–1921.

Griffin, R., Nally, R., Nolan, Y., McCartney, Y., Linden, J., and Lynch, M.A. (2006). The age-related

attenuation in long-term potentiation is associated with microglial activation. J Neurochem *99*, 1263–1272.

Gründemann, J., and Clark, B.A. (2015). Calcium-Activated Potassium Channels at Nodes of Ranvier Secure Axonal Spike Propagation. Cell Rep *12*, 1715–1722.

Hagemeyer, N., Hanft, K.-M., Akriditou, M.-A., Unger, N., Park, E.S., Stanley, E.R., Staszewski, O., Dimou, L., and Prinz, M. (2017). Microglia contribute to normal myelinogenesis and to oligodendrocyte progenitor maintenance during adulthood. Acta Neuropathol *134*, 441–458.

Hamada, M.S., Popovic, M.A., and Kole, M.H.P. (2017). Loss of Saltation and Presynaptic Action Potential Failure in Demyelinated Axons. Front Cell Neurosci *11*, 45.

Hamilton, S.P., and Rome, L.H. (1994). Stimulation of in vitro myelin synthesis by microglia. Glia *11*, 326–335.

Hammond, T.R., Dufort, C., Dissing-Olesen, L., Giera, S., Young, A., Wysoker, A., Walker, A.J., Gergits, F., Segel, M., Nemesh, J., et al. (2019). Single-Cell RNA Sequencing of Microglia throughout the Mouse Lifespan and in the Injured Brain Reveals Complex Cell-State Changes. Immunity *50*, 253-271.e6.

Heppner, F.L., Greter, M., Marino, D., Falsig, J., Raivich, G., Hövelmeyer, N., Waisman, A., Rülicke, T., Prinz, M., Priller, J., et al. (2005). Experimental autoimmune encephalomyelitis repressed by microglial paralysis. Nat Med *11*, 146–152.

Hickman, S.E., Kingery, N.D., Ohsumi, T.K., Borowsky, M.L., Wang, L., Means, T.K., and El Khoury, J. (2013). The microglial sensome revealed by direct RNA sequencing. Nat Neurosci *16*, 1896–1905.

Hines, J.H., Ravanelli, A.M., Schwindt, R., Scott, E.K., and Appel, B. (2015). Neuronal activity biases axon selection for myelination in vivo. Nat Neurosci *18*, 683–689.

Hirono, M., Ogawa, Y., Misono, K., Zollinger, D.R., Trimmer, J.S., Rasband, M.N., and Misonou, H. (2015). BK Channels Localize to the Paranodal Junction and Regulate Action Potentials in Myelinated Axons of Cerebellar Purkinje Cells. J Neurosci *35*, 7082–7094.

Ho, T.S.-Y., Zollinger, D.R., Chang, K.-J., Xu, M., Cooper, E.C., Stankewich, M.C., Bennett, V., and Rasband, M.N. (2014). A hierarchy of ankyrin-spectrin complexes clusters sodium channels at nodes of Ranvier. Nat Neurosci *17*, 1664–1672.

Hodgkin, A.L., and Huxley, A.F. (1952). A quantitative description of membrane current and its application to conduction and excitation in nerve. J Physiol *117*, 500–544.

Hollopeter, G., Jantzen, H.M., Vincent, D., Li, G., England, L., Ramakrishnan, V., Yang, R.B., Nurden, P., Nurden, A., Julius, D., et al. (2001). Identification of the platelet ADP receptor targeted by antithrombotic drugs. Nature *409*, 202–207.

Hoshiko, M., Arnoux, I., Avignone, E., Yamamoto, N., and Audinat, E. (2012). Deficiency of the microglial receptor CX3CR1 impairs postnatal functional development of thalamocortical synapses in the barrel cortex. J Neurosci *32*, 15106–15111.

Howell, O.W., Palser, A., Polito, A., Melrose, S., Zonta, B., Scheiermann, C., Vora, A.J., Brophy, P.J., and Reynolds, R. (2006). Disruption of neurofascin localization reveals early changes preceding demyelination and remyelination in multiple sclerosis. Brain *129*, 3173–3185.

Howell, O.W., Rundle, J.L., Garg, A., Komada, M., Brophy, P.J., and Reynolds, R. (2010). Activated

Microglia Mediate Axoglial Disruption That Contributes to Axonal Injury in Multiple Sclerosis. J Neuropathol Exp Neurol *69*, 1017–1033.

Hughes, A.N., and Appel, B. (2020). Microglia phagocytose myelin sheaths to modify developmental myelination. Nat Neurosci *23*, 1055–1066.

Hughes, E.G., Kang, S.H., Fukaya, M., and Bergles, D.E. (2013). Oligodendrocyte progenitors balance growth with self-repulsion to achieve homeostasis in the adult brain. Nat Neurosci *16*, 668–676.

Huxley, A.F., and Stämpfli, R. (1949). Evidence for saltatory conduction in peripheral myelinated nerve fibres. J Physiol *108*, 315–339.

Irvine, K.A., and Blakemore, W.F. (2008). Remyelination protects axons from demyelination-associated axon degeneration. Brain *131*, 1464–1477.

Jäckle, K., Zeis, T., Schaeren-Wiemers, N., Junker, A., van der Meer, F., Kramann, N., Stadelmann, C., and Brück, W. (2020). Molecular signature of slowly expanding lesions in progressive multiple sclerosis. Brain *143*, 2073–2088.

Jäkel, S., Agirre, E., Mendanha Falcão, A., van Bruggen, D., Lee, K.W., Knuesel, I., Malhotra, D., Ffrench-Constant, C., Williams, A., and Castelo-Branco, G. (2019). Altered human oligodendrocyte heterogeneity in multiple sclerosis. Nature *566*, 543–547.

Kanda, H., Ling, J., Tonomura, S., Noguchi, K., Matalon, S., and Gu, J.G. (2019). TREK-1 and TRAAK Are Principal K+ Channels at the Nodes of Ranvier for Rapid Action Potential Conduction on Mammalian Myelinated Afferent Nerves. Neuron *104*, 960-971.e7.

Kaplan, M.R., Meyer-Franke, A., Lambert, S., Bennett, V., Duncan, I.D., Levinson, S.R., and Barres, B.A. (1997). Induction of sodium channel clustering by oligodendrocytes. Nature *386*, 724–728.

Kato, G., Inada, H., Wake, H., Akiyoshi, R., Miyamoto, A., Eto, K., Ishikawa, T., Moorhouse, A.J., Strassman, A.M., and Nabekura, J. (2016). Microglial Contact Prevents Excess Depolarization and Rescues Neurons from Excitotoxicity. ENeuro *3*.

Kazen-Gillespie, K.A., Ragsdale, D.S., D'Andrea, M.R., Mattei, L.N., Rogers, K.E., and Isom, L.L. (2000). Cloning, localization, and functional expression of sodium channel beta1A subunits. J Biol Chem *275*, 1079–1088.

Keirstead, H.S., and Blakemore, W.F. (1997). Identification of post-mitotic oligodendrocytes incapable of remyelination within the demyelinated adult spinal cord. J Neuropathol Exp Neurol *56*, 1191–1201.

Kigerl, K.A., Gensel, J.C., Ankeny, D.P., Alexander, J.K., Donnelly, D.J., and Popovich, P.G. (2009). Identification of two distinct macrophage subsets with divergent effects causing either neurotoxicity or regeneration in the injured mouse spinal cord. J Neurosci *29*, 13435–13444.

Kimelberg, H.K., and Nedergaard, M. (2010). Functions of astrocytes and their potential as therapeutic targets. Neurotherapeutics *7*, 338–353.

Komada, M., and Soriano, P. (2002). [Beta]IV-spectrin regulates sodium channel clustering through ankyrin-G at axon initial segments and nodes of Ranvier. J Cell Biol *156*, 337–348.

Kornek, B., Storch, M.K., Weissert, R., Wallstroem, E., Stefferl, A., Olsson, T., Linington, C., Schmidbauer, M., and Lassmann, H. (2000). Multiple sclerosis and chronic autoimmune encephalomyelitis: a comparative quantitative study of axonal injury in active, inactive, and

remyelinated lesions. Am J Pathol *157*, 267–276.

Kotter, M.R., Setzu, A., Sim, F.J., Van Rooijen, N., and Franklin, R.J. (2001). Macrophage depletion impairs oligodendrocyte remyelination following lysolecithin-induced demyelination. Glia *35*, 204–212.

Kotter, M.R., Zhao, C., van Rooijen, N., and Franklin, R.J.M. (2005). Macrophage-depletion induced impairment of experimental CNS remyelination is associated with a reduced oligodendrocyte progenitor cell response and altered growth factor expression. Neurobiology of Disease *18*, 166–175.

Kuhlmann, T., Ludwin, S., Prat, A., Antel, J., Brück, W., and Lassmann, H. (2017). An updated histological classification system for multiple sclerosis lesions. Acta Neuropathol *133*, 13–24.

Lampron, A., Larochelle, A., Laflamme, N., Préfontaine, P., Plante, M.-M., Sánchez, M.G., Yong, V.W., Stys, P.K., Tremblay, M.-È., and Rivest, S. (2015). Inefficient clearance of myelin debris by microglia impairs remyelinating processes. J Exp Med *212*, 481–495.

Landon, D.N., and Williams, P.L. (1963). ULTRASTRUCTURE OF THE NODE OF RANVIER. Nature *199*, 575–577.

Lasiene, J., Matsui, A., Sawa, Y., Wong, F., and Horner, P.J. (2009). Age-related myelin dynamics revealed by increased oligodendrogenesis and short internodes. Aging Cell *8*, 201–213.

Lawson, L.J., Perry, V.H., Dri, P., and Gordon, S. (1990). Heterogeneity in the distribution and morphology of microglia in the normal adult mouse brain. Neuroscience *39*, 151–170.

Lee, S., Leach, M.K., Redmond, S.A., Chong, S.Y.C., Mellon, S.H., Tuck, S.J., Feng, Z.-Q., Corey, J.M., and Chan, J.R. (2012). A culture system to study oligodendrocyte myelination processes using engineered nanofibers. Nat Methods *9*, 917–922.

Letiembre, M., Hao, W., Liu, Y., Walter, S., Mihaljevic, I., Rivest, S., Hartmann, T., and Fassbender, K. (2007). Innate immune receptor expression in normal brain aging. Neuroscience *146*, 248–254.

Levine, J.M., and Reynolds, R. (1999). Activation and proliferation of endogenous oligodendrocyte precursor cells during ethidium bromide-induced demyelination. Exp Neurol *160*, 333–347.

Levine, J.M., Stincone, F., and Lee, Y.S. (1993). Development and differentiation of glial precursor cells in the rat cerebellum. Glia *7*, 307–321.

Li, W.-W., Setzu, A., Zhao, C., and Franklin, R.J.M. (2005). Minocycline-mediated inhibition of microglia activation impairs oligodendrocyte progenitor cell responses and remyelination in a non-immune model of demyelination. J Neuroimmunol *158*, 58–66.

Li, Y., Du, X.-F., Liu, C.-S., Wen, Z.-L., and Du, J.-L. (2012). Reciprocal regulation between resting microglial dynamics and neuronal activity in vivo. Dev Cell *23*, 1189–1202.

Lien, C.-C., and Jonas, P. (2003). Kv3 potassium conductance is necessary and kinetically optimized for high-frequency action potential generation in hippocampal interneurons. J Neurosci *23*, 2058–2068.

Liu, C.-H., Stevens, S.R., Teliska, L.H., Stankewich, M., Mohler, P.J., Hund, T.J., and Rasband, M.N. (2020). Nodal β spectrins are required to maintain Na+ channel clustering and axon integrity. Elife *9*.

Lloyd, A.F., Davies, C.L., Holloway, R.K., Labrak, Y., Ireland, G., Carradori, D., Dillenburg, A., Borger, E., Soong, D., Richardson, J.C., et al. (2019). Central nervous system regeneration is driven by microglia necroptosis and repopulation. Nat Neurosci *22*, 1046–1052.

Locatelli, G., Theodorou, D., Kendirli, A., Jordão, M.J.C., Staszewski, O., Phulphagar, K., Cantuti-Castelvetri, L., Dagkalis, A., Bessis, A., Simons, M., et al. (2018). Mononuclear phagocytes locally specify and adapt their phenotype in a multiple sclerosis model. Nat Neurosci *21*, 1196–1208.

Lu, W., Bhasin, M., and Tsirka, S.E. (2002). Involvement of tissue plasminogen activator in onset and effector phases of experimental allergic encephalomyelitis. J Neurosci *22*, 10781–10789.

Lubetzki, C., Sol-Foulon, N., and Desmazières, A. (2020). Nodes of Ranvier during development and repair in the CNS. Nat Rev Neurol *16*, 426–439.

Lucchinetti, C., Brück, W., Parisi, J., Scheithauer, B., Rodriguez, M., and Lassmann, H. (1999). A quantitative analysis of oligodendrocytes in multiple sclerosis lesions. A study of 113 cases. Brain *122 (Pt 12)*, 2279–2295.

Lucchinetti, C., Bruck, W., Parisi, J., Scheithauer, B., Rodriguez, M., and Lassmann, H. (2000). Heterogeneity of multiple sclerosis lesions: Implications for the pathogenesis of demyelination. 11.

Luchetti, S., Fransen, N.L., van Eden, C.G., Ramaglia, V., Mason, M., and Huitinga, I. (2018). Progressive multiple sclerosis patients show substantial lesion activity that correlates with clinical disease severity and sex: a retrospective autopsy cohort analysis. Acta Neuropathol *135*, 511–528.

Madry, C., Kyrargyri, V., Arancibia-Cárcamo, I.L., Jolivet, R., Kohsaka, S., Bryan, R.M., and Attwell, D. (2018). Microglial Ramification, Surveillance, and Interleukin-1β Release Are Regulated by the Two-Pore Domain K+ Channel THIK-1. Neuron *97*, 299-312.e6.

Makinodan, M., Rosen, K.M., Ito, S., and Corfas, G. (2012). A critical period for social experience-dependent oligodendrocyte maturation and myelination. Science *337*, 1357–1360.

Maldonado, P.P., Vélez-Fort, M., Levavasseur, F., and Angulo, M.C. (2013). Oligodendrocyte precursor cells are accurate sensors of local K+ in mature gray matter. J Neurosci *33*, 2432–2442.

Mantovani, A., Sica, A., and Locati, M. (2007). New vistas on macrophage differentiation and activation. Eur J Immunol *37*, 14–16.

Martini, R., and Schachner, M. (1986). Immunoelectron microscopic localization of neural cell adhesion molecules (L1, N-CAM, and MAG) and their shared carbohydrate epitope and myelin basic protein in developing sciatic nerve. J Cell Biol *103*, 2439–2448.

Mason, J.L., Suzuki, K., Chaplin, D.D., and Matsushima, G.K. (2001). Interleukin-1beta promotes repair of the CNS. J Neurosci *21*, 7046–7052.

Matthews, M.A. (1968). An electron microscopic study of the relationship between axon diameter and the initiation of myelin production in the peripheral nervous system. Anat Rec *161*, 337–351.

Mei, F., Lehmann-Horn, K., Shen, Y.-A.A., Rankin, K.A., Stebbins, K.J., Lorrain, D.S., Pekarek, K., A Sagan, S., Xiao, L., Teuscher, C., et al. (2016). Accelerated remyelination during inflammatory demyelination prevents axonal loss and improves functional recovery. Elife *5*.

Menegoz, M., Gaspar, P., Le Bert, M., Galvez, T., Burgaya, F., Palfrey, C., Ezan, P., Arnos, F., and Girault, J.A. (1997). Paranodin, a glycoprotein of neuronal paranodal membranes. Neuron *19*, 319–331.

Mensch, S., Baraban, M., Almeida, R., Czopka, T., Ausborn, J., El Manira, A., and Lyons, D.A. (2015). Synaptic vesicle release regulates myelin sheath number of individual oligodendrocytes in vivo. Nat Neurosci *18*, 628–630.

Metuzals, J. (1963). Ultrastructure of myelinated nerve fibers in the central nervous system of the frog. Journal of Ultrastructure Research *8*, 30–47.

Mi, S., Miller, R.H., Lee, X., Scott, M.L., Shulag-Morskaya, S., Shao, Z., Chang, J., Thill, G., Levesque, M., Zhang, M., et al. (2005). LINGO-1 negatively regulates myelination by oligodendrocytes. Nat Neurosci *8*, 745–751.

Mildner, A., Mack, M., Schmidt, H., Brück, W., Djukic, M., Zabel, M.D., Hille, A., Priller, J., and Prinz, M. (2009). CCR2+Ly-6Chi monocytes are crucial for the effector phase of autoimmunity in the central nervous system. Brain *132*, 2487–2500.

Mildner, A., Huang, H., Radke, J., Stenzel, W., and Priller, J. (2017). P2Y $_{12}$ receptor is expressed on human microglia under physiological conditions throughout development and is sensitive to neuroinflammatory diseases: P2Y $_{12}$ Expression on Human Microglia. Glia *65*, 375–387.

Miron, V.E., and Franklin, R.J.M. (2014). Macrophages and CNS remyelination. J. Neurochem. *130*, 165–171.

Miron, V.E., Boyd, A., Zhao, J.-W., Yuen, T.J., Ruckh, J.M., Shadrach, J.L., van Wijngaarden, P., Wagers, A.J., Williams, A., Franklin, R.J.M., et al. (2013). M2 microglia and macrophages drive oligodendrocyte differentiation during CNS remyelination. Nat Neurosci *16*, 1211–1218.

Mitew, S., Gobius, I., Fenlon, L.R., McDougall, S.J., Hawkes, D., Xing, Y.L., Bujalka, H., Gundlach, A.L., Richards, L.J., Kilpatrick, T.J., et al. (2018). Pharmacogenetic stimulation of neuronal activity increases myelination in an axon-specific manner. Nat Commun *9*, 306.

Mosser, D.M., and Edwards, J.P. (2008). Exploring the full spectrum of macrophage activation. Nat Rev Immunol *8*, 958–969.

Natrajan, M.S., de la Fuente, A.G., Crawford, A.H., Linehan, E., Nuñez, V., Johnson, K.R., Wu, T., Fitzgerald, D.C., Ricote, M., Bielekova, B., et al. (2015). Retinoid X receptor activation reverses age-related deficiencies in myelin debris phagocytosis and remyelination. Brain *138*, 3581–3597.

Nawaz, S., Sánchez, P., Schmitt, S., Snaidero, N., Mitkovski, M., Velte, C., Brückner, B.R., Alexopoulos, I., Czopka, T., Jung, S.Y., et al. (2015). Actin filament turnover drives leading edge growth during myelin sheath formation in the central nervous system. Dev Cell *34*, 139–151.

Neumann, B., Foerster, S., Zhao, C., Bodini, B., Reich, D.S., Bergles, D.E., Káradóttir, R.T., Lubetzki, C., Lairson, L.L., Zalc, B., et al. (2020). Problems and Pitfalls of Identifying Remyelination in Multiple Sclerosis. Cell Stem Cell *26*, 617–619.

Neumann, H., Kotter, M.R., and Franklin, R.J.M. (2009). Debris clearance by microglia: an essential link between degeneration and regeneration. Brain *132*, 288–295.

Nikić, I., Merkler, D., Sorbara, C., Brinkoetter, M., Kreutzfeldt, M., Bareyre, F.M., Brück, W., Bishop, D., Misgeld, T., and Kerschensteiner, M. (2011). A reversible form of axon damage in experimental autoimmune encephalomyelitis and multiple sclerosis. Nat Med *17*, 495–499.

Nimmerjahn, A., Kirchhoff, F., and Helmchen, F. (2005). Resting microglial cells are highly dynamic surveillants of brain parenchyma in vivo. Science *308*, 1314–1318.

Nishiyama, A., Lin, X.H., Giese, N., Heldin, C.H., and Stallcup, W.B. (1996). Co-localization of NG2 proteoglycan and PDGF alpha-receptor on O2A progenitor cells in the developing rat brain. J Neurosci Res *43*, 299–314.

Ogiwara, I., Miyamoto, H., Morita, N., Atapour, N., Mazaki, E., Inoue, I., Takeuchi, T., Itohara, S.,

Yanagawa, Y., Obata, K., et al. (2007). Nav1.1 localizes to axons of parvalbumin-positive inhibitory interneurons: a circuit basis for epileptic seizures in mice carrying an Scn1a gene mutation. J Neurosci *27*, 5903–5914.

Oluich, L.-J., Stratton, J.A.S., Lulu Xing, Y., Ng, S.W., Cate, H.S., Sah, P., Windels, F., Kilpatrick, T.J., and Merson, T.D. (2012). Targeted Ablation of Oligodendrocytes Induces Axonal Pathology Independent of Overt Demyelination. Journal of Neuroscience *32*, 8317–8330.

Oohashi, T., Hirakawa, S., Bekku, Y., Rauch, U., Zimmermann, D.R., Su, W.-D., Ohtsuka, A., Murakami, T., and Ninomiya, Y. (2002). Bral1, a brain-specific link protein, colocalizing with the versican V2 isoform at the nodes of Ranvier in developing and adult mouse central nervous systems. Mol Cell Neurosci *19*, 43–57.

Ortiz, F.C., Habermacher, C., Graciarena, M., Houry, P.-Y., Nishiyama, A., Nait Oumesmar, B., and Angulo, M.C. (2019). Neuronal activity in vivo enhances functional myelin repair. JCI Insight *5*.

Pan, Z., Kao, T., Horvath, Z., Lemos, J., Sul, J.-Y., Cranstoun, S.D., Bennett, V., Scherer, S.S., and Cooper, E.C. (2006). A common ankyrin-G-based mechanism retains KCNQ and NaV channels at electrically active domains of the axon. J Neurosci *26*, 2599–2613.

Paolicelli, R.C., and Gross, C.T. (2011). Microglia in development: linking brain wiring to brain environment. Neuron Glia Biol *7*, 77–83.

Paolicelli, R.C., Bolasco, G., Pagani, F., Maggi, L., Scianni, M., Panzanelli, P., Giustetto, M., Ferreira, T.A., Guiducci, E., Dumas, L., et al. (2011). Synaptic pruning by microglia is necessary for normal brain development. Science *333*, 1456–1458.

Parkhurst, C.N., Yang, G., Ninan, I., Savas, J.N., Yates, J.R., Lafaille, J.J., Hempstead, B.L., Littman, D.R., and Gan, W.-B. (2013). Microglia promote learning-dependent synapse formation through brain-derived neurotrophic factor. Cell *155*, 1596–1609.

Patani, R., Balaratnam, M., Vora, A., and Reynolds, R. (2007). Remyelination can be extensive in multiple sclerosis despite a long disease course. Neuropathol Appl Neurobiol *33*, 277–287.

Patrikios, P., Stadelmann, C., Kutzelnigg, A., Rauschka, H., Schmidbauer, M., Laursen, H., Sorensen, P.S., Bruck, W., Lucchinetti, C., and Lassmann, H. (2006). Remyelination is extensive in a subset of multiple sclerosis patients. Brain *129*, 3165–3172.

Patton, D.E., Isom, L.L., Catterall, W.A., and Goldin, A.L. (1994). The adult rat brain beta 1 subunit modifies activation and inactivation gating of multiple sodium channel alpha subunits. J Biol Chem *269*, 17649–17655.

Pekny, M., Wilhelmsson, U., and Pekna, M. (2014). The dual role of astrocyte activation and reactive gliosis. Neurosci Lett *565*, 30–38.

Peles, E., Nativ, M., Lustig, M., Grumet, M., Schilling, J., Martinez, R., Plowman, G.D., and Schlessinger, J. (1997). Identification of a novel contactin-associated transmembrane receptor with multiple domains implicated in protein-protein interactions. EMBO J *16*, 978–988.

Perry, V.H., Matyszak, M.K., and Fearn, S. (1993). Altered antigen expression of microglia in the aged rodent CNS. Glia *7*, 60–67.

Peters, A. (1960). THE FORMATION AND STRUCTURE OF MYELIN SHEATHS IN THE CENTRAL NERVOUS SYSTEM. The Journal of Biophysical and Biochemical Cytology *8*, 431–446.

Pfeiffer, F., Frommer-Kaestle, G., and Fallier-Becker, P. (2019). Structural adaption of axons during

de- and remyelination in the Cuprizone mouse model. Brain Pathol *29*, 675–692.

Pfeiffer, S.E., Warrington, A.E., and Bansal, R. (1993). The oligodendrocyte and its many cellular processes. Trends Cell Biol *3*, 191–197.

Piaton, G., Aigrot, M.-S., Williams, A., Moyon, S., Tepavcevic, V., Moutkine, I., Gras, J., Matho, K.S., Schmitt, A., Soellner, H., et al. (2011). Class 3 semaphorins influence oligodendrocyte precursor recruitment and remyelination in adult central nervous system. Brain *134*, 1156–1167.

Plemel, J.R., Manesh, S.B., Sparling, J.S., and Tetzlaff, W. (2013). Myelin inhibits oligodendroglial maturation and regulates oligodendrocytic transcription factor expression. Glia *61*, 1471–1487.

Pohl, H.B.F., Porcheri, C., Mueggler, T., Bachmann, L.C., Martino, G., Riethmacher, D., Franklin, R.J.M., Rudin, M., and Suter, U. (2011). Genetically induced adult oligodendrocyte cell death is associated with poor myelin clearance, reduced remyelination, and axonal damage. J Neurosci *31*, 1069–1080.

Ponomarev, E.D., Shriver, L.P., Maresz, K., and Dittel, B.N. (2005). Microglial cell activation and proliferation precedes the onset of CNS autoimmunity. J Neurosci Res *81*, 374–389.

Prineas, J.W., and Connell, F. (1979). Remyelination in multiple sclerosis. Ann Neurol *5*, 22–31.

Prineas, J.W., Barnard, R.O., Revesz, T., Kwon, E.E., Sharer, L., and Cho, E.S. (1993). Multiple sclerosis. Pathology of recurrent lesions. Brain *116 (Pt 3)*, 681–693.

Prineas, J.W., Kwon, E.E., Cho, E.S., Sharer, L.R., Barnett, M.H., Oleszak, E.L., Hoffman, B., and Morgan, B.P. (2001). Immunopathology of secondary-progressive multiple sclerosis. Ann Neurol *50*, 646–657.

Pringle, N.P., Mudhar, H.S., Collarini, E.J., and Richardson, W.D. (1992). PDGF receptors in the rat CNS: during late neurogenesis, PDGF alpha-receptor expression appears to be restricted to glial cells of the oligodendrocyte lineage. Development *115*, 535–551.

Psachoulia, K., Chamberlain, K.A., Heo, D., Davis, S.E., Paskus, J.D., Nanescu, S.E., Dupree, J.L., Wynn, T.A., and Huang, J.K. (2016). IL4I1 augments CNS remyelination and axonal protection by modulating T cell driven inflammation. Brain *139*, 3121–3136.

Ragozzino, D., Di Angelantonio, S., Trettel, F., Bertollini, C., Maggi, L., Gross, C., Charo, I.F., Limatola, C., and Eusebi, F. (2006). Chemokine fractalkine/CX3CL1 negatively modulates active glutamatergic synapses in rat hippocampal neurons. J Neurosci *26*, 10488–10498.

Ransohoff, R.M., Liu, L., and Cardona, A.E. (2007). Chemokines and chemokine receptors: multipurpose players in neuroinflammation. Int Rev Neurobiol *82*, 187–204.

Rasband, M.N. (2010). Clustered K+ channel complexes in axons. Neurosci Lett *486*, 101–106.

Rasband, M.N., Peles, E., Trimmer, J.S., Levinson, S.R., Lux, S.E., and Shrager, P. (1999). Dependence of nodal sodium channel clustering on paranodal axoglial contact in the developing CNS. J Neurosci *19*, 7516–7528.

Rasband, M.N., Kagawa, T., Park, E.W., Ikenaka, K., and Trimmer, J.S. (2003). Dysregulation of axonal sodium channel isoforms after adult-onset chronic demyelination. J Neurosci Res *73*, 465–470.

Rasband, M.N., Tayler, J., Kaga, Y., Yang, Y., Lappe-Siefke, C., Nave, K.-A., and Bansal, R. (2005). CNP is required for maintenance of axon-glia interactions at nodes of Ranvier in the CNS. Glia *50*, 86–90.

Reich, D.S., Lucchinetti, C.F., and Calabresi, P.A. (2018). Multiple Sclerosis. N Engl J Med *378*, 169–180.

Remahl, S., and Hildebrand, C. (1982). Changing relation between onset of myelination and axon diameter range in developing feline white matter. Journal of the Neurological Sciences *54*, 33–45.

Rio-Hortega, D.P. (1921). Histogenesis y evolucion normal; exodo y distribucion regional de la microglia. pp. 213–268.

Rio-Hortega, R.D. (1928). Tercera Aportacion Al Conocimiento Morfologico E Interpretacion Funcional De La Oligodendroglia. pp. 5–122.

Rios, J.C., Rubin, M., St Martin, M., Downey, R.T., Einheber, S., Rosenbluth, J., Levinson, S.R., Bhat, M., and Salzer, J.L. (2003). Paranodal interactions regulate expression of sodium channel subtypes and provide a diffusion barrier for the node of Ranvier. J Neurosci *23*, 7001–7011.

Robinson, S., and Miller, R.H. (1999). Contact with central nervous system myelin inhibits oligodendrocyte progenitor maturation. Dev Biol *216*, 359–368.

Rommer, P.S., Milo, R., Han, M.H., Satyanarayan, S., Sellner, J., Hauer, L., Illes, Z., Warnke, C., Laurent, S., Weber, M.S., et al. (2019). Immunological Aspects of Approved MS Therapeutics. Front Immunol *10*, 1564.

Ruckh, J.M., Zhao, J.-W., Shadrach, J.L., van Wijngaarden, P., Rao, T.N., Wagers, A.J., and Franklin, R.J.M. (2012). Rejuvenation of regeneration in the aging central nervous system. Cell Stem Cell *10*, 96–103.

Rushton, W. a. H. (1951). A theory of the effects of fibre size in medullated nerve. J Physiol *115*, 101–122.

Saab, A.S., Tzvetavona, I.D., Trevisiol, A., Baltan, S., Dibaj, P., Kusch, K., Möbius, W., Goetze, B., Jahn, H.M., Huang, W., et al. (2016). Oligodendroglial NMDA Receptors Regulate Glucose Import and Axonal Energy Metabolism. Neuron *91*, 119–132.

Salter, M.W., and Stevens, B. (2017). Microglia emerge as central players in brain disease. Nat Med *23*, 1018–1027.

Salzer, J.L. (2003). Polarized domains of myelinated axons. Neuron *40*, 297–318.

Satoh, J., Kino, Y., Asahina, N., Takitani, M., Miyoshi, J., Ishida, T., and Saito, Y. (2016). TMEM119 marks a subset of microglia in the human brain: Human microglial marker TMEM119. Neuropathology *36*, 39–49.

Schafer, D.P., Lehrman, E.K., Kautzman, A.G., Koyama, R., Mardinly, A.R., Yamasaki, R., Ransohoff, R.M., Greenberg, M.E., Barres, B.A., and Stevens, B. (2012). Microglia sculpt postnatal neural circuits in an activity and complement-dependent manner. Neuron *74*, 691–705.

Schaller, K.L., and Caldwell, J.H. (2003). Expression and distribution of voltage-gated sodium channels in the cerebellum. Cerebellum *2*, 2–9.

Scholz, J., Klein, M.C., Behrens, T.E.J., and Johansen-Berg, H. (2009). Training induces changes in white-matter architecture. Nat Neurosci *12*, 1370–1371.

Schwarz, J.R., Glassmeier, G., Cooper, E.C., Kao, T.-C., Nodera, H., Tabuena, D., Kaji, R., and Bostock, H. (2006). KCNQ channels mediate IKs, a slow K+ current regulating excitability in the rat node of Ranvier. J Physiol *573*, 17–34.

Seidl, A.H., Rubel, E.W., and Barría, A. (2014). Differential conduction velocity regulation in ipsilateral and contralateral collaterals innervating brainstem coincidence detector neurons. J Neurosci *34*, 4914–4919.

Serwanski, D.R., Jukkola, P., and Nishiyama, A. (2017). Heterogeneity of astrocyte and NG2 cell insertion at the node of ranvier: Frequency of glial insertion at the node. J. Comp. Neurol. *525*, 535–552.

Shields, S.A., Gilson, J.M., Blakemore, W.F., and Franklin, R.J. (1999). Remyelination occurs as extensively but more slowly in old rats compared to young rats following gliotoxin-induced CNS demyelination. Glia *28*, 77–83.

Silvin, A., and Ginhoux, F. (2018). Microglia heterogeneity along a spatio-temporal axis: More questions than answers. Glia *66*, 2045–2057.

Sim, F.J., Zhao, C., Penderis, J., and Franklin, R.J.M. (2002). The age-related decrease in CNS remyelination efficiency is attributable to an impairment of both oligodendrocyte progenitor recruitment and differentiation. J Neurosci *22*, 2451–2459.

Sims, T.J., Waxman, S.G., Black, J.A., and Gilmore, S.A. (1985). Perinodal astrocytic processes at nodes of ranvier in developing normal and glial cell deficient rat spinal cord. Brain Research *337*, 321–331.

Skripuletz, T., Hackstette, D., Bauer, K., Gudi, V., Pul, R., Voss, E., Berger, K., Kipp, M., Baumgärtner, W., and Stangel, M. (2013). Astrocytes regulate myelin clearance through recruitment of microglia during cuprizone-induced demyelination. Brain *136*, 147–167.

Smith, K.J., and Lassmann, H. (2002). The role of nitric oxide in multiple sclerosis. Lancet Neurol *1*, 232–241.

Smith, R.S., and Koles, Z.J. (1970). Myelinated nerve fibers: computed effect of myelin thickness on conduction velocity. Am J Physiol *219*, 1256–1258.

Smith, K.J., Blakemore, W.F., and McDonald, W.I. (1979). Central remyelination restores secure conduction. Nature *280*, 395–396.

Smith, K.J., Bostock, H., and Hall, S.M. (1982). Saltatory conduction precedes remyelination in axons demyelinated with lysophosphatidyl choline. Journal of the Neurological Sciences *54*, 13–31.

Snaidero, N., Möbius, W., Czopka, T., Hekking, L.H.P., Mathisen, C., Verkleij, D., Goebbels, S., Edgar, J., Merkler, D., Lyons, D.A., et al. (2014). Myelin Membrane Wrapping of CNS Axons by PI(3,4,5)P3-Dependent Polarized Growth at the Inner Tongue. Cell *156*, 277–290.

Solly, S.K., Thomas, J.L., Monge, M., Demerens, C., Lubetzki, C., Gardinier, M.V., Matthieu, J.M., and Zalc, B. (1996). Myelin/oligodendrocyte glycoprotein (MOG) expression is associated with myelin deposition. Glia *18*, 39–48.

Susuki, K., Chang, K.-J., Zollinger, D.R., Liu, Y., Ogawa, Y., Eshed-Eisenbach, Y., Dours-Zimmermann, M.T., Oses-Prieto, J.A., Burlingame, A.L., Seidenbecher, C.I., et al. (2013). Three Mechanisms Assemble Central Nervous System Nodes of Ranvier. Neuron *78*, 469–482.

Syed, Y.A., Hand, E., Möbius, W., Zhao, C., Hofer, M., Nave, K.A., and Kotter, M.R. (2011). Inhibition of CNS remyelination by the presence of semaphorin 3A. J Neurosci *31*, 3719–3728.

Szalay, G., Martinecz, B., Lénárt, N., Környei, Z., Orsolits, B., Judák, L., Császár, E., Fekete, R., West, B.L., Katona, G., et al. (2016). Microglia protect against brain injury and their selective

elimination dysregulates neuronal network activity after stroke. Nat Commun *7*, 11499.

Tait, S., Gunn-Moore, F., Collinson, J.M., Huang, J., Lubetzki, C., Pedraza, L., Sherman, D.L., Colman, D.R., and Brophy, P.J. (2000). An oligodendrocyte cell adhesion molecule at the site of assembly of the paranodal axo-glial junction. J Cell Biol *150*, 657–666.

Targett, M.P., Sussman, J., Scolding, N., O'Leary, M.T., Compston, D.A., and Blakemore, W.F. (1996). Failure to achieve remyelination of demyelinated rat axons following transplantation of glial cells obtained from the adult human brain. Neuropathol Appl Neurobiol *22*, 199–206.

Thetiot, M., Freeman, S.A., Roux, T., Dubessy, A., Aigrot, M., Rappeneau, Q., Lejeune, F., Tailleur, J., Sol-Foulon, N., Lubetzki, C., et al. (2020). An alternative mechanism of early nodal clustering and myelination onset in GABAergic neurons of the central nervous system. Glia *68*, 1891–1909.

Tomasi, S., Caminiti, R., and Innocenti, G.M. (2012). Areal differences in diameter and length of corticofugal projections. Cereb Cortex *22*, 1463–1472.

Tomassy, G.S., Berger, D.R., Chen, H.-H., Kasthuri, N., Hayworth, K.J., Vercelli, A., Seung, H.S., Lichtman, J.W., and Arlotta, P. (2014). Distinct profiles of myelin distribution along single axons of pyramidal neurons in the neocortex. Science *344*, 319–324.

Torres, L., Danver, J., Ji, K., Miyauchi, J.T., Chen, D., Anderson, M.E., West, B.L., Robinson, J.K., and Tsirka, S.E. (2016). Dynamic microglial modulation of spatial learning and social behavior. Brain Behav Immun *55*, 6–16.

Trapp, B.D., Wujek, J.R., Criste, G.A., Jalabi, W., Yin, X., Kidd, G.J., Stohlman, S., and Ransohoff, R. (2007). Evidence for synaptic stripping by cortical microglia. Glia *55*, 360–368.

Tremblay, M.-È., Lowery, R.L., and Majewska, A.K. (2010). Microglial interactions with synapses are modulated by visual experience. PLoS Biol *8*, e1000527.

Tripathi, R.B., Rivers, L.E., Young, K.M., Jamen, F., and Richardson, W.D. (2010). NG2 glia generate new oligodendrocytes but few astrocytes in a murine experimental autoimmune encephalomyelitis model of demyelinating disease. J Neurosci *30*, 16383–16390.

Tvrdik, P., and Kalani, M.Y.S. (2017). In Vivo Imaging of Microglial Calcium Signaling in Brain Inflammation and Injury. Int J Mol Sci *18*.

Ueno, M., Fujita, Y., Tanaka, T., Nakamura, Y., Kikuta, J., Ishii, M., and Yamashita, T. (2013). Layer V cortical neurons require microglial support for survival during postnatal development. Nat Neurosci *16*, 543–551.

van der Valk, P., and Amor, S. (2009). Preactive lesions in multiple sclerosis: Current Opinion in Neurology 1.

Vogel, D.Y., Vereyken, E.J., Glim, J.E., Heijnen, P.D., Moeton, M., van der Valk, P., Amor, S., Teunissen, C.E., van Horssen, J., and Dijkstra, C.D. (2013). Macrophages in inflammatory multiple sclerosis lesions have an intermediate activation status. J Neuroinflammation *10*, 809.

Voss, E.V., Škuljec, J., Gudi, V., Skripuletz, T., Pul, R., Trebst, C., and Stangel, M. (2012). Characterisation of microglia during de- and remyelination: can they create a repair promoting environment? Neurobiol Dis *45*, 519–528.

Wake, H., Moorhouse, A.J., Jinno, S., Kohsaka, S., and Nabekura, J. (2009). Resting microglia directly monitor the functional state of synapses in vivo and determine the fate of ischemic terminals. J Neurosci *29*, 3974–3980.

Wake, H., Lee, P.R., and Fields, R.D. (2011). Control of local protein synthesis and initial events in myelination by action potentials. Science *333*, 1647–1651.

Wake, H., Ortiz, F.C., Woo, D.H., Lee, P.R., Angulo, M.C., and Fields, R.D. (2015). Nonsynaptic junctions on myelinating glia promote preferential myelination of electrically active axons. Nat Commun *6*, 7844.

Wang, H., Kunkel, D.D., Martin, T.M., Schwartzkroin, P.A., and Tempel, B.L. (1993). Heteromultimeric K+ channels in terminal and juxtaparanodal regions of neurons. Nature *365*, 75–79.

Wang, S., Sdrulla, A.D., diSibio, G., Bush, G., Nofziger, D., Hicks, C., Weinmaster, G., and Barres, B.A. (1998). Notch receptor activation inhibits oligodendrocyte differentiation. Neuron *21*, 63–75.

Watkins, T.A., Emery, B., Mulinyawe, S., and Barres, B.A. (2008). Distinct stages of myelination regulated by gamma-secretase and astrocytes in a rapidly myelinating CNS coculture system. Neuron *60*, 555–569.

Waxman, S.G., and Black, J.A. (1984). Freeze-fracture ultrastructure of the perinodal astrocyte and associated glial junctions. Brain Research *308*, 77–87.

Waxman, S.G., and Ritchie, J.M. (1993). Molecular dissection of the myelinated axon. Ann Neurol *33*, 121–136.

Waxman, S.G., and Swadlow, H.A. (1976). Ultrastructure of visual callosal axons in the rabbit. Exp Neurol *53*, 115–127.

Wlodarczyk, A., Holtman, I.R., Krueger, M., Yogev, N., Bruttger, J., Khorooshi, R., Benmamar-Badel, A., Boer-Bergsma, J.J., Martin, N.A., Karram, K., et al. (2017). A novel microglial subset plays a key role in myelinogenesis in developing brain. EMBO J *36*, 3292–3308.

Wolswijk, G. (1998). Chronic stage multiple sclerosis lesions contain a relatively quiescent population of oligodendrocyte precursor cells. J Neurosci *18*, 601–609.

Wood, P.M., and Bunge, R.P. (1991). The origin of remyelinating cells in the adult central nervous system: the role of the mature oligodendrocyte. Glia *4*, 225–232.

Yamasaki, R., Lu, H., Butovsky, O., Ohno, N., Rietsch, A.M., Cialic, R., Wu, P.M., Doykan, C.E., Lin, J., Cotleur, A.C., et al. (2014). Differential roles of microglia and monocytes in the inflamed central nervous system. Journal of Experimental Medicine *211*, 1533–1549.

Yang, Y., Ogawa, Y., Hedstrom, K.L., and Rasband, M.N. (2007). betaIV spectrin is recruited to axon initial segments and nodes of Ranvier by ankyrinG. J Cell Biol *176*, 509–519.

Young, K.M., Psachoulia, K., Tripathi, R.B., Dunn, S.-J., Cossell, L., Attwell, D., Tohyama, K., and Richardson, W.D. (2013). Oligodendrocyte dynamics in the healthy adult CNS: evidence for myelin remodeling. Neuron *77*, 873–885.

Zalc, B., Monge, M., Dupouey, P., Hauw, J.J., and Baumann, N.A. (1981). Immunohistochemical localization of galactosyl and sulfogalactosyl ceramide in the brain of the 30-day-old mouse. Brain Res *211*, 341–354.

Zamora, N.N., Cheli, V.T., Santiago González, D.A., Wan, R., and Paez, P.M. (2020). Deletion of Voltage-Gated Calcium Channels in Astrocytes during Demyelination Reduces Brain Inflammation and Promotes Myelin Regeneration in Mice. J Neurosci *40*, 3332–3347.

Zeis, T., Graumann, U., Reynolds, R., and Schaeren-Wiemers, N. (2008). Normal-appearing white

matter in multiple sclerosis is in a subtle balance between inflammation and neuroprotection. Brain *131*, 288–303.

Zhang, J., Yang, X., Zhou, Y., Fox, H., and Xiong, H. (2019). Direct contacts of microglia on myelin sheath and Ranvier's node in the corpus callosum in rats. J Biomed Res *33*, 192–200.

Zonta, B., Tait, S., Melrose, S., Anderson, H., Harroch, S., Higginson, J., Sherman, D.L., and Brophy, P.J. (2008). Glial and neuronal isoforms of Neurofascin have distinct roles in the assembly of nodes of Ranvier in the central nervous system. J Cell Biol *181*, 1169–1177.

Zrzavy, T., Hametner, S., Wimmer, I., Butovsky, O., Weiner, H.L., and Lassmann, H. (2017). Loss of 'homeostatic' microglia and patterns of their activation in active multiple sclerosis. Brain *140*, 1900–1913.

Zuchero, J.B., Fu, M.-M., Sloan, S.A., Ibrahim, A., Olson, A., Zaremba, A., Dugas, J.C., Wienbar, S., Caprariello, A.V., Kantor, C., et al. (2015). CNS myelin wrapping is driven by actin disassembly. Dev Cell *34*, 152–167.

RESUME

La sclérose en plaques (SEP) est une maladie inflammatoire démyélinisante et neurodégénérative du système nerveux central (SNC), sans traitement disponible capable de ralentir la progression du handicap. Ainsi, de nouvelles thérapeutiques favorisant remyélinisation et neuroprotection sont nécessaires. Mieux caractériser les processus de réparation après un évènement démyélinisant est une étape cruciale vers cet objectif. Dans les fibres myélinisées, l'agrégation des canaux sodiques voltage-dépendants aux nœuds de Ranvier favorise la propagation rapide des potentiels d'action via la conduction saltatoire. Les nœuds de Ranvier sont connus comme une cible immunitaire préférentielle lors de la démyélinisation et il a été démontré qu'ils peuvent se reconstituer tôt avant même la remyélinisation, ce qui suggère qu'ils pourraient y participer. En outre, les cellules microgliales, cellules immunitaires résidentes du SNC, sont des régulateurs majeurs de la remyélinisation, en soutenant la survie neuronale et en favorisant la différenciation oligodendrogliale. Le rôle de l'interaction entre les neurones et la microglie sur le comportement des cellules microgliales et la remyélinisation est cependant inconnu.

Mon projet de thèse avait pour but de déchiffrer les interactions entre la microglie et les nœuds de Ranvier, notamment pendant la remyélinisation. Ainsi, dans la première partie de mon travail, nous avons recherché des interactions entre la microglie et les nœuds de Ranvier dans des modèles expérimentaux. Nous avons montré des interactions microglies-nœuds stables, qui sont renforcées lors de la remyélinisation. Cette interaction dépend de l'activité neuronale et des courants potassiques existants aux nœuds. Nous avons également montré que l'inhibition des contacts nœud-microglie était en corrélation avec une diminution du switch microglial vers un phénotype pro-régénératif et une diminution du taux de remyélinisation.

La deuxième partie de ma thèse, portant sur des travaux en cours, vise à caractériser les interactions nœud-microglie dans des tissus humains contrôle et SEP. L'interaction nœud-microglie est observée dans les deux contextes, mais est diminuée dans la substance blanche d'apparence normale des patients SEP. La microglie dans son phénotype homéostatique réapparaît dans les « shadow plaques » malgré la persistance d'un phénotype microglial inflammatoire. L'interaction nœud-microglie est également rétablie.

Au total, nos résultats placent l'interaction entre neurone et microglie comme un acteur central durant la remyélinisation et ouvrent la voie vers de nouvelles cibles thérapeutiques dans la SEP.

Mots clés : nœuds de Ranvier, microglie, remyélinisation, Sclérose en plaques, shadow plaques

SUMMARY

Multiple sclerosis (MS) is a central nervous system (CNS) inflammatory demyelinating disease, which leads to neurodegeneration, without any available treatment able to slow associated progressive handicap. Thus, new molecules enhancing repair and neuroprotection are an unmet need. To better decipher the repair processes after a demyelinating insult is a crucial step towards this goal. In myelinated fibers, the clustering of voltage-gated sodium channels at the nodes of Ranvier support the rapid propagation of action potentials by saltatory conduction. Nodes of Ranvier are known as a preferential immune target during demyelination and it was shown that they can recluster early at the onset of remyelination, suggesting they could participate in repair. Furthermore, microglia, the resident immune cells of the CNS, have been shown to be major regulators of remyelination, by supporting neuronal survival and promoting oligodendroglial lineage differentiation. How the crosstalk between neurons and microglia can affect microglial behavior and remyelination is however unknown.

My thesis project aimed at deciphering the interactions between microglia and nodes of Ranvier, in particular in repair. Thus, for the first part of my work, we searched for interactions between microglia and nodes of Ranvier in experimental models. We showed stable microglia-nodes interactions, which are further reinforced during remyelination. This interaction depends on neuronal activity and related potassium fluxes. We also showed that inhibiting node-microglia contacts correlates with a diminution of the microglial switch towards a pro-repair state and with a decreased remyelination.

The second part of my thesis, which corresponds to work in progress, aims at characterizing node-microglia interactions in human control and MS tissues. Node-microglia interaction is observed in both contexts but is altered in normal appearing white matter of MS tissues. Homeostatic microglia reappear in shadow plaques despite the persistence of inflammatory microglia and node-microglia interaction is restored following nodal reclustering in these areas.

Taken together, our results put neuron-microglia crosstalk as a central player in repair and open new avenues for therapeutic targets in MS.

Keywords: nodes of Ranvier, microglia, remyelination, Multiple Sclerosis, shadow plaques, neuron-glial crosstalk